



INSTITUTO DE FÍSICA

Universidade Federal Fluminense

David MÖCKLI

**SPONTANEOUS FERROMAGNETISM IN
HIGH- T_c SUPERCONDUCTORS**

Niterói
March 2013

DAVID MÖCKLI

SPONTANEOUS FERROMAGNETISM IN HIGH- T_c SUPERCONDUCTORS

This dissertation is submitted to the graduate program in Physics of Universidade Federal Fluminense, in partial fulfilment of the requirements for the degree Master in Physics.

Advisor: Dr. EVANDRO VIDOR LINS DE MELLO

Niterói
March 2013

To Carlo and Geane

Acknowledgements

I thank the Father for the privilege to explore His handiwork.

I owe everything to Carlo and Geane, my parents.

I thank Bruna for unlimited love.

Nothing of this would have been possible without Paulo Viana.

I am grateful to Daniel and Raquel Salvador, Flávio and Fabricia Lins, Daniel and Débora Oliveira, Silas and Selma Esteves.

I obviously thank my advisor Evandro for his orientation, integrity and patience.

I am grateful to Gustavo, my friend, from whom I learn so much.

I am grateful to Orlando, my friend and neighbour, for useful discussions and leading me out of the obvious.

I thank CAPES for financial aid.

Abstract

We propose a model based on the charge disorder of the high- T_c superconductors to explain the weak ferromagnetic signal observed in compounds such as $\text{YBa}_2\text{Cu}_3\text{O}_{6+x}$. In order to set the framework, we develop the basic elements of second quantization for fermions, and introduce important elements of both the microscopic and phenomenological theory of superconductivity. Our basic model relies on an electronic phase separation with the formation of low and high density domains. At low temperatures this system may act as a granular superconductor where the grains are formed by isolated regions with varying charge density and superconducting amplitudes. These isolated regions may have different local critical temperatures (T_c), that is, not the same onset of superconducting amplitudes, forming a Josephson network and the whole system undergoes the superconducting or resistivity transition through phase coherence among the grains. The main point of this dissertation is that the low electronic density of the grains in conjunction with intrinsic electronic disorder, two well known properties of cuprates, may produce a negative Josephson coupling that provokes spontaneous frustration. Spontaneous current loops are produced that are responsible for the overall observed weak ferromagnetic order. We show that this model provides a novel explanation and reproduces the experimental data of the observed magnetic signal.

Resumo

Sugerimos um modelo para os supercondutores de altas temperaturas críticas para explicar o sinal ferromagnético fraco observado em compostos como $\text{YBa}_2\text{Cu}_3\text{O}_{6+x}$. Afim de estabelecer o cenário, desenvolvemos elementos básicos da teoria microscópica da supercondutividade. O modelo base se firma numa separação eletrônica com domínios de baixas e altas densidades. A baixas temperaturas esse sistema pode se comportar como um supercondutor granular, onde os grãos são formados por regiões isoladas com densidade de carga e amplitude supercondutora variável, formando uma rede Josephson e o sistema sofre uma transição supercondutora através do estabelecimento de coerência de fase entre os grãos. O ponto principal desta dissertação afirma que a baixa densidade dos grãos em conjunção com desordem eletrônica intrínseca – duas características bem conhecidas dos cupratos – produzem um acoplamento Josephson negativo que provoca frustração espontânea. Circuitos espontâneos são produzidos e são responsáveis pelo sinal ferromagnético fraco observado. Mostramos que este modelo provê uma explicação inovadora e reproduz os dados experimentais do sinal magnético observado.

List of Figures

- 1.1 **Left:** As Onnes reduced the temperature of mercury, he saw an abrupt transition to zero resistance at 4.2 K. **Right:** Diagram of the Meissner effect. Magnetic field lines, represented as arrows, are excluded from a superconductor when it is below its critical temperature T_c 2
- 1.2 **Left:** Evolution of superconductors. **Right:** Schematic phase diagram of high- T_c superconductors, temperature versus hole doping concentration. The left AF region shows the anti-ferromagnetic region, the superconducting dome in the middle, with the crossover temperature T^* of the "normal" pseudogap phase. 3
- 3.1 **Left:** The wave packet $\phi(\mathbf{r}_1 - \mathbf{r}_2)$ embodying the two electrons at \mathbf{r}_1 and \mathbf{r}_2 , with energies ϵ_1 and ϵ_2 above the Fermi level ϵ_F . **Right:** The Cooper problem: two electrons outside a fully occupied Fermi sea, but restricted to a band $\hbar\omega_D$ due to the attractive potential provided by the electron-phonon interaction. 21
- 3.2 Behaviour of elementary quasiparticle excitations: Dashed line - normal state with $\Delta = 0$; Continuous line - superconducting state where $\Delta \neq 0$. . . 31
- 3.3 **Left:** The BCS wave function parameters $|u_k|^2$ and $|v_k|^2$ for \mathbf{k} near the Fermi surface. **Right:** Temperature dependence of the energy gap in the BCS theory. 32
- 3.4 **Left:** Part of the lattice structure of yttrium barium copper oxide. **Right:** d-wave symmetry of the gap parameter with four gap nodes on the Fermi surface. The square is the first Brillouin zone. 34

3.5	Top left: The values of the gap of $\Delta_\delta(i)$ varying in a 24 x 24 square lattice at temperature 50 K. Top right: Correspondent hole concentration $\rho(i)$ also at 50 K. Bottom left: The gaps at 190 K. Bottom right: Hole concentration at 190 K.	42
3.6	The temperature evolution of $\Delta_\delta(i)$ at five randomly chosen locations i of an average $\bar{\rho} = 0.15$ compound. The mean field Bogoliubov-deGennes calculations vanish at the same temperature $T^*(0.15) = 165$ K, above $T_c(0.15) = 92$ K.	43
4.1	Left (Equation 4.4): The free energy density difference between the superconducting and the normal state. The dashed line describes the normal state in which $a(T) > 0$, admitting one minimum. The continuous line describes the superconducting state in which $a(T) < 0$ with two minima at $\pm\sqrt{\alpha(T_c - T)/\beta}$. Right (Equation 4.5): The order parameter magnitude $ \psi $ as a function of the temperature in the Ginzburg-Landau model. This is worth comparing with figure 3.3.	46
4.2	Left: Diagram of a single Josephson junction. A and B represent superconductors, and C the weak link between them. Right: Boundary conditions of the junction as described by equation (4.24).	49
4.3	Left: An experimental setup of ARPES. Right: ARPES measurements through the Fermi surface (c) of a film of Bi2212 showing the superconducting gaps defined by the dots in (a) and (b) [27].	52
4.4	Left: Idealized diagram of the spin and charge stripe pattern within a Ni ₂ plane observed in hole doped La ₂ Ni ₄ with the hole density of 25%. Right: Hypothesized stripe pattern in a copper-oxide plane of hole doped oxygen atoms, which surround the metal sites in a square planar array. Arrows indicate the orientation of magnetic moments on metal atoms, which are locally anti-parallel.	53
4.5	Temperature dependence of the distribution in local hole concentration Δx_{hole} as deduced by ⁶³ Cu nuclear quadrupole resonance in La _{2-x} Sr _x CuO ₄ [(▲) $x = 0.04$, (○) $x = 0.07$, (●) $x = 0.115$, (△) $x = 0.16$].	54
4.6	Measured $\Delta(\mathbf{r})$, gap maps, of four different hole dopings: (a) 89 K with $\rho = 0.19$; (b) 79 K with $\rho = 0.15$; (c) 75 K with $\rho = 0.13$; and (d) 65 K with $\rho = 0.11$ [33].	55
4.7	Electronic phase diagram for cuprates. The temperature $T_{\text{PS}}(\rho)$ marks the onset of phase separation into two main densities corresponding to the two minima of the Ginzburg-Landau potential. As the temperature decreases below $T_{\text{PS}}(\rho)$, the potential barrier E_g increases and the two minima $\pm A(T)/B$ separate from each other.	57

4.8	<p>Left: The charge density on a 105 x 105 square lattice system after 6400 time steps. The fraction $A(T)/B = 0.6$, which corresponds to values of T close to the line T_1 plotted in figure 4.7 – with $0.05 < \rho < 0.18$. The dark blue grains are in the verge of becoming insulators (low density) and the red ones have metallic character (high density). Right: Density profile of the local free energy in the same location and temperature as in the left figure. The red lines show the potential barrier between the grain boundaries. The system becomes a mixture of two disordered metals with high and low densities (DM1+DM2).</p>	58
5.1	<p>Left: The onset of the polar Kerr-effect signal T_s in circles and T_c as red squares for $\text{YBa}_2\text{Cu}_3\text{O}_{6+x}$ samples [52]. Right: The same behaviour is confirmed by zero field muon spin relaxation [44].</p>	61
5.2	<p>Josephson junction between two d-wave superconductors. The circles show the orientation of the crystal lattice and the pair wave function $\psi(\mathbf{k}) \propto \cos k_x - \cos k_y$ on both sides of the junction. This example corresponds to a π-junction.</p>	62
5.3	<p>A schematic example of a sequence of intermediate states for a Cooper pair tunnelling across a barrier that contains a spin up and leads to a negative coupling along the junction. Between steps c and d it is necessary to permute the two electrons to be in canonical order of a pair, and this exchange is responsible for the negative sign [45].</p>	64
5.4	<p>Superconducting loop with three π-junctions. If there were only two junctions, the system would manage to minimize the overall free energy and no current would arise. With an odd number of junctions (three in this case) the system is frustrated and the overall effect of one junction generates a spontaneous current around the loop.</p>	64
5.5	<p>The simplest model for a frustrated loop with a single junction.</p>	65
5.6	<p>The induced current in a frustrated loop for three values of the parameter γ_c as a function of the external flux. For the zero flux case $\Phi_{ex} = 0$, the figure shows that for $\gamma_c > 1$ a spontaneous current may arise while there is none for $\gamma_c < 1$.</p>	67
5.7	<p>The temperature evolution of $\Delta_{\delta,max}(\rho, T)$ of six different values of the average doping $\bar{\rho}$. The line at ≈ 40 meV shows the experimental onset of spontaneous magnetization and the intersections yield the temperature onset for different compounds.</p>	68

5.8 This dissertation's main result [17]: The calculated onset of spontaneous magnetization derived from the intersections in figure 5.7. The results from polar Kerr-effect are drawn as black squares, while muon spin relaxation is indicated by open circles. The line connecting the theoretical points is just a guide to the eye. The insets from left to right are respectively from polar Kerr-effect and muon spin relaxation. 69

Contents

1	Introduction	1
1.1	Historical background	1
1.2	The cuprates	3
1.3	Pseudogap and inhomogeneity	4
1.4	Ferromagnetic signal	5
1.5	Overview	5
2	Second quantization for fermions	7
2.1	Introductory remarks	7
2.2	Properties	7
2.2.1	Basic definitions	8
2.2.2	The anti-commutation relations for fermions	10
2.2.3	The number operator	11
2.3	Change of basis – field operators	11
2.4	Representation of operators	12
2.4.1	Additive one-body operator	12
2.4.2	Additive pair operator	14
2.5	A product of four Fermi operators	15
2.5.1	Wick’s theorem	15
2.5.2	The quadratic mean field approximation	16
2.6	Concluding remarks	18
3	Microscopic theory of superconductivity	19
3.1	Introductory remarks	19
3.2	BCS theory	19
3.2.1	The Cooper problem	19

3.2.2	The BCS Hamiltonian	23
3.2.3	The Bogoliubov transformation	25
3.2.4	The Bogoliubov equations	26
3.2.5	The ground state	27
3.2.6	Conjugate variables	29
3.2.7	Calculations at finite temperature	30
3.3	Intermission – d-wave superconductors	33
3.4	The Bogoliubov-deGennes formalism	34
3.4.1	The Hubbard model	35
3.4.2	The extended Hubbard Hamiltonian	36
3.4.3	Bogoliubov equations	38
3.4.4	The gaps and the electronic density	40
3.4.5	Numerical evaluation	41
3.5	Concluding remarks	43
4	Phenomenological theory of superconductivity	44
4.1	Introductory remarks	44
4.2	Ginzburg-Landau theory	44
4.2.1	The phenomenological parameters	45
4.2.2	The Ginzburg-Landau differential equations	46
4.2.3	Flux quantization	48
4.3	The Josephson Effect	49
4.3.1	Deriving the Josephson equations	50
4.4	Intermission – experimental survey	51
4.4.1	Evidence for the pseudogap from ARPES	51
4.4.2	Evidence for inhomogeneity	51
4.5	Theory of electronic phase separation	56
4.5.1	Cahn-Hilliard theory of phase separation	56
4.6	Concluding remarks	59
5	Ferromagnetism in high temperature superconductors	60
5.1	Introductory remarks	60
5.2	Paramagnetic effect in cuprates	61
5.3	Phase fluctuations	63
5.4	Spontaneous frustration	64
5.5	Doping and temperature dependence	67
5.6	Bogoliubov-deGennes calculations	67
5.7	Concluding remarks	69
6	Conclusion and perspectives	70

1.1 Historical background

Superconducting phenomena were discovered more than a century ago, in 1911 by the Dutch physicist Heike Kamerlingh Onnes. Below we list three major characteristics that define a superconductor in its context of discovery:

1. Kamerlingh noted that for certain metals, the electric resistance vanished abruptly below a critical temperature T_c , see figure 1.1;
2. Walther Meissner and Robert Ochsenfeld discovered in 1933 that a superconductor can behave as a perfect diamagnet (Meissner effect) when exposed to a magnetic field, see figure 1.1;
3. Pure superconductors have a gap in energy of width 2Δ centred about the Fermi energy in the set of allowed one-electron levels. This means that electrons form pairs, called Cooper pairs that are the basic current unit in superconductors, and one needs an energy Δ to extract an electron from a superconductor.

These three characteristics summarize the properties of a superconductor, which is much more than simply a perfect conductor. Also, superconductors are categorized into two types.

- Type 1: Those who expel an external magnetic field completely from the bulk;
- Type 2: Those who lock little vortices of magnetic strands into the bulk in a certain temperature range to minimize the overall free energy.

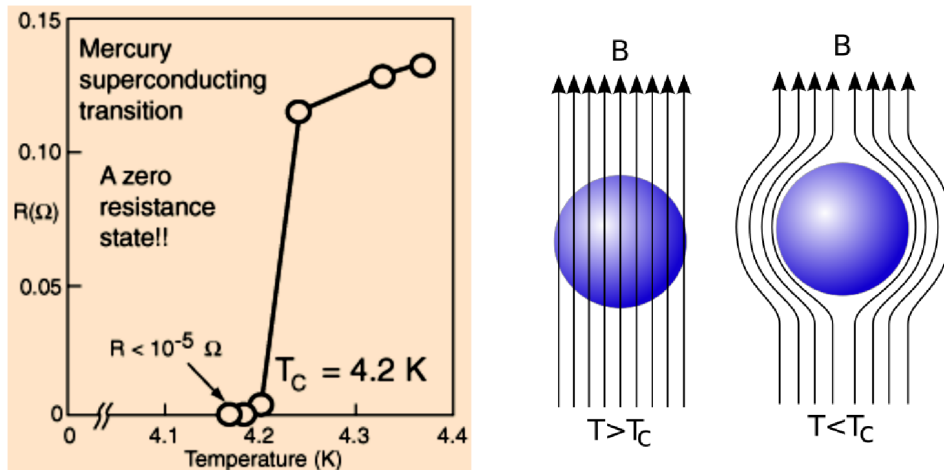


Figure 1.1: **Left:** As Onnes reduced the temperature of mercury, he saw an abrupt transition to zero resistance at 4.2 K. **Right:** Diagram of the Meissner effect. Magnetic field lines, represented as arrows, are excluded from a superconductor when it is below its critical temperature T_c .

Many theories emerged to describe this new state of matter. In 1935, the London brothers, Fritz and Heinz, developed an electromagnetic theory of superconductors. However, only in 1950, Vitaly Lazarevich Ginzburg and Lev Landau developed a successful phenomenological theory, which described the thermodynamics of the phase transition from the normal to the superconducting state. This guaranteed the Nobel prize of 1962 to Ginzburg. A fundamental microscopic theory of superconductivity arose in 1956, when Leon Cooper discovered that the basic mechanism for superconducting condensation consisted of pairing electrons with bound energy Δ . Due to him, these pairs are called Cooper pairs and account for the resistance free current. Finally, in 1957, John Bardeen, Leon Cooper and Robert Schrieffer (the BCS trio) presented a complete quantum mechanical theory of superconductivity able to describe conventional superconductors, which were the ones known by that time. This theory, BCS theory, was held as a triumph, because of the vast application it has. Until 1975, a variety of superconductors were discovered that BCS theory embraced well – this is referred to as the "classic" era of superconductivity. Classic superconductors are characterized by a number of common properties; below we list the most important ones:

1. The vast majority of classic superconductors have a transition temperature T_c below 25 K;
2. The normal state is described by Landau Fermi-liquid theory;
3. The superconducting phase transition is isolated from other phase transitions;
4. The order parameter is of the s-wave type (constant superconducting amplitude Δ);

5. Cooper pairs are formed by an attractive interaction resulting from the exchange of virtual phonons;
6. Crystal structure is simple.

Everything changed in 1986, when Johannes Georg Bednorz and Karl Alexander Müller discovered a new class of superconductors – the cuprates – that violate all of the six conditions above, with critical temperatures above the previous known superconductors. This inaugurated the quest in understanding the basic mechanism behind high- T_c superconductors, which BCS theory did not cover.

1.2 The cuprates

The discovery of the first high- T_c superconductor $\text{La}_{2-x}\text{Sr}_x\text{CuO}_4$, by Berdnorz and Müller [5], was of huge impact, not just because of the critical temperature of 32 K, but mainly because it was a group of materials that with zero doping ($x = 0$) are insulators and present anti-ferromagnetic order at low temperatures (see figure 1.2). In 1987, Chu et. al. synthesized a new cuprate $\text{YBa}_2\text{Cu}_3\text{O}_7$, which has a critical temperature of 94 K [51]. This was the first superconductor with a critical temperature beyond the barrier of liquid nitrogen (77K). For this reason, the compound $\text{YBa}_2\text{Cu}_3\text{O}_7$ gained increasing attention because of its technological implications. Since then, several families of cuprates were discovered; all characterized by cooper-oxide (CuO_2) crystal planes.

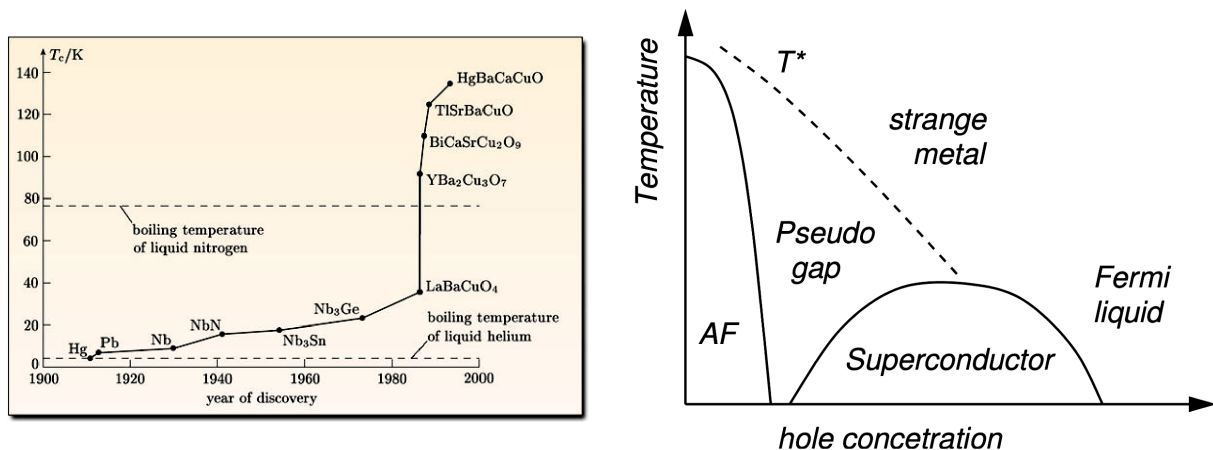


Figure 1.2: **Left:** Evolution of superconductors. **Right:** Schematic phase diagram of high- T_c superconductors, temperature versus hole doping concentration. The left AF region shows the anti-ferromagnetic region, the superconducting dome in the middle, with the crossover temperature T^* of the "normal" pseudogap phase.

With time it became evident that cuprates are more complex than expected. Differently from metallic conventional superconductors where the normal phase is described in terms of the properties of the Fermi liquid, the cuprates presents a normal phase with

new properties that remains a challenge for over 25 years. Simply put, the properties of the normal state: specific heat, magnetic susceptibility, electric resistivity, etc..., differ from a metal. Even due the increasing experimental techniques, the origin of superconductivity and the description of the basic properties is still an open problem. However, valuable knowledge about the cuprates was constructed over the past three decades. This knowledge is summarized below [31]:

- Superconductivity in the cuprates is due to formation of Cooper pairs;
- The main location of superconductivity in the cuprates is the CuO_2 planes;
- The order parameter is a spin singlet;
- The orbital symmetry of the order parameter is strongly suspected to be $d_{x^2-y^2}$;
- The formation of Cooper pairs takes place independently within different multilayers;
- The electron-phonon interaction is not the dominant mechanism of the formation of Cooper pairs.

1.3 Pseudogap and inhomogeneity

Beyond the different properties of cuprates, two completely new features were observed:

1. Unlike conventional superconductors where the gap is an exclusive property of the superconducting phase of matter, high- T_c superconductors present partial gapping above T_c ;
2. Inhomogeneous electronic distribution.

In conventional metallic superconductors, the superconducting gap amplitude $\Delta(T)$ is an exclusive feature of the superconducting phase of matter. However, in the cuprates, there also are local stable gaps above the critical temperature. This feature is referred to as partial gapping. In other words, an energy gap $\Delta(T > T_c)$ is observed in the supposed "normal" phase of cuprates, which caused great perplexity [47]. There is no clear vision of the nature of these local gaps. This partial (pseudo) gap appears at a temperature denoted by $T^*(x)$ and extends way above $T_c(x)$, see figure 1.2. One of the challenges is explaining the dome-like shape of the superconducting critical temperature versus the hole concentration. This continues as a major focus condensed matter physics. More thwarting is the lack of a thorough explanation of the "normal" state of high- T_c superconductors – the pseudogap phase.

In this dissertation we present a model of electronic phase separation, which is capable to explain many features of the mysterious pseudogap region. Our model relies essentially on the intrinsic electronic charge distribution in the cooper-oxide planes of cuprates. This is still a hot topic of debate. However, the inhomogeneous charge distribution was measured by several different experiments that indicate that the local densities of high- T_c superconductors is disordered, varying at nanoscales [7, 25]. This differs radically from a metal, where the charge distribution is uniform. Increasing evidence suggest that the inhomogeneity is intrinsic to cuprates, and is not related with impurities or crystallographic defects [49, 6, 43, 42, 37, 33, 22, 39, 12, 28, 24].

There is a general consensus that the unveiling of the nature the pseudogap region is crucial to the understanding of high- T_c superconductors. A reason for the lack of a widely accepted theory for the pseudogap is because of the intrinsic complexity of the electronic distribution of high- T_c superconductors. Such systems are not easily treated mathematically. Mathematical methods such as quantum field theory, present itself effective for homogeneous systems. Quantum field theory relies on simplifications, which wash out the existence of inhomogeneity – a crucial factor for treating high- T_c superconductors mathematically. An important issue about the pseudogap is whether the gaps measured in the normal state are evidence of a new state of matter, which therefore would compete with superconductivity. Here we adopt the thesis that the local gaps are superconducting in nature, announcing and abrupt phase transition to come.

1.4 Ferromagnetic signal

Among the many unexplained features of the pseudogap phase is the weak ferromagnetic signal observed in compounds such as $\text{YBa}_2\text{Cu}_3\text{O}_{6+x}$. The diamagnetic and paramagnetic characters of high- T_c superconductors are known, but the weak ferromagnetism lacks a theoretical explanation. This signal was measured by two independent experimental techniques [44, 52], which suggest that this weak magnetic signal might be related with the properties of the pseudogap. Therefore, understanding the underlining mechanism of this ferromagnetic signal should shed light on the nature of the pseudogap phase. This is the main issue addressed in this dissertation. *We suggest a new model for high- T_c superconductors to explain the weak ferromagnetic signal observed compounds such as $\text{YBa}_2\text{Cu}_3\text{O}_{6+x}$.*

1.5 Overview

This dissertation is organized in the following sequence: introduction, formalism, phenomenology, problem, conclusion. We would like to state that most of chapters 2 to 4 was developed with the aim to help to understand the aspects of the problem.

Chapter 2 sets the mathematical framework that is suitable for the quantum theory of superconductivity. We develop the properties of creation and annihilation operators that are adequate to describe collective systems. We limit ourselves to electrons, which will suffice. The fundamental anti-commutation relations are established. Furthermore, we show how to represent dynamical variables in this framework. Lastly, we introduce the approximation methods that will be convenient throughout this dissertation.

In chapter 3 we apply the formal framework to develop the microscopic (quantum) theory of superconductivity for both conventional metallic and unconventional cuprate superconductors. We open with the Cooper problem, which is a cornerstone for all superconducting phenomena. Then we develop the BCS theory in a suitable notation that can be naturally extended beyond the BCS framework. Fundamental concepts such as the superconducting ground state, the Bogoliubov equations, phase fluctuations, and the BCS equation are discussed. We switch to the formal framework of high- T_c superconductivity with a brief intermission on d-wave symmetry, in contrast to the conventional BCS s-wave symmetry. The extended Hubbard model is introduced, which is especially useful for strongly correlated electron systems. We develop and apply the formalism of Bogoliubov deGennes to the two dimensional copper-oxide lattice, which is responsible for the properties of cuprates, and permits us to determine the local gap $\Delta(i)$.

In chapter 4 we develop the essential elements of the elegant and powerful phenomenological theory of superconductivity developed by Ginzburg and Landau. The theory's main results that are relevant for this dissertation are presented, which includes: flux quantization, boundary conditions, and the Josephson (tunnelling) effect. Again, to make the transition of the phenomenological description of conventional to unconventional (cuprate) superconductors, we present an intermission surveying the most recent experimental data, which support our fundamental model of electronic phase separation. Then, we use the ideas of Ginzburg and Landau of their description of second order phase transition to construct our quantitative model of electronic phase separation, which is the basic background to solve our main problem.

With the background model laid, we attack our main problem in chapter 5 – the description of the weak ferromagnetic signal of high- T_c superconductors. The role of strong correlation effects due to phase fluctuations are discussed. We show that our system will behave as a network of frustrated π -junctions, which is the underlining mechanism responsible for the weak signal. This discussion finally integrates the phenomenological background model, the effects of spontaneous frustration with the formalism of Bogoliubov deGennes that will yield a theoretical confirmation to the experiments.

We conclude stating the most important result of our calculations presented in chapter 5 and we discuss some perspectives for future working using some of the concepts learned in this dissertation.

Second quantization for fermions

2.1 Introductory remarks

Here we deal only with fermions. Superconductivity is a cooperative phenomena between many fermions – the electrons. Therefore, before developing basic elements of the physics of superconductivity, we set a mathematical framework to describe fermionic systems (superconductors in our case). We need a formalism that focuses on just a few degrees of freedom, but treats the system’s total number of particles as a dynamical variable [3]. This because the number of electrons will vary at a critical temperature that marks the superconducting phase transition. Pascual Jordan and Eugene Wigner created our mathematical structure of interest - the formalism of creation and annihilation operators, also known as second quantization. This formalism permits mathematical manipulations with ease. It is nice because it keeps track of the anti-symmetrization requirement for fermions, which reads

$$\Psi(\mathbf{r}_2, \mathbf{r}_1) = -\Psi(\mathbf{r}_1, \mathbf{r}_2). \quad (2.1)$$

Second quantization is applicable both to fermions and bosons. However, we will restrict ourselves to fermions, because this is all we need. The name second quantization alludes to the fact that some operators will obey a Schrödinger-like equation. Let us start by looking at the space in which our states live.

2.2 Properties

The orthonormal basis vectors of Fock space can be summarized as follows:

- A single state with no particles in it $|0\rangle$;
- A complete set of one-particle vectors $\{|\alpha\rangle\}$;
- A complete set of two-particle state vectors $\{|\alpha\rangle \otimes |\beta\rangle\}$;
- A complete set of three-particle state vectors $\{|\alpha\rangle \otimes |\beta\rangle \otimes |\gamma\rangle\}$.

The numbers α , β and γ are any natural numbers that stand for all necessary quantum numbers to describe a certain state. Since all sets contain only fermions, they are complete in the anti-symmetric invariant subspace. Also note that Fock space is much larger than Hilbert space because it is the direct sum of all Hilbert spaces of each fermion. Now let us develop the basic properties of our formalism beginning with some basic definitions.

2.2.1 Basic definitions

We define a *creation operator* C_α^\dagger , that when acted upon a vector that does not contain the state $|\alpha\rangle$, will create it. In the most simple case

$$C_\alpha^\dagger|0\rangle = |\alpha\rangle. \quad (2.2)$$

The fact that C_α^\dagger is the hermitian adjoint of an other operator C_α is a convention. We say that C_α^\dagger occupies the α orbital of a quantum state. If C_α^\dagger acted upon the state with occupied β orbital, we would write

$$C_\alpha^\dagger|\beta\rangle = C_\alpha^\dagger C_\beta^\dagger|0\rangle = |\alpha\beta\rangle \stackrel{(2.1)}{=} -|\beta\alpha\rangle. \quad (2.3)$$

This last step is crucial and shows anti-symmetrization under interchange. We can continue inductively and write

$$C_\alpha^\dagger|\beta\gamma\rangle = C_\alpha^\dagger C_\beta^\dagger C_\gamma^\dagger|0\rangle = |\alpha\beta\gamma\rangle = -|\alpha\gamma\beta\rangle = |\gamma\alpha\beta\rangle. \quad (2.4)$$

For the sake of exercise, the normalized three-particle state $|\alpha\beta\gamma\rangle$ can be expressed as

$$|\alpha\beta\gamma\rangle = \frac{1}{\sqrt{6}} \left(|\alpha\rangle|\beta\rangle|\gamma\rangle - |\beta\rangle|\alpha\rangle|\gamma\rangle - |\alpha\rangle|\gamma\rangle|\beta\rangle - |\gamma\rangle|\beta\rangle|\alpha\rangle + |\gamma\rangle|\alpha\rangle|\beta\rangle + |\beta\rangle|\alpha\rangle|\gamma\rangle \right), \quad (2.5)$$

where $|\alpha\rangle|\beta\rangle|\gamma\rangle$ is an abbreviation for $|\alpha\rangle \otimes |\beta\rangle \otimes |\gamma\rangle$. In coordinate representation, where $\langle \mathbf{r} | \alpha \rangle = \phi_\alpha(\mathbf{r})$, a two-particle state vector reads

$$\langle \mathbf{r}_1, \mathbf{r}_2 | \alpha\beta \rangle = \frac{\phi_\alpha(\mathbf{r}_1)\phi_\beta(\mathbf{r}_2) - \phi_\beta(\mathbf{r}_1)\phi_\alpha(\mathbf{r}_2)}{\sqrt{2}} = \frac{1}{\sqrt{2}} \begin{vmatrix} \phi_\alpha(\mathbf{r}_1) & \phi_\beta(\mathbf{r}_1) \\ \phi_\alpha(\mathbf{r}_2) & \phi_\beta(\mathbf{r}_2) \end{vmatrix}, \quad (2.6)$$

where the last term was written in terms of the *slater determinant* for a two-particle state – which is especially useful to generalize to state vectors with more particles. The properties of the creation operator can be neatly written as

$$C_\alpha^\dagger|\mathcal{A}\rangle = |\alpha\mathcal{A}\rangle, \quad (2.7)$$

where \mathcal{A} stands for "anything", but it must be the same on both sides of the equation. We know from the Pauli exclusion principle that when C_α^\dagger acts on a vector with the α orbital occupied this must yield zero, because two identical states cannot occupy the same orbital. Indeed

$$C_\alpha^\dagger|\alpha\mathcal{A}\rangle = |\alpha\alpha\mathcal{A}\rangle \stackrel{(2.1)}{=} -|\alpha\alpha\mathcal{A}\rangle = 0. \quad (2.8)$$

Equations (2.7) and (2.8) fully define the creation operator, which enables us to deduce the properties of C_α that in advance will be called the annihilation operator. We introduce a notation to indicate a state with a specific orbital unoccupied. For instance, the vector $|\tilde{\alpha}\mathcal{A}\rangle$ is a generic state, but with the α orbital empty. The symbol tilde above the α stands for "not." Then we would have $C_\alpha^\dagger|\tilde{\alpha}\mathcal{A}\rangle = |\alpha\mathcal{A}\rangle$ and write

$$\begin{aligned} \langle\alpha\mathcal{A}|C_\alpha^\dagger|\tilde{\alpha}\mathcal{A}\rangle &= 1, \\ \langle\psi|C_\alpha^\dagger|\tilde{\alpha}\mathcal{A}\rangle &= 0, \quad \text{if } \langle\psi|\alpha\mathcal{A}\rangle = 0, \end{aligned} \quad (2.9)$$

where the state $|\psi\rangle$ is arbitrary, but different from $|\mathcal{A}\rangle$. From (2.7) we see that $\langle\alpha\mathcal{A}|C_\alpha = 0$, and in the same way we rewrite equations (2.9) as

$$\begin{aligned} \langle\tilde{\alpha}\mathcal{A}|C_\alpha|\alpha\mathcal{A}\rangle &= 1, \\ \langle\tilde{\alpha}\mathcal{A}|C_\alpha|\psi\rangle &= 0, \quad \text{if } \langle\psi|\alpha\mathcal{A}\rangle = 0. \end{aligned} \quad (2.10)$$

Obviously, if $\langle\alpha\mathcal{A}|C_\alpha = 0$ then

$$\langle\alpha\mathcal{A}|C_\alpha|\psi\rangle = 0. \quad (2.11)$$

Let us analyse the information that equations (2.10) and (2.11) contain for three relevant cases: $|\psi\rangle = |0\rangle$, $|\psi\rangle = |\alpha\rangle$ and $|\psi\rangle = |\tilde{\alpha}\mathcal{A}\rangle$ respectively.

If we take $|\psi\rangle = |0\rangle$, then the second equation of (2.10) tells us that $C_\alpha|0\rangle$ is orthogonal to any vector with the α orbital unoccupied. Simultaneously, equation (2.11) says that the very same vector $C_\alpha|0\rangle$ is also orthogonal to any state vector in which the α orbital is occupied. As an inevitable consequence, we must conclude that $C_\alpha|0\rangle = 0$.

The second interesting case to consider is the one in which $|\psi\rangle = |\alpha\rangle$. Equation (2.11) asserts that $C_\alpha|\alpha\rangle$ is orthogonal to any state vector in which the α orbital is filled. Nevertheless, the second equation of (2.10) shows us that $C_\alpha|\alpha\rangle$ is orthogonal to all vector with unoccupied α orbital – except one, which is $\langle 0|C_\alpha|\alpha\rangle = 1$ – according to the first

equation of (2.10). It is imminent that $C_\alpha|\alpha\rangle = 0$. By means of a similar argument one shows that $C_\alpha|\alpha\mathcal{A}\rangle = |\tilde{\alpha}\mathcal{A}\rangle$.

The last relevant case, $|\psi\rangle = |\tilde{\alpha}\mathcal{A}\rangle$, in the same line of reasoning gives us $C_\alpha|\tilde{\alpha}\mathcal{A}\rangle = 0$. Hence, C_α destroys the vector if the α orbital is occupied, and empties the α orbital if it is occupied. Now the name annihilation operator is justified.

To summarize, the creation operator C_α^\dagger adds a fermion to the α orbital if it is empty. Its hermitian adjoint, the annihilation operator C_α , removes a fermion from the α orbital if it is occupied; otherwise, these operators yield zero.

2.2.2 The anti-commutation relations for fermions

It should be easy to see from (2.4) that the anti-commutator $\{C_\alpha^\dagger, C_\beta^\dagger\}|0\rangle = 0$. Now we are able to extend the application of the anti-commutator on $|0\rangle$ to a completely general state $|\psi\rangle$. We can see from (2.8) that $C_\alpha^\dagger C_\alpha^\dagger|\psi\rangle = 0$. Since $|\psi\rangle$ is arbitrary we safely write $C_\alpha^\dagger C_\alpha^\dagger = 0$, and consequently $C_\alpha C_\alpha = 0$. Now it is interesting to consider $\{C_\alpha^\dagger, C_\beta^\dagger\}|\psi\rangle$, because it will summarize some of the properties of these operators. We have

$$\left(C_\alpha^\dagger C_\beta^\dagger + C_\beta^\dagger C_\alpha^\dagger\right)|\psi\rangle = |\alpha\beta\psi\rangle + |\beta\alpha\psi\rangle = |\alpha\beta\psi\rangle - |\alpha\beta\psi\rangle = 0. \quad (2.12)$$

This leads to

$$\{C_\alpha^\dagger, C_\beta^\dagger\} = 0 \quad \text{and} \quad \{C_\alpha, C_\beta\} = 0, \quad (2.13)$$

which are the first two anti-commutation relations. At last, we inspect the last case $\{C_\alpha, C_\beta^\dagger\}$ involving a creation and an annihilation operator. We will examine the cases $\alpha = \beta$ and $\alpha \neq \beta$ separately. For $\alpha = \beta$ we must separate the analysis in two cases, one where $|\psi\rangle = |\alpha\mathcal{A}\rangle$ and another with $|\psi\rangle = |\tilde{\alpha}\mathcal{A}\rangle$:

- $(C_\alpha C_\alpha^\dagger + C_\alpha^\dagger C_\alpha)|\alpha\mathcal{A}\rangle = 0 + C_\alpha^\dagger|\tilde{\alpha}\mathcal{A}\rangle = |\alpha\mathcal{A}\rangle$;
- $(C_\alpha C_\alpha^\dagger + C_\alpha^\dagger C_\alpha)|\tilde{\alpha}\mathcal{A}\rangle = C_\alpha|\alpha\mathcal{A}\rangle + 0 = |\tilde{\alpha}\mathcal{A}\rangle$.

It is clear that $\{C_\alpha, C_\alpha^\dagger\} = I$, where I is the identity matrix. From our previous result (2.13) it is apparent that $\{C_\alpha, C_\beta^\dagger\}$ will yield zero if either the α orbital is empty or the β orbital is occupied. Thus, it is only necessary to examine its effect on $|\alpha\tilde{\beta}\mathcal{A}\rangle$. In our notation, it is not important where to place $\tilde{\alpha}$ in the argument of $|\ \rangle$, because the orbital is unoccupied. However, special attention must be given to the order of an occupied orbital in $|\ \rangle$. This observation is important for the following manipulations. We have

$$\begin{aligned}
(C_\alpha C_\beta^\dagger + C_\beta^\dagger C_\alpha) |\alpha\tilde{\beta}\mathcal{A}\rangle &= C_\alpha |\beta\alpha\mathcal{A}\rangle + C_\beta^\dagger |\tilde{\alpha}\tilde{\beta}\mathcal{A}\rangle \\
&= -C_\alpha |\alpha\beta\mathcal{A}\rangle + C_\beta^\dagger |\tilde{\alpha}\tilde{\beta}\mathcal{A}\rangle \\
&= -|\tilde{\alpha}\beta\mathcal{A}\rangle + |\tilde{\alpha}\beta\mathcal{A}\rangle = 0.
\end{aligned}$$

Both cases are summarized by the equation

$$\{C_\alpha, C_\beta^\dagger\} = \delta_{\alpha\beta} I. \quad (2.14)$$

Equations (2.13) and (2.14) constitute the anti-commutation relations for fermions and they contain all necessary information about this formalism for fermions.

2.2.3 The number operator

At last, note that all vectors in Fock space are eigenvectors of the operator $C_\alpha^\dagger C_\alpha$. If acted on $|\tilde{\alpha}\mathcal{A}\rangle$ the eigenvalue is zero; and if acted on $|\alpha\mathcal{A}\rangle$ the eigenvalue is one. For this reason, it is quite intuitive to call $C_\alpha^\dagger C_\alpha$ the number operator for the α orbital. The total number operator is equal to

$$N = \sum_\alpha C_\alpha^\dagger C_\alpha. \quad (2.15)$$

One could ask why we did not define the number operator N as $C_\alpha C_\alpha^\dagger$. As we know, there are zero particles in the vacuum state $|0\rangle$, which would not be the case with $C_\alpha C_\alpha^\dagger$ as the number operator.

2.3 Change of basis – field operators

Until now we have defined our creation and annihilation operators with respect to a particular set of discrete one-particle state vectors $|\alpha\rangle = C_\alpha^\dagger |0\rangle$. Sometimes it is much more convenient to use other state vectors as basis. Let us consider an important case. Instead of considering operators that create "discrete" one-particle states as C_α^\dagger does, let us see what happens with a continuous case; that is, the family of operators $\psi^\dagger(\mathbf{r})$ that create position eigenvectors $|\mathbf{r}\rangle$. The new creation operator $\psi^\dagger(\mathbf{r})$ creates the position state vector $|\mathbf{r}\rangle$ at position \mathbf{r} in ordinary configuration space. For this reason the operators ψ are called field operators. These operators should not be confused with the wavefunction.

We want to perform the following change of basis

$$|\alpha\rangle = C_\alpha^\dagger |0\rangle \quad \longrightarrow \quad |\mathbf{r}\rangle = \psi^\dagger(\mathbf{r}) |0\rangle. \quad (2.16)$$

We change from a discrete base $|\alpha\rangle$ to a continuous one $|\mathbf{r}\rangle$. Let us relate the two bases. Since both bases span Fock space, we can express $|\mathbf{r}\rangle$ as a linear combination of the $|\alpha\rangle$ in the usual way as

$$|\mathbf{r}\rangle = \sum_{\alpha} \langle \alpha | \mathbf{r} \rangle |\alpha\rangle \quad \Rightarrow \quad \psi^{\dagger}(\mathbf{r})|0\rangle = \sum_{\alpha} \langle \alpha | \mathbf{r} \rangle C_{\alpha}^{\dagger}|0\rangle. \quad (2.17)$$

From here we can write the new operators as linear combinations of the old ones

$$\psi^{\dagger}(\mathbf{r}) = \sum_{\alpha} \langle \alpha | \mathbf{r} \rangle C_{\alpha}^{\dagger}; \quad \psi(\mathbf{r}) = \sum_{\alpha} \langle \mathbf{r} | \alpha \rangle C_{\alpha}. \quad (2.18)$$

In condensed matter applications the coefficients $\langle \mathbf{r} | \alpha \rangle$ are usually assumed to be Block waves. The new operators (2.18) must also obey the fermi anti-commutation relations (2.13) and (2.14), since these characterize the essential properties of creation and annihilation operators. They read

$$\{\psi^{\dagger}(\mathbf{r}), \psi^{\dagger}(\mathbf{r}')\} = 0 \quad (2.19a)$$

$$\{\psi(\mathbf{r}), \psi(\mathbf{r}')\} = 0 \quad (2.19b)$$

$$\{\psi(\mathbf{r}), \psi^{\dagger}(\mathbf{r}')\} = \delta(\mathbf{r} - \mathbf{r}') I. \quad (2.19c)$$

In analogy to the number operator in the discrete case, $\psi^{\dagger}(\mathbf{r})\psi(\mathbf{r})$ is the *number density operator*. The total number operator (2.15) is equal to

$$N = \int d\mathbf{r} \psi^{\dagger}(\mathbf{r})\psi(\mathbf{r}), \quad (2.20)$$

where $d\mathbf{r}$ is a volume element and should not be confused with a line element.

2.4 Representation of operators

Let us see how dynamical variables are represented in second quantized form.

2.4.1 Additive one-body operator

Our states are expressed utilizing creation and annihilation operators. Accordingly, the representation of our dynamic variables, such as momentum, kinetic energy, potential, the Hamiltonian, etc., also must involve creation and annihilation operators. Some would say that these operators must undergo second quantization. The simplest operator representations in our formalism will be those who are additive over each particle. For instance, in the conventional Schrödinger treatment, the kinetic energy is expressed as

$$K = -\frac{\hbar^2}{2m} \sum_{i=1}^n \nabla_i^2. \quad (2.21)$$

Each element of this sum acts only on a single particle, which means that each particle is labelled with an index i . Nonetheless, one of the foundational aspects of the formalism of second quantization is that there is absolutely no significance in labelling the particles – they are identical. We need an operator representation that does not tag particles, and does not depend on particle number. In particular for the kinetic energy, the following form covers both requirements:

$$K = -\frac{\hbar^2}{2m} \sum_{\alpha} \sum_{\beta} \langle \alpha | \nabla^2 | \beta \rangle C_{\alpha}^{\dagger} C_{\beta}. \quad (2.22)$$

Let us show that the conventional Schrödinger kinetic energy (2.21) operator is equivalent to the second quantized kinetic energy (2.22). First, we have to confirm that K in second quantized form is invariant under change of basis. Writing K in another basis we have

$$K' = -\frac{\hbar^2}{2m} \sum_j \sum_k \langle j | \nabla^2 | k \rangle \gamma_j^{\dagger} \gamma_k. \quad (2.23)$$

Transforming the γ 's similar to (2.18), but now for discrete operators, we have

$$K' = -\frac{\hbar^2}{2m} \sum_{\alpha} \sum_{\beta} \sum_j \sum_k \langle \alpha | j \rangle \langle j | \nabla^2 | k \rangle \langle k | \beta \rangle C_{\alpha}^{\dagger} C_{\beta}. \quad (2.24)$$

Here, the completeness relations $\sum |i\rangle\langle i|$ are explicit. Using them we get

$$K' = -\frac{\hbar^2}{2m} \sum_{\alpha} \sum_{\beta} \langle \alpha | \nabla^2 | \beta \rangle C_{\alpha}^{\dagger} C_{\beta} = K. \quad (2.25)$$

We have used the kinetic energy to illustrate the invariance under change of basis of an additive operator. Our illustration is valid for any general operator that sums over individual particles. We can choose any convenient basis to demonstrate the equivalency between the Schrödinger form and the second quantized one. Have us choose the basis vectors $\{|i\rangle\}$ with associated creation and annihilation operators b to diagonalize the single particle operator ∇^2 : $\nabla^2|i\rangle = k_i^2|i\rangle$, which from (2.22) yields

$$K = -\frac{\hbar^2}{2m} \sum_i k_i^2 b_i^{\dagger} b_i = -\frac{\hbar^2}{2m} \sum_i k_i^2 n_i, \quad (2.26)$$

where n_i is the occupancy of the i orbital. This is clearly in agreement with the matrix elements of (2.21) provided that $\sum_i n_i = N$ is finite. We have chosen the kinetic energy operator as an additive one-body operator to represent it in second quantized form (2.22).

The same is valid for any generic additive one-body operator $R = \sum_i R_i$ in ordinary representation. Thus, any general additive one-body operator has

$$R = \sum_{\alpha} \sum_{\beta} \langle \alpha | R_1 | \beta \rangle C_{\alpha}^{\dagger} C_{\beta}, \quad (2.27)$$

as its second quantized form.

2.4.2 Additive pair operator

There is another kind of operator that must be considered. The most important one is the interaction potential V , which is an *additive pair operator*. In ordinary representation such a pair operator reads generically

$$V = \frac{1}{2} \sum_i \sum_{\substack{j \\ i \neq j}} v(\mathbf{r}_i, \mathbf{r}_j). \quad (2.28)$$

In terms of creation and annihilation operators we suggest

$$V = \frac{1}{4} \sum_{\alpha} \sum_{\beta} \sum_{\gamma} \sum_{\delta} \langle \alpha\beta | v | \gamma\delta \rangle C_{\alpha}^{\dagger} C_{\beta}^{\dagger} C_{\delta} C_{\gamma}. \quad (2.29)$$

In order to show that (2.29) is equivalent to (2.28) we choose a representation that diagonalizes $\langle \alpha\beta | v | \gamma\delta \rangle$, so that $\langle \alpha\beta | v | \gamma\delta \rangle = \langle \alpha\beta | v | \alpha\beta \rangle \delta_{\alpha\beta, \gamma\delta}$, where we have introduced a variant of the Kroenecker delta with the property that $\langle \alpha\beta | v | \alpha\beta \rangle \delta_{\alpha\beta, \gamma\delta} = 1$ only if $|\alpha\beta\rangle$ and $|\gamma\delta\rangle$ describe the same state. Taking this into consideration we write

$$\begin{aligned} V &= \frac{1}{4} \sum_{\alpha, \beta} \left[\langle \alpha\beta | v | \alpha\beta \rangle C_{\alpha}^{\dagger} C_{\beta}^{\dagger} C_{\beta} C_{\alpha} + \langle \alpha\beta | v | \beta\alpha \rangle C_{\alpha}^{\dagger} C_{\beta}^{\dagger} C_{\alpha} C_{\beta} \right] \\ &= \frac{1}{2} \sum_{\alpha, \beta} \langle \alpha\beta | v | \alpha\beta \rangle C_{\alpha}^{\dagger} C_{\alpha} C_{\beta}^{\dagger} C_{\beta}. \end{aligned} \quad (2.30)$$

This is the second quantized form of (2.28) and will be used extensively throughout this work.

2.5 A product of four Fermi operators

Such products are frequent and there are a variety of techniques to address them. This section is devoted to establish the means by which a product of four Fermi operators will be treated here.

2.5.1 Wick's theorem

A product of four (or more) creation/annihilation operators as found in the interaction potential (2.29) is difficult to handle. In this section we present a theorem due to Wick, that simplifies such products considerably. We show Wick's Theorem only for products of two and four operators, because this is all we need. It can be extended to a general product of operators which is essential in quantum field theory and developing Feynman diagrams.

Let us begin stating Wick's Theorem for two operators and subsequently explain it. The product of two operators A and B can be written as

$$AB = N(AB) + \langle AB \rangle, \quad (2.31)$$

where $N(AB)$ is the *normal product* of the operators A and B and $\langle AB \rangle$ is the expectation value of AB calculated in the ground state $|G\rangle$, which in this case is $|0\rangle$. The normal product of a product of creation and annihilation operators puts the creation operators to the left of the annihilation operators, multiplying by a factor (-1) for every pair interchange for fermions. For instance, $N(C_\alpha C_\alpha^\dagger) = -C_\alpha^\dagger C_\alpha$. Also, the expectation value in the ground state $\langle AB \rangle$, in this case the vacuum matrix element $\langle 0|AB|0\rangle$, is generally called a *contraction*. As we will see, this nomenclature suits Wick's Theorem's context. One can verify that with $|G\rangle = |0\rangle$, the only non-zero contraction involves a creation and an annihilation operator.

We state Wick's Theorem in words and then show it for the statement (2.31). Wick's Theorem for fermi operators says that:

A product of a finite number of fermi operators can be written as the sum of the normal products from which 0,1,2,3... contractions have been removed in all possible ways.

In equation (2.31) we wrote the normal product $N(AB)$ and then removed the only possible contraction $\langle AB \rangle$. Note that $\langle N(\mathcal{A}) \rangle = 0$, which reflects that the only non-zero contraction is $\langle CC^\dagger \rangle$. For the cases in which AB is of the type CC or $C^\dagger C^\dagger$, the validity of (2.31) is easy to see. The less obvious case is the one in which AB is of the type CC^\dagger . To see that this case satisfies (2.31) we may write $CC^\dagger = \{C, C^\dagger\} - C^\dagger C$. The effect of

$\{C, C^\dagger\}$ over a state is the same as $\langle CC^\dagger \rangle$, because

$$\{C, C^\dagger\} |\psi\rangle = I|\psi\rangle = \langle 0|CC^\dagger|0\rangle. \quad (2.32)$$

Therefore we have shown the validity of (2.31). According to Wick's Theorem stated above, a product of four fermion operators would yield:

$$\begin{aligned} ABCD &= + \overbrace{N(ABCD)}^{\text{no contraction}} \\ &+ N(AB)\langle CD \rangle - N(AC)\langle BD \rangle + N(AD)\langle BC \rangle \\ &+ N(BC)\langle AD \rangle - N(BD)\langle AC \rangle + N(CD)\langle AB \rangle \\ &+ \langle AB \rangle \langle CD \rangle - \langle AC \rangle \langle BD \rangle + \langle AD \rangle \langle BC \rangle. \end{aligned} \quad (2.33)$$

An immediate corollary of this is

$$\langle ABCD \rangle = \langle AB \rangle \langle CD \rangle - \langle AC \rangle \langle BD \rangle + \langle AD \rangle \langle BC \rangle, \quad (2.34)$$

which often is also referred to as Wick's theorem. It is of utter importance to have in mind that Wick's theorem is defined with respect to a particular ground state, which in this section is $|0\rangle$. However, we could have chosen any suitable state that we would have wanted.

2.5.2 The quadratic mean field approximation

Another useful way to deal with a product of four fermion operators is the mean field approach. The main disadvantage with respect to Wick's theorem is that it is not exact. On the other hand, it is much simpler and more convenient in certain contexts. In fact, throughout the literature, this is the preferred approach [32, 18]. The mean field approach writes the product of two fermion operators as

$$AB = \langle AB \rangle + \overbrace{(AB - \langle AB \rangle)}^{\delta}, \quad (2.35)$$

where δ is supposed to be small and terms of order $\mathcal{O}(\delta^2)$ will be neglected. At first this can seem strange since $\langle AB \rangle$ is a number and AB is not. However, what we are saying is that when δ acts on a state of interest, its effect will be negligible. The expectation values $\langle \rangle$ are taken with respect to any preferred state. This provides an advantage over Wick's theorem, because the latter is useful for the expectation values taken with respect

to $|G\rangle$. Therefore, we can write a product of four fermi operators as

$$\begin{aligned} ABCD &= [\langle AB \rangle + (AB - \langle AB \rangle)] [\langle CD \rangle + (CD - \langle CD \rangle)] \\ &= \langle AB \rangle CD + \langle CD \rangle AB - \langle AB \rangle \langle CD \rangle + \delta^2. \end{aligned} \quad (2.36)$$

When $ABCD$ is part of the Hamiltonian, as is the case for the interaction potential, then the constant term $\langle AB \rangle \langle CD \rangle$ will not contribute to the dynamics of the Hamiltonian. However, it would contribute to expectation values; but in such a case it would be much more interesting to use Wick's theorem's corollary (2.34). For this reason, the mean field approximation[2] is mostly encountered as [36]

$$ABCD \longrightarrow \langle AB \rangle CD + \langle CD \rangle AB, \quad (2.37)$$

which is clearly simpler than Wick's theorem (2.33).

Particular case: The interaction potential

Let us analyse a particular case of interest. Generally, the interaction potential has the form $c_\alpha^\dagger c_\alpha c_\beta^\dagger c_\beta$, or equivalently $c_\alpha^\dagger c_\beta^\dagger c_\beta c_\alpha$ and $-c_\alpha^\dagger c_\beta^\dagger c_\alpha c_\beta$. Therefore, according to the mean field approximation (2.37) we could have the following cases

$$c_\alpha^\dagger c_\alpha c_\beta^\dagger c_\beta \rightarrow \begin{cases} \langle c_\alpha^\dagger c_\alpha \rangle c_\beta^\dagger c_\beta + \langle c_\beta^\dagger c_\beta \rangle c_\alpha^\dagger c_\alpha \\ \langle c_\alpha^\dagger c_\beta^\dagger \rangle c_\beta c_\alpha + \langle c_\beta c_\alpha \rangle c_\alpha^\dagger c_\beta^\dagger \\ -\langle c_\alpha^\dagger c_\beta^\dagger \rangle c_\alpha c_\beta - \langle c_\alpha c_\beta \rangle c_\alpha^\dagger c_\beta^\dagger \end{cases}$$

which could be written as

$$\begin{aligned} 3c_\alpha^\dagger c_\alpha c_\beta^\dagger c_\beta &= + \langle c_\alpha^\dagger c_\alpha \rangle c_\beta^\dagger c_\beta + \langle c_\beta^\dagger c_\beta \rangle c_\alpha^\dagger c_\alpha + \langle c_\alpha^\dagger c_\beta^\dagger \rangle c_\beta c_\alpha \\ &\quad + \langle c_\beta c_\alpha \rangle c_\alpha^\dagger c_\beta^\dagger - \langle c_\alpha^\dagger c_\beta^\dagger \rangle c_\alpha c_\beta - \langle c_\alpha c_\beta \rangle c_\alpha^\dagger c_\beta^\dagger. \end{aligned} \quad (2.38)$$

These two lines are part of (2.33), but with no normal ordering and is sometimes called the Hartree-Fock-Bogoliubov[53] approximation. Furthermore, if $\alpha \neq \beta$, then we can rewrite this neatly as

$$N_\alpha N_\beta = \frac{1}{3} \left(\langle N_\alpha \rangle N_\beta + \langle N_\beta \rangle N_\alpha + 2 \langle c_\alpha^\dagger c_\beta^\dagger \rangle c_\beta c_\alpha + 2 \langle c_\beta c_\alpha \rangle c_\alpha^\dagger c_\beta^\dagger \right). \quad (2.39)$$

The question is then, which approximation should we use? According to Annett[2], we use the approximation that contains the terms responsible for the physics of interest. In advance for the case of Cooper pairing, the amplitude of interest is $\langle c_\alpha^\dagger c_\beta^\dagger \rangle$, because it describes the formation of a pairs of electrons. The other "uninteresting" amplitudes, such as $\langle c_\alpha^\dagger c_\alpha \rangle$ are not included because they are part of the physics of the normal state. Since we are studying specific properties of the superconducting state, we drop such terms.

2.6 Concluding remarks

In this chapter we have developed a mathematical method called second quantization suitable to treat quantum mechanical systems with many particles. This method does not label particles, which guarantees that all particles involved are indistinguishable. At the same time it incorporates the anti-symmetrization postulate for fermions into the two basic anti-commutation relations that summarize all properties of creation and annihilation operators. We showed how to represent operators in this formalism and presented some useful methods approximations that can be used to treat a product of four Fermi operators.

Microscopic theory of superconductivity

3.1 Introductory remarks

In this chapter we present well established aspects of the theory of superconductivity that are relevant for this dissertation. We begin with the foundational aspects of BCS theory that describe successfully conventional superconductors. The acronym BCS refers to Bardeen, Cooper and Schrieffer, which are the ones who submitted a first coherent explanation of superconductivity [26]. First, we discuss the Cooper Problem – a cornerstone in the theory of superconductivity. With this ground laid, we develop the most important elements of uniform superconductivity (BCS theory) in a language and notation that is easily extended to the formalism of nonuniform superconductivity – the self-consistent mean field method of Bogoliubov-deGennes. We transition from conventional to unconventional superconductivity with an intermission on d-wave symmetry. Finally, we introduce the extended Hubbard model, which is almost regarded as the ”standard model” for strongly correlated electron systems. This model is suitable to study the evolution of superconductivity in a plane. Computational simulation will give us the relevant parameters of the microscopic theory: the d-wave gap Δ_δ and hole concentration ρ in the copper-oxide planes.

3.2 BCS theory

3.2.1 The Cooper problem

Leon Cooper addressed the problem of considering two electrons with momenta \mathbf{k}_1 and \mathbf{k}_2 above a filled Fermi sea up to k_F [10]. Cooper’s calculation showed that these two electrons

present a bound state (the Cooper pair) in the presence of an arbitrarily weak attractive potential. In the superconducting condensate, this attractive potential is provided by the electron-phonon interaction, and can be reviewed for instance in Taylor [46]. In our discussion, however, the nature of the attractive potential will not be explicit, but rather postulated. Our discussion follows closely references [13, 29]. In order to describe the two electrons at positions \mathbf{r}_1 and \mathbf{r}_2 , Cooper proposed the time independent wavefunction

$$\psi(\mathbf{r}_1, \sigma_1, \mathbf{r}_2, \sigma_2) = \phi(\mathbf{r}_1 - \mathbf{r}_2) e^{i\mathbf{k}_{cm} \cdot \mathbf{R}_{cm}} |\chi(\sigma_1, \sigma_2)\rangle, \quad (3.1)$$

where $\phi(\mathbf{r}_1 - \mathbf{r}_2)$ is the wave-packet embodying the two electrons, \mathbf{k}_{cm} and \mathbf{R}_{cm} are the momenta and position of the center of mass representing the wave-packet, and the spin wavefunction $|\chi\rangle$. These three parts allow three simplifications:

1. We expand $\phi(\mathbf{r}_1 - \mathbf{r}_2)$ in terms of Bloch waves;
2. The minimum energy will correspond to a pair of electrons with $\mathbf{k}_{cm} = 0$;
3. And lastly, we assume for the sake of simplicity that the spin wavefunction is in the singlet state $|\chi\rangle = \frac{1}{\sqrt{2}}(|\uparrow\downarrow\rangle - |\downarrow\uparrow\rangle)$. (This is indeed the case of most conventional metallic superconductors.)

With this in mind, Fermion antisymmetry implies that $\psi(\mathbf{r}_1, \mathbf{r}_2) = -\psi(\mathbf{r}_2, \mathbf{r}_1)$ and hence $\phi(\mathbf{r}_1 - \mathbf{r}_2) = \phi(\mathbf{r}_2 - \mathbf{r}_1)$. Therefore, we rewrite (3.1) as

$$\psi(\mathbf{r}_1, \mathbf{r}_2) = \overbrace{\sum_{\mathbf{k}} g(\mathbf{k}) e^{i\mathbf{k} \cdot (\mathbf{r}_1 - \mathbf{r}_2)}}^{\phi(\mathbf{r}_1 - \mathbf{r}_2)}, \quad \text{with } g(\mathbf{k}) = g(-\mathbf{k}). \quad (3.2)$$

Since both electrons hover above the Fermi level, the energy of the electron at $\mathbf{r}_{1(2)}$ is $E_{1(2)} = \frac{\hbar^2 k_F^2}{2m} + \epsilon_{1(2)}$, where $\epsilon_{1(2)}$ is the electron's energy above the Fermi surface. With this, in advance, we define the bound state energy $\epsilon = \epsilon_1 + \epsilon_2$, which will turn out to be negative. Now we write the Schrödinger equation for (3.2) assuming translational invariance for the potential, that is $V(\mathbf{r}_1, \mathbf{r}_2) = V(\mathbf{r}_1 - \mathbf{r}_2)$, in the same way we have for $\phi(\mathbf{r}_1 - \mathbf{r}_2)$. This gives

$$\left[-\frac{\hbar^2}{2m} (\nabla_{\mathbf{r}_1}^2 + \nabla_{\mathbf{r}_2}^2) + V(\mathbf{r}_1 - \mathbf{r}_2) \right] \psi(\mathbf{r}_1, \mathbf{r}_2) = \left(\epsilon + 2 \frac{\hbar^2 k_F^2}{2m} \right) \psi(\mathbf{r}_1, \mathbf{r}_2). \quad (3.3)$$

In this equation we explicitly wrote the bound state energy ϵ because this is the quantity that we are ultimately interested in. We substitute the simplified wavefunction (3.2) into (3.3) to obtain

$$\sum_{\mathbf{k}} \left[\frac{\hbar^2}{m} k^2 + V \right] g(\mathbf{k}) e^{i\mathbf{k} \cdot (\mathbf{r}_1 - \mathbf{r}_2)} = \left(\epsilon + \frac{\hbar^2 k_F^2}{m} \right) \sum_{\mathbf{k}} g(\mathbf{k}) e^{i\mathbf{k} \cdot (\mathbf{r}_1 - \mathbf{r}_2)}. \quad (3.4)$$

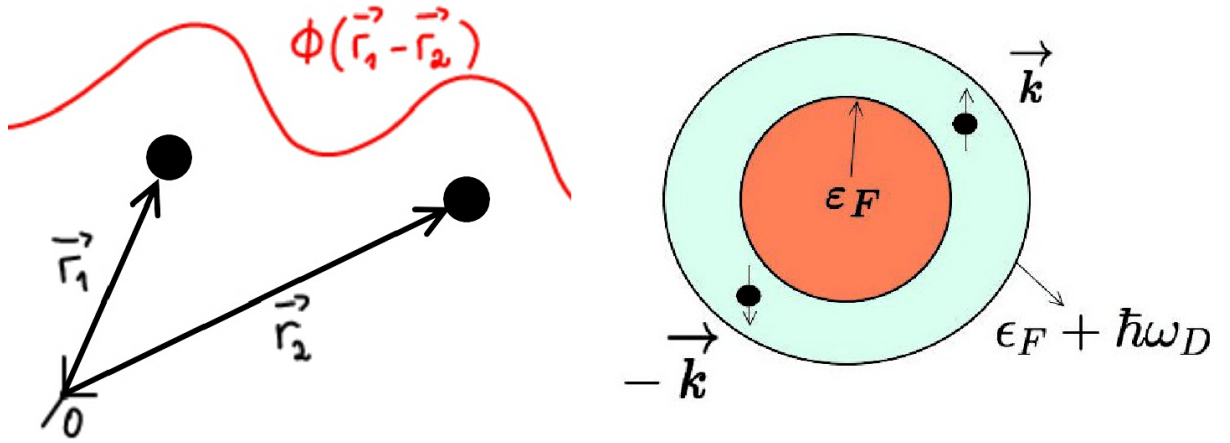


Figure 3.1: **Left:** The wave packet $\phi(\mathbf{r}_1 - \mathbf{r}_2)$ embodying the two electrons at \mathbf{r}_1 and \mathbf{r}_2 , with energies ϵ_1 and ϵ_2 above the Fermi level ϵ_F . **Right:** The Cooper problem: two electrons outside a fully occupied Fermi sea, but restricted to a band $\hbar\omega_D$ due to the attractive potential provided by the electron-phonon interaction.

The form of the exponentials suggest that we can simplify this substantially using the exponential definition of the delta function. Carrying on with this idea we multiply this equation by $e^{-i\mathbf{k}'\cdot(\mathbf{r}_1-\mathbf{r}_2)}$ and integrate over $d(\mathbf{r}_1 - \mathbf{r}_2)$ to obtain

$$\begin{aligned}
\frac{\hbar^2}{m} \sum_{\mathbf{k}} k^2 g(\mathbf{k}) \int d(\mathbf{r}_1 - \mathbf{r}_2) \overbrace{e^{i(\mathbf{k}-\mathbf{k}')\cdot(\mathbf{r}_1-\mathbf{r}_2)}}^{L^3 \delta_{\mathbf{k}\mathbf{k}'}} \\
+ \sum_{\mathbf{k}} g(\mathbf{k}) \int d(\mathbf{r}_1 - \mathbf{r}_2) \overbrace{V(\mathbf{r}_1 - \mathbf{r}_2) e^{i(\mathbf{k}-\mathbf{k}')\cdot(\mathbf{r}_1-\mathbf{r}_2)}}^{V_{\mathbf{k}\mathbf{k}'}} \\
= \left(\epsilon + \frac{\hbar^2 k_F^2}{m} \right) \sum_{\mathbf{k}} g(\mathbf{k}) \int d(\mathbf{r}_1 - \mathbf{r}_2) \overbrace{e^{i(\mathbf{k}-\mathbf{k}')\cdot(\mathbf{r}_1-\mathbf{r}_2)}}^{L^3 \delta_{\mathbf{k}\mathbf{k}'}}. \quad (3.5)
\end{aligned}$$

Here we have introduced the quantity $V_{\mathbf{k}\mathbf{k}'}$. This big equation simplifies to

$$\frac{\hbar^2}{m} k^2 g(\mathbf{k}) + \sum_{\mathbf{k}'} g(\mathbf{k}') V_{\mathbf{k}\mathbf{k}'} = (\epsilon + 2\epsilon_F) g(\mathbf{k}), \quad (3.6)$$

which is known as the Bethe-Goldstone equation for the two-electron problem. Also remember that $g(\mathbf{k}) = 0$ for $k < k_F$. It is not easy to treat this problem for general $V_{\mathbf{k}\mathbf{k}'}$. Because of this, let us continue in our journey of the art of mathematical simplifications without losing the essential physics. Therefore, we set

$$V_{\mathbf{k}\mathbf{k}'} = \begin{cases} -\frac{V}{L^3}, & \frac{\hbar^2 k'^2}{2m} < \epsilon_F + \hbar\omega_D \\ 0, & \text{otherwise} \end{cases}$$

This interaction is attractive and constant in an energy band $\hbar\omega_D$ above the Fermi surface, see figure 3.1. Substituting this into equation (3.6) we obtain

$$g(\mathbf{k}) = \frac{V}{L^3} \frac{1}{\frac{\hbar^2 k^2}{m} - \epsilon - 2\epsilon_F} \sum_{\mathbf{k}'} g(\mathbf{k}'). \quad (3.7)$$

Summing over \mathbf{k} on both sides of this equation we are left with the self-consistency condition

$$\frac{V}{L^3} \sum_{\mathbf{k}} \frac{1}{\frac{\hbar^2 k^2}{m} - \epsilon - 2\epsilon_F} = 1. \quad (3.8)$$

For the sake of brevity we define $\xi = \frac{\hbar^2 k^2}{2m} - \epsilon_F$, which is the energy above the Fermi level. Now we convert the sum in (3.8) into an integral. For this we must introduce the density of states per spin $\mathcal{N}(\xi)$ whose exact form is not relevant. With this

$$V \int_0^{\hbar\omega_D} d\xi \frac{\mathcal{N}(\xi)}{2\xi - \epsilon} = 1. \quad (3.9)$$

Since $\mathcal{N}(\xi)$ does not vary much from the Fermi surface, we can assume that $\mathcal{N}(\xi) \approx \mathcal{N}(0)$. We easily carry out the integration to obtain

$$\frac{1}{2} \mathcal{N}(0) V \ln \left(\frac{\epsilon - 2\hbar\omega_D}{\epsilon} \right) = 1. \quad (3.10)$$

At last, we assume that $|\epsilon| \ll \hbar\omega_D$, and therefore equation (3.10) simplifies to

$$\epsilon = -2\hbar\omega_D e^{-\frac{2}{\mathcal{N}(0)V}}. \quad (3.11)$$

This is our desired bound state energy for two electrons above but near the Fermi surface subjected to an attractive potential. This result was unexpected, because two electrons in free space would not bind with the same weak attractive interaction. Some observations are worth to point out. The sign of the binding energy ϵ is negative as expected. A bound state generally implies a discrete energy spectrum, which is consistent with the exponentially falling heat capacity observed experimentally. And impressively, we obtain a bound state regardless of how small V is! Moreover, our final result (3.11) could not be obtained by perturbation methods, because (3.11) cannot be expanded in power series in V . Also, note that if we write the the energy of the electron at position \mathbf{r}_1 we have $E_1 = \epsilon_F + \epsilon_1$. However, we know that $\epsilon = \epsilon_1 + \epsilon_2 < 0$ and therefore $E_1 < \epsilon_F$. This is an apparent paradox, since we started with the impression that $E_1 > \epsilon_F$. The paradox is resolved by understanding that the electron pair has in fact condensed into a different

state of matter – a bose like state. This provided the foundation for the development of the theory of superconductivity. The Cooper problem is a historical foundation for the description of a different state of matter - the superconducting condensate. This condensate consists of a cooperative phenomena between all condensed Cooper pairs governed by a single wavefunction.

3.2.2 The BCS Hamiltonian

The objective of this section is to develop the basic machinery used to describe conventional superconductors. The interaction Hamiltonian responsible for Cooper pairing will be of crucial importance. In order to introduce the elements of the BCS Hamiltonian we define an operator $\psi_\sigma^{(\dagger)}(\mathbf{r})$, which annihilates (creates) an electron of spin σ at position \mathbf{r} . Evidently, these field operators will obey the anti-symmetric commutation relations

$$\left\{ \psi_\sigma(\mathbf{r}), \psi_{\sigma'}^\dagger(\mathbf{r}') \right\} = \delta(\mathbf{r} - \mathbf{r}') \delta_{\sigma\sigma'} I. \quad (3.12)$$

$$\left\{ \psi_\sigma(\mathbf{r}), \psi_{\sigma'}(\mathbf{r}') \right\} = 0. \quad (3.13)$$

In the section below we develop the appropriate pairing (BCS) Hamiltonian which will lead us to the equation that describes the superconducting state. We start our discussion at zero temperature, and then introduce thermal averages to treat calculations at finite temperatures. At last, we will apply the equations that describe superconductivity to a uniform superconductor. This discussion is mainly inspired by reference [36].

The Hamiltonian

We split our Hamiltonian \mathcal{H} into two parts: \mathcal{H}_0 and \mathcal{H}_c . The term \mathcal{H}_0 includes the dynamics of the electrons in the normal state of matter, including interactions. In second quantized form, we write

$$\mathcal{H}_0 = \int d\mathbf{r} \sum_{\sigma} K \psi_{\sigma}^{\dagger}(\mathbf{r}) \psi_{\sigma}(\mathbf{r}), \quad \text{with} \quad K = \frac{p^2}{2m} + U - \mu. \quad (3.14)$$

Here, U represents the interactions present between electrons in the normal state of matter, and μ is the Fermi level. The more interesting part, \mathcal{H}_c , is the coupling Hamiltonian that contains the interactions responsible for Cooper pairing. Let us take a closer look on this term.

Following the definition (2.30), the electron-electron coupling Hamiltonian in terms of electron creation(annihilation) field operators is written as

$$\mathcal{H}_c = \frac{1}{2} \int d\mathbf{r} \int d\mathbf{r}' \sum_{\sigma} \sum_{\sigma'} \langle \sigma\sigma' | v(\mathbf{r} - \mathbf{r}') | \sigma\sigma' \rangle \psi_{\sigma}^{\dagger}(\mathbf{r}) \psi_{\sigma}(\mathbf{r}) \psi_{\sigma'}^{\dagger}(\mathbf{r}') \psi_{\sigma'}(\mathbf{r}'). \quad (3.15)$$

We simplify \mathcal{H}_c until we retain the essential physics. Having this in mind, we set

$$\frac{1}{2}\langle\sigma\sigma'|v(\mathbf{r}-\mathbf{r}')|\sigma\sigma'\rangle=-\frac{V}{2}\delta(\mathbf{r}-\mathbf{r}')\delta_{\sigma,-\sigma'}. \quad (3.16)$$

The minus sign is motivated from the attractive potential in the Cooper problem induced by phonons. We rearrange the operators using the commutation relations to pair up the opposite spins, which will yield the relevant amplitudes. We get

$$\mathcal{H}_c=-\frac{V}{2}\int d\mathbf{r}\sum_{\sigma}\psi_{\sigma}^{\dagger}(\mathbf{r})\psi_{-\sigma}^{\dagger}(\mathbf{r})\psi_{-\sigma}(\mathbf{r})\psi_{\sigma}(\mathbf{r}). \quad (3.17)$$

Since we have introduced the most important element of the Cooper problem, that is, the attractive potential between pairs, the Hamiltonian (3.17) should be responsible for the condensation of Cooper pairs above the Fermi sea as discussed in the previous section. Let us work out some simplifications by starting with the mean field approximation (2.37)

$$\begin{aligned} \psi_{\sigma}^{\dagger}(\mathbf{r})\psi_{-\sigma}^{\dagger}(\mathbf{r})\psi_{-\sigma}(\mathbf{r})\psi_{\sigma}(\mathbf{r}) &\longrightarrow \psi_{\sigma}^{\dagger}(\mathbf{r})\psi_{-\sigma}^{\dagger}(\mathbf{r})\langle\psi_{-\sigma}(\mathbf{r})\psi_{\sigma}(\mathbf{r})\rangle \\ &+ \langle\psi_{\sigma}^{\dagger}(\mathbf{r})\psi_{-\sigma}^{\dagger}(\mathbf{r})\rangle\psi_{-\sigma}(\mathbf{r})\psi_{\sigma}(\mathbf{r}), \end{aligned} \quad (3.18)$$

where the averages now are supposed to be taken in the superconducting ground state $|G\rangle$ at zero temperature where thermal fluctuations do not exist. We perform the sums over $\sigma=\uparrow,\downarrow$ in (3.17), having in mind that $\langle\psi_{\downarrow}\psi_{\uparrow}\rangle=-\langle\psi_{\uparrow}\psi_{\downarrow}\rangle$ to obtain

$$\mathcal{H}_c=-V\int d\mathbf{r}\left[\langle\psi_{\downarrow}(\mathbf{r})\psi_{\uparrow}(\mathbf{r})\rangle\psi_{\uparrow}^{\dagger}(\mathbf{r})\psi_{\downarrow}^{\dagger}(\mathbf{r})+\langle\psi_{\uparrow}^{\dagger}(\mathbf{r})\psi_{\downarrow}^{\dagger}(\mathbf{r})\rangle\psi_{\downarrow}(\mathbf{r})\psi_{\uparrow}(\mathbf{r})\right]. \quad (3.19)$$

At last, we introduce the following fundamental quantity below

$$\begin{aligned} \Delta(\mathbf{r}) &= -V\langle\psi_{\downarrow}(\mathbf{r})\psi_{\uparrow}(\mathbf{r})\rangle \\ \Delta^*(\mathbf{r}) &= -V\langle\psi_{\uparrow}^{\dagger}(\mathbf{r})\psi_{\downarrow}^{\dagger}(\mathbf{r})\rangle, \end{aligned} \quad (3.20)$$

and arrive at

$$\mathcal{H}_c=\int d\mathbf{r}\left(\Delta(\mathbf{r})\psi_{\uparrow}^{\dagger}(\mathbf{r})\psi_{\downarrow}^{\dagger}(\mathbf{r})+\Delta^*(\mathbf{r})\psi_{\downarrow}(\mathbf{r})\psi_{\uparrow}(\mathbf{r})\right). \quad (3.21)$$

The function Δ is the central parameter defining \mathcal{H}_c and therefore this must be the parameter that measures the strength of condensed Cooper pairs. Indeed, Δ is called the superconducting amplitude, or simply gap. As it must be, for a free non-interacting electron gas, Δ is zero since the total numbers of particles is fixed. The nature of paired electrons is very different from free ones. At a critical temperature T_c the number of electrons flow from one state of matter (the normal state) to another one (the superconducting state) regulated by a chemical potential μ . Throughout the discussion we hope

to develop an intuition for Δ .

At last, we write the full Hamiltonian as

$$\begin{aligned}\mathcal{H} &= \int d\mathbf{r} \left[\sum_{\sigma} K \psi_{\sigma}^{\dagger}(\mathbf{r}) \psi_{\sigma}(\mathbf{r}) + \Delta \psi_{\uparrow}^{\dagger}(\mathbf{r}) \psi_{\downarrow}^{\dagger}(\mathbf{r}) + \Delta^* \psi_{\downarrow}(\mathbf{r}) \psi_{\uparrow}(\mathbf{r}) \right] \\ &= \int d\mathbf{r} \left[K \psi_{\uparrow}^{\dagger}(\mathbf{r}) \psi_{\uparrow}(\mathbf{r}) + K \psi_{\downarrow}^{\dagger}(\mathbf{r}) \psi_{\downarrow}(\mathbf{r}) + \Delta \psi_{\uparrow}^{\dagger}(\mathbf{r}) \psi_{\downarrow}^{\dagger}(\mathbf{r}) + \Delta^* \psi_{\downarrow}(\mathbf{r}) \psi_{\uparrow}(\mathbf{r}) \right].\end{aligned}\quad (3.22)$$

This is the effective (mean field) Hamiltonian that describes the physics of pairing. Furthermore, we can write (3.22) neatly by introducing a spinor and a Hamiltonian matrix respectively written as

$$\mathbf{\Psi}(\mathbf{r}) = \begin{pmatrix} \psi_{\uparrow}(\mathbf{r}) \\ \psi_{\downarrow}^{\dagger}(\mathbf{r}) \end{pmatrix}, \quad \text{and} \quad \mathbf{H} = \begin{pmatrix} K & \Delta \\ \Delta^* & -K^* \end{pmatrix}.\quad (3.23)$$

In order to see this better we rewrite (3.22) using the anti-commutation relations (3.12) as

$$\begin{aligned}\mathcal{H} &= \int d\mathbf{r} K \delta(0) + \int d\mathbf{r} \left[K \psi_{\uparrow}^{\dagger} \psi_{\uparrow} - K \psi_{\downarrow} \psi_{\downarrow}^{\dagger} + \Delta \psi_{\uparrow}^{\dagger} \psi_{\downarrow}^{\dagger} + \Delta^* \psi_{\downarrow} \psi_{\uparrow} \right] \\ &= K(0) + \int d\mathbf{r} \mathbf{\Psi}^{\dagger} \mathbf{H} \mathbf{\Psi},\end{aligned}\quad (3.24)$$

where we have used the property that $K = K^*$.

3.2.3 The Bogoliubov transformation

Observe that, as any mean field Hamiltonian, equation (3.24) is quadratic in the ψ 's. For this reason, we can diagonalize \mathcal{H} by a transformation \mathcal{B} such that

$$\mathbf{\Psi}(\mathbf{r}) = \sum_n \mathcal{B}_n(\mathbf{r}) \mathbf{\Phi}_n, \quad \text{where} \quad \mathbf{\Phi}_n = \begin{pmatrix} \gamma_{n\uparrow} \\ \gamma_{n\downarrow}^{\dagger} \end{pmatrix}.\quad (3.25)$$

Note that $\mathbf{\Phi}_n$ is similar to $\mathbf{\Psi}$, but does not depend on \mathbf{r} , which means that the $\gamma_{n\sigma}$'s are not field operators. The quantum number n stands for all quantum numbers necessary to completely described a given state. Evidently, the $\gamma_{n\sigma}$'s must also obey the fermi anti-commutation relations since they are fermi operators. Also we must have that

$$\mathbf{\Phi}_n = \int d\mathbf{r} \mathcal{B}_n^{-1}(\mathbf{r}) \mathbf{\Psi}(\mathbf{r}),\quad (3.26)$$

which implies the orthogonality relations

$$\sum_n \mathcal{B}_n^{-1}(\mathbf{r}) \mathcal{B}_n(\mathbf{r}') = \delta(\mathbf{r} - \mathbf{r}') I\quad (3.27)$$

$$\int d\mathbf{r} \mathcal{B}_n^{-1}(\mathbf{r}) \mathcal{B}_m(\mathbf{r}) = \delta_{nm} I, \quad (3.28)$$

where I is just the identity matrix. One can verify that the matrices

$$\mathcal{B}_n(\mathbf{r}) = \begin{pmatrix} u_n(\mathbf{r}) & -v_n^*(\mathbf{r}) \\ v_n(\mathbf{r}) & u_n^*(\mathbf{r}) \end{pmatrix} \quad \text{and} \quad \mathcal{B}_n^{-1}(\mathbf{r}) = \begin{pmatrix} u_n^*(\mathbf{r}) & v_n^*(\mathbf{r}) \\ -v_n(\mathbf{r}) & u_n(\mathbf{r}) \end{pmatrix} \quad (3.29)$$

do satisfy the orthogonality relations above. The matrix \mathcal{B}_n is known as the Bogoliubov transformation. The normalization condition on the matrix elements is fixed by (3.28), which is expressed as

$$\int d\mathbf{r} (|u_n(\mathbf{r})|^2 + |v_n(\mathbf{r})|^2) = 1. \quad (3.30)$$

We can also observe that the Bogoliubov transformation \mathcal{B}_n is unitary ($\mathcal{B}^{-1} = \mathcal{B}^\dagger$). More importantly, \mathcal{B} diagonalizes the mean field Hamiltonian (3.24) into

$$\mathcal{H} = \sum_n \sum_\sigma \epsilon_n \gamma_{n\sigma}^\dagger \gamma_{n\sigma}, \quad (3.31)$$

where the corresponding eigenvalue of \mathcal{H} – the energy E – is measured from the ground state. In the same way we have done with equation (3.22), we can express this in terms of matrices. Again, we use the anti-commutation relations to obtain

$$\mathcal{H} = \overbrace{\sum_n \epsilon_n}^{K(0)} + \sum_n \epsilon_n \left(\gamma_{n\uparrow}^\dagger \gamma_{n\uparrow} - \gamma_{n\downarrow} \gamma_{n\downarrow}^\dagger \right) = K(0) + \sum_n \epsilon_n \Phi_n^\dagger \sigma_z \Phi_n, \quad (3.32)$$

where σ_z is the *Pauli matrix*

$$\sigma_z = \begin{pmatrix} 1 & 0 \\ 0 & -1 \end{pmatrix}. \quad (3.33)$$

Now we must establish a proper connection of the full mean Hamiltonian with the diagonalized Hamiltonian.

3.2.4 The Bogoliubov equations

We compare equations (3.24) and (3.32) to determine u_n , v_n and ϵ_n . We substitute the transformation (3.25) into (3.24), and find

$$\mathcal{H} = K(0) + \int d\mathbf{r} \sum_n \sum_m \Phi_n^\dagger \mathcal{B}_n^\dagger(\mathbf{r}) \mathbf{H}(\mathbf{r}) \mathcal{B}_m(\mathbf{r}) \Phi_m \stackrel{(3.32)}{=} K(0) + \sum_n \epsilon_n \Phi_n^\dagger \sigma_z \Phi_n. \quad (3.34)$$

Here we have established the essential connection between the two equivalent Hamiltonians. In this comparison we see that we have to require

$$\sum_m \int d\mathbf{r} \mathcal{B}_n^\dagger(\mathbf{r}) \mathbf{H}(\mathbf{r}) \mathcal{B}_m(\mathbf{r}) = \epsilon_n \delta_{mn} \sigma_z. \quad (3.35)$$

Therefore, we operate $\mathcal{B}_m(\mathbf{r})$ to the left of (3.35) and obtain the so called Bogoliubov Equation:

$$\mathbf{H}(\mathbf{r}) \mathcal{B}_n(\mathbf{r}) = \epsilon_n \mathcal{B}_n(\mathbf{r}) \sigma_z. \quad (3.36)$$

This equation determines u_n , v_n and ϵ_n . Writing the matrices we get

$$\begin{pmatrix} K & \Delta \\ \Delta^* & -K^* \end{pmatrix} \begin{pmatrix} u_n & -v_n^* \\ v_n & u_n^* \end{pmatrix} = \epsilon_n \begin{pmatrix} u_n & -v_n^* \\ v_n & u_n^* \end{pmatrix} \begin{pmatrix} 1 & 0 \\ 0 & -1 \end{pmatrix}. \quad (3.37)$$

The essential information contained in this is expressed by the two Bogoliubov equations that read

$$\epsilon_n u_n(\mathbf{r}) = K u_n(\mathbf{r}) + \Delta v_n(\mathbf{r}) \quad (3.38)$$

$$\epsilon_n v_n(\mathbf{r}) = -K^* v_n(\mathbf{r}) + \Delta^* u_n(\mathbf{r}). \quad (3.39)$$

We also can rewrite this in standard matrix form as

$$\epsilon_n \begin{pmatrix} u_n(\mathbf{r}) \\ v_n(\mathbf{r}) \end{pmatrix} = \begin{pmatrix} K & \Delta \\ \Delta^* & -K^* \end{pmatrix} \begin{pmatrix} u_n(\mathbf{r}) \\ v_n(\mathbf{r}) \end{pmatrix}. \quad (3.40)$$

An important fact to notice about our discussion is that we have mapped the problem of pairing of electrons into a problem of free fermions, which are called quasi-particles created by $\gamma_{n\sigma}^\dagger$. It should be clear that solving (3.40) is a nonlinear problem. In most useful applications, there is almost no hope for an analytical solution. For this reason, this problem often involves computational techniques. Before exploring the Bogoliubov equations further, we examine the nature of the superconducting ground state.

3.2.5 The ground state

In order to infer the properties of the ground state, let us investigate the occupation of quasi-particles along the energy spectrum. The occupation number is naturally given by the Fermi distribution

$$f_n = \langle \gamma_{n\sigma}^\dagger \gamma_{n\sigma} \rangle = \frac{1}{e^{\beta \epsilon_n} + 1}, \quad (3.41)$$

where $\beta = 1/k_B T$ and the brackets are thermal averages, not a ground state average. From the Fermi distribution (3.41) we see that at $T = 0$, the number of quasi-particles is zero. With this, the ground state $|G\rangle$ must be such that $\gamma_{n\sigma}|G\rangle = 0$. Let us consider the

particular case in which $\sigma = \uparrow$. In this case, from equation (3.26) we have

$$\gamma_{n\uparrow} = \int d\mathbf{r} [u_n^*(\mathbf{r})\psi_{\uparrow}(\mathbf{r}) + v_n^*(\mathbf{r})\psi_{\downarrow}(\mathbf{r})]. \quad (3.42)$$

Our discussion will proceed smoother in momentum space. Therefore, let us Fourier transform this making

$$\begin{aligned} \psi_{\sigma}(\mathbf{r}) &= \frac{1}{\sqrt{\mathcal{V}}} \sum_{\mathbf{k}} e^{i\mathbf{k}\cdot\mathbf{r}} \psi_{\sigma}(\mathbf{k}) \\ u_n(\mathbf{r}) &= \frac{1}{\sqrt{\mathcal{V}}} \int d\mathbf{k} e^{i\mathbf{k}\cdot\mathbf{r}} u_n(\mathbf{k}), \end{aligned} \quad (3.43)$$

where \mathcal{V} is the correspondent volume in momentum \mathbf{k} -space. One should pay special attention in distinguishing the operators $u_n(\mathbf{r})$ and $\psi_{\sigma}(\mathbf{r})$, which live in configuration space, from $u_n(\mathbf{k})$ and $\psi_{\sigma}(\mathbf{k})$, which live in Fourier transformed \mathbf{k} -space. We substitute (3.43) into (3.42), identify the δ -functions in the integrals and obtain

$$\left[u_n^*(\mathbf{k})\psi_{\uparrow}(\mathbf{k}) + v_n^*(\mathbf{k})\psi_{\downarrow}^{\dagger}(\mathbf{k}) \right] |G\rangle = 0, \quad (3.44)$$

which is the condition from which we can suggest a ground state $|G\rangle$. Let us consider as a test ground state the Fermi sea $|F\rangle$ described by

$$|F\rangle = \prod_{\mathbf{k},\sigma}^{k < k_F} \psi_{\sigma}^{\dagger}(\mathbf{k})|0\rangle. \quad (3.45)$$

As one can easily verify, $|F\rangle$ cannot be $|G\rangle$ because it does not satisfy the fundamental condition (3.44). Bardeen, Cooper and Schrieffer [26] suggested the following BCS ground state

$$|G\rangle \equiv |BCS\rangle = \prod_{\mathbf{k},n} \left(u_n(\mathbf{k}) + v_n(\mathbf{k})\psi_{\uparrow}^{\dagger}(\mathbf{k})\psi_{\downarrow}^{\dagger}(-\mathbf{k}) \right) |0\rangle, \quad (3.46)$$

which satisfies (3.44). One also can show that $\langle G|G\rangle = 1$. This ground state gives a well defined physical meaning to the coefficients $u_n(\mathbf{k})$ and $v_n(\mathbf{k})$. The quantity $|u_n(\mathbf{k})|^2$ is the probability of a state n of a pair of electrons with opposite momenta and spin to be unoccupied. Obviously, $|v_n(\mathbf{k})|^2$ is the probability of this Cooper pair to be occupied. Since the number of Cooper pairs in the system of half of the number of condensed electrons, we must have

$$\langle G|N|G\rangle = 2 \sum_{n,\mathbf{k}} |v_n(\mathbf{k})|^2. \quad (3.47)$$

The BCS ground state is not an eigenstate of the number operator N . This is an important characteristic, because $|G\rangle$ does not have a well defined number of particles. We explore the nuances associated to the number operator in the next section.

3.2.6 Conjugate variables

In this section we attempt to identify the uncertainty principle relevant to BCS theory. Every quantum description of matter has an uncertainty principle associated to it. When an operator has a large variance in its spectrum of eigenvalues, then there must be another operator conjugated to the first that has a small variance. This is Heisenberg's uncertainty principle. It is not clear from our discussion, however, what operators are conjugated to one another. To address this problem, let us look at a fundamental quantity in BCS theory – the gap $\Delta(\mathbf{r})$. This gap amplitude is the complex superconducting wave function, which implies that it always can be written as

$$\Delta(\mathbf{r}) = |\Delta(\mathbf{r})| e^{i\varphi(\mathbf{r})}, \quad (3.48)$$

where $\varphi(\mathbf{r})$ is the phase of the order parameter and $|\Delta(\mathbf{r})|$ is the amplitude. We can associate a physical interpretation to the phase $\varphi(\mathbf{r})$: the phase of condensed Cooper pairs described as

$$|\varphi\rangle = \prod_{\mathbf{k},n} \left(|u_n(\mathbf{k})| + e^{i\varphi} |v_n(\mathbf{k})| \psi_{\uparrow}^{\dagger}(\mathbf{k}) \psi_{\downarrow}^{\dagger}(-\mathbf{k}) \right) |0\rangle, \quad (3.49)$$

which is a state with a well defined phase φ . If we take the product in this last equation seriously, it can be rewritten as

$$|\varphi\rangle = \sum_M \sum_{\mathbf{k}_1, \dots, \mathbf{k}_M} \underbrace{\prod_{\mathbf{k},n} |u_n(\mathbf{k})| \prod_{\mathbf{k}',n} e^{i\varphi} |v_n(\mathbf{k}')| \prod_M \psi_{\uparrow}^{\dagger}(\mathbf{k}_M) \psi_{\downarrow}^{\dagger}(-\mathbf{k}_M)}_{C(\mathbf{k}_1, \mathbf{k}_2, \dots, \mathbf{k}_M)}. \quad (3.50)$$

The $C(\mathbf{k}_1, \mathbf{k}_2, \dots, \mathbf{k}_M)$ are constants where \mathbf{k} runs over the unoccupied states and \mathbf{k}' over the occupied states. Here M is the number of states available for \mathbf{k} . If the total number of electrons is N , then we have $N/2$ states occupied by Cooper pairs, such that

$$C(\mathbf{k}_1, \mathbf{k}_2, \dots, \mathbf{k}_M) = e^{i\frac{N}{2}\varphi} \prod_{\mathbf{k},n} |u_n(\mathbf{k})| \prod_{\mathbf{k}',n} |v_n(\mathbf{k}')|. \quad (3.51)$$

Therefore, we can shorten equation (3.50) with convenient notation to obtain

$$|\varphi\rangle = \sum_N e^{i\frac{N}{2}\varphi} |C_N||N\rangle, \quad (3.52)$$

which gives the state with a well defined phase as a linear combination of states with well defined number. This means that the number and phase operators are related, and speculate that they are conjugate to each other. To confirm this we Fourier transform

(3.52), which yields

$$|N\rangle = \frac{1}{|C_N|} \int_{-\pi}^{\pi} \frac{d\varphi}{2\pi} e^{-i\frac{N}{2}\varphi} |\varphi\rangle. \quad (3.53)$$

The physical interpretation of the Fourier transform is simple – by integrating over φ , we make the phase uncertain, and the number of particles N becomes fixed. Therefore, the Heisenberg uncertainty relation is $\delta N \delta \varphi > 1$. This discussion shows us that the superconducting phase as an operator will be conjugated with the number operator. This implies the commutation relation

$$[N, \varphi] = 1 \quad (3.54)$$

for the number and phase operator. Observe that the BCS ground state (3.46) has a well defined phase ($\varphi = 0$) and an ill defined number of particles.

3.2.7 Calculations at finite temperature

To extend our discussion to finite temperatures we have to introduce thermal states as in (3.41), which are excited states at a certain temperature T . Observe that the thermal averages $\langle \gamma_{n\sigma} \gamma_{m\sigma'} \rangle$ are zero. The only relevant thermal averages are $\langle \gamma_{n\sigma}^\dagger \gamma_{m\sigma'} \rangle = \delta_{nm} \delta_{\sigma\sigma'} f_n$. Now that we have mapped the problem into quasi-particles, we could write any operator in terms of the quasi-particles operators γ . As an example of this machinery, let us calculate the number of electrons in the system N and its thermal average $\langle N \rangle$. Therefore

$$\begin{aligned} N &= \int d\mathbf{r} \sum_{\sigma} \psi_{\sigma}^{\dagger} \psi_{\sigma} = \int d\mathbf{r} \delta(0) + \int d\mathbf{r} \Psi^{\dagger} \sigma_{\mathbf{z}} \Psi \\ &= 1 + \int d\mathbf{r} \sum_n \Phi_n^{\dagger} \mathcal{B}_n^{\dagger} \sigma_{\mathbf{z}} \mathcal{B}_n \Phi_n \\ &= 1 + \sum_n \int d\mathbf{r} \left\{ (|u_n|^2 - |v_n|^2) \sum_{\sigma} \left(\gamma_{n\sigma}^{\dagger} \gamma_{n\sigma} - \frac{1}{2} \right) \right. \\ &\quad \left. - 2u_n v_n \gamma_{n\downarrow} \gamma_{n\uparrow} - 2u_n^* v_n^* \gamma_{n\uparrow}^{\dagger} \gamma_{n\downarrow}^{\dagger} \right\}. \end{aligned} \quad (3.55)$$

Remembering (3.30) and the properties of thermal averages, we write

$$\begin{aligned} \langle N \rangle &= +2 \sum_n \left(f_n - \frac{1}{2} \right) \int d\mathbf{r} (|u_n|^2 - |v_n|^2) \\ &= 1 + 2 \sum_n \left(f_n - \frac{1}{2} \right) \left(1 - 2 \int d\mathbf{r} |v_n|^2 \right) \\ &= 2 \sum_n \left[f_n + \tanh \left(\frac{\beta \epsilon_n}{2} \right) \int d\mathbf{r} |v_n|^2 \right]. \end{aligned} \quad (3.56)$$

This reduces precisely to (3.47) at $T = 0$. Now let us calculate $\Delta(\mathbf{r}) = V\langle\psi_{\uparrow}\psi_{\downarrow}\rangle$. We Bogoliubov transform this again from (3.25) such that

$$\begin{pmatrix} \psi_{\uparrow} \\ \psi_{\downarrow} \end{pmatrix} = \sum_n \begin{pmatrix} u_n \gamma_{n\uparrow} - v_n^* \gamma_{n\downarrow}^{\dagger} \\ v_n^* \gamma_{n\uparrow}^{\dagger} + u_n \gamma_{n\downarrow} \end{pmatrix}. \quad (3.57)$$

This equation shows the Bogoliubov transformation explicitly. With this we write

$$\Delta(\mathbf{r}) = V \sum_n u_n v_n^* (1 - 2f_n) = V \sum_n u_n v_n^* \tanh\left(\frac{\beta\epsilon_n}{2}\right). \quad (3.58)$$

The complete solution of the problem depends on (3.40) together with (3.58). For real life problems, all the integrals are converted into sums for computational implementation.

The translational invariant problem

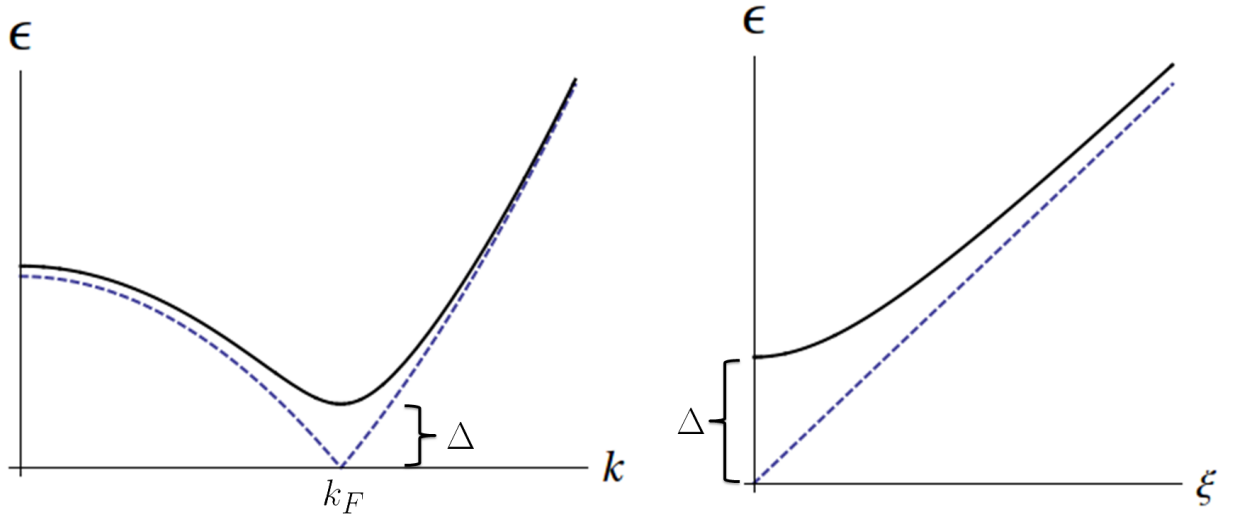


Figure 3.2: Behaviour of elementary quasiparticle excitations: Dashed line - normal state with $\Delta = 0$; Continuous line - superconducting state where $\Delta \neq 0$.

We want to solve the self-consistent problem, that is, equation (3.40) in conjunction with (3.58). To simplify our discussion, we consider the gap parameter to be constant throughout our superconducting sample, that is $\Delta(\mathbf{r}) = \Delta$. This allows us to write the Bogoliubov equations (3.40) as

$$\begin{pmatrix} K - \epsilon_k & \Delta \\ \Delta^* & -K^* - \epsilon_k \end{pmatrix} \begin{pmatrix} u_k \\ v_k \end{pmatrix} = 0. \quad (3.59)$$

In this last equation we have Fourier transformed the $u_n(\mathbf{r})$ to u_k and the quantum number

n is now \mathbf{k} itself. Assuming that $K \equiv \xi_k$ is real, we avoid trivial solutions by imposing

$$\det \begin{pmatrix} \xi_k - \epsilon_k & \Delta \\ \Delta^* & -\xi_k - \epsilon_k \end{pmatrix} = 0 \quad \Rightarrow \quad \epsilon_k^2 = \xi_k^2 + |\Delta|^2, \quad (3.60)$$

which is the dispersion relation of the quasi-particle excitations. Moreover, equation (3.59) together with the Fourier transformed normalization condition $|u_k|^2 + |v_k|^2 = 1$ fix the values of u_k and v_k . Consider the two lines of (3.59). We isolate Δ from the second line and substitute it into the first. Multiply the first line by u_k^* and use the normalization condition. This procedure gives $|u_k|^2$. An analogous procedure gives $|v_k|^2$. With this done, we obtain:

$$\begin{aligned} |u_k|^2 &= \frac{1}{2} \left(1 + \frac{\xi_k}{\epsilon_k} \right) \\ |v_k|^2 &= \frac{1}{2} \left(1 - \frac{\xi_k}{\epsilon_k} \right). \end{aligned} \quad (3.61)$$

These equations enable us to write the fundamental BCS equation that determines Δ . To do so we substitute the coefficients (3.61) into (3.58) to obtain

$$\Delta = \frac{1}{\mathcal{V}} \sum_k \frac{V\Delta}{\epsilon_k} \tanh \left(\frac{\beta\epsilon_k}{2} \right). \quad (3.62)$$

For zero temperature, the solution of $|\Delta(0)|$ for the fundamental BCS equation (3.62) is identical to the Cooper solution (3.11). We also can evaluate the integral equivalent to (3.62) numerically to plot the temperature dependence of the gap. This looks like figure 3.3.

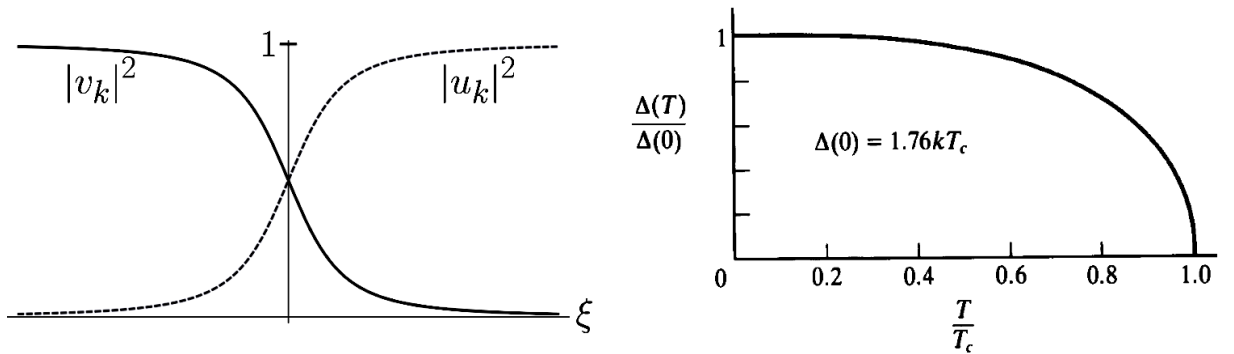


Figure 3.3: **Left:** The BCS wave function parameters $|u_k|^2$ and $|v_k|^2$ for \mathbf{k} near the Fermi surface. **Right:** Temperature dependence of the energy gap in the BCS theory.

3.3 Intermission – d-wave superconductors

One of the essential open question regarding unconventional superconductors is: Is the superconducting pairing mechanism in these materials of the familiar BCS s-wave type, or is some other form of pairing, of which the most likely appears to be d-wave pairing? There is no doubt that the superconducting mechanism of high- T_c superconductors is based on Cooper pairs $q = 2e$ with zero net momentum because the usual Josephson frequency $q\Delta V/\hbar$ is observed. Also, experiments show pairing is of the spin singlet form as in BCS theory [48].

High- T_c cuprate superconductors have gained attention since its discovery. Although all the enlightening efforts invested until now, it is fair to say that our knowledge of the essential points is limited. However, there is one aspect that is becoming well established – the so called d-wave state – because of the overwhelming experimental evidence and nice symmetry arguments from the theoretical point of view. Even more intriguing is the fact that the superconducting phase emerges from a strongly correlated electron system with a pronounced trend towards anti-ferromagnetism.

Unconventional superconductors have Cooper pairs with lower symmetry in contrast to the the conventional BCS ground state (3.46), which is the most symmetric Cooper pair possible. As we saw in BCS theory, the gap parameter Δ is independent of k . However, we can easily generalize this to a symmetry depended gap Δ_k . Given a certain symmetry operation \hat{R} that acts on the first Brillouin zone of a crystal, conventional symmetry is defined as $\Delta_{\hat{R}k} = \Delta_k$. Conversely, unconventional superconductors satisfy the condition $\Delta_{\hat{R}k} \neq \Delta_k$ for at least one symmetry operation \hat{R} . In practice, one simply refers to the pairing symmetries as s-wave ($l = 0$), p-wave ($l = 1$), d-wave ($l = 2$) or f-wave ($l = 3$). Unfortunately, these nomenclatures are mathematically relaxed [2]. Experimental evidence suggest that high- T_c superconductors such as $\text{La}_{2-x}\text{Sr}_x\text{CuO}_4$ and $\text{YBa}_2\text{Cu}_3\text{O}_7$ present d-wave symmetry. These materials are complex in structure. However, a common feature is that they contain two dimensional layers of copper and oxygen (CuO_2), which confer fundamental properties for unconventional pairing. Therefore, any k_z dependence can be neglected. To examine the energy gaps, we can restrict ourselves to a two-dimensional square. Below we list some of the known pairing states

Symmetry	Short	Proportion	Gap	l
BCS s-wave	s	1	$\Delta_k = \Delta$	0
Extended s-wave	s^-	$k_x^2 + k_y^2$	$\Delta_k = \frac{\Delta}{2} (\cos k_x a + \cos k_y a)$	0
d-wave symmetry	$d_{x^2-y^2}$	$k_x^2 - k_y^2$	$\Delta_k = \frac{\Delta}{2} (\cos k_x a - \cos k_y a)$	2
d_{xy} -wave symmetry	d_{xy}	$k_x k_y$	$\Delta_k = \Delta \sin k_x a \sin k_y a$	2

Table 3.1: Table of some of the possible pairing states. The quantity a is the crystal lattice constant of the square cooper-oxide plane.

We give special attention to d-wave symmetry in as depicted in figure 3.4 because it

is the most important symmetry in this dissertation. In this case Δ_k changes sign under rotation of the square by $\pi/2$ ($k_x \rightarrow k_y, k_y \rightarrow -k_x$). Also note that Δ_k vanishes at four point on the Fermi surface. Alternative pairing mechanisms and strong correlation effects are key elements to prevents electrons from undergoing conventional s-wave pairing.

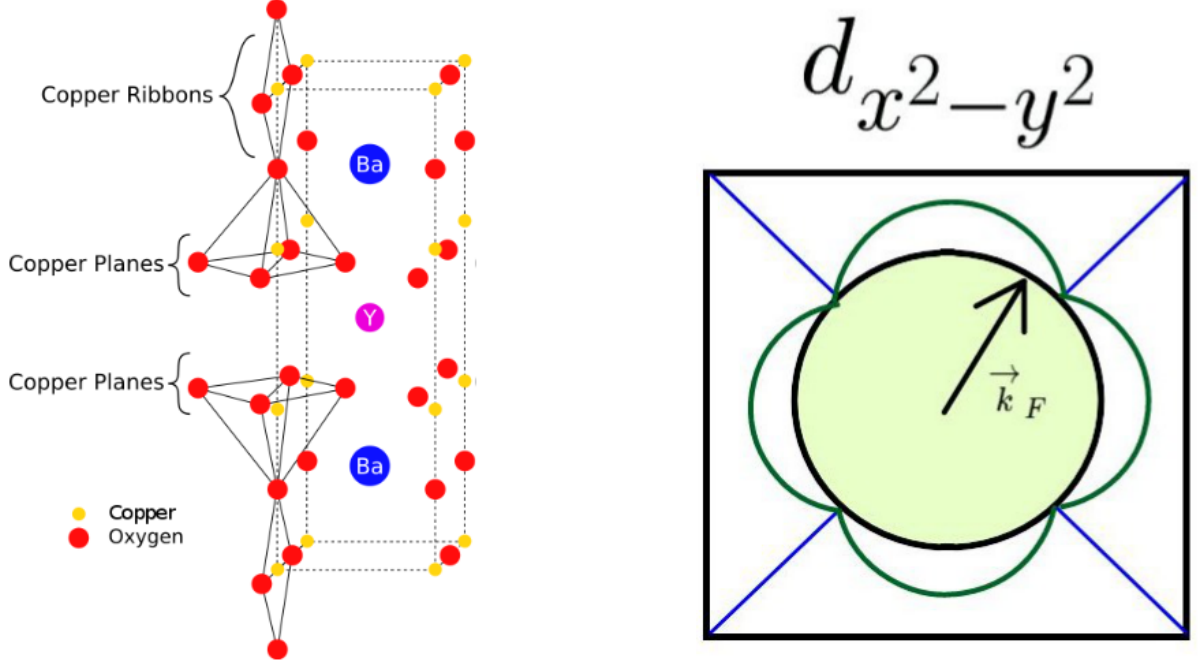


Figure 3.4: **Left:** Part of the lattice structure of yttrium barium copper oxide. **Right:** d-wave symmetry of the gap parameter with four gap nodes on the Fermi surface. The square is the first Brillouin zone.

3.4 The Bogoliubov-deGennes formalism

In this section we develop the formalism of Bogoliubov-deGennes [13, 18] that is an extension of BCS theory for inhomogeneous superconductors. In BCS theory we wrote the Hamiltonian as (3.22) and inferred an adequate matrix \mathbf{H} to simplify our mathematical discussion. However, for a Hamiltonian describing inhomogeneous superconductors, inferring a matrix is difficult. Because of this, we develop a formalism where no inferences are made. This method allows us to treat intrinsic inhomogeneities – which are supposed to be characteristic of high- T_c superconductors – without appealing to complex mathematical methods. Our objective aims to determine the local hole doping ρ in the copper-oxide planes. This approach also permits us to calculate the local gap parameters in inhomogeneous systems. Since electrons in high- T_c superconductors are strongly correlated, we use an adapted (extended) Hubbard model to describe our two dimensional lattice (the planes) [20].

3.4.1 The Hubbard model

In simple metals it is easy for the electron-phonon interaction to overcome the Coloumb repulsion. In so called strongly correlated electron systems, electrons retain more of their localized character. In this case the Coloumb interaction is larger, such that the attractive electron-phonon interaction will not suffice.

The Hubbard model is almost the standard model for strongly correlated systems [40]. The reason of its popularity is the inclusion of electron correlation, its simplicity and the rich physics contained in the model. Here we present this model briefly. It can be solved exactly in one dimension, which is not our case. For this reason, we present the Hubbard model for a two dimensional discrete square lattice, which will be used to model the copper-oxide plane. Let us first write the Hamiltonian describing a system of non-interacting fermions. Inspired on equation (2.22), we can write this Hamiltonian as

$$\mathcal{H}_0 = \sum_{i,k} \sum_{\sigma} t(i,k) c_{\sigma}^{\dagger}(i) c_{\sigma}(k), \quad (3.63)$$

where i and k are labels of the lattice's sites, and $c_{\sigma}^{\dagger}(i)$ ($c_{\sigma}(i)$) creates (annihilates) a fermion in a single particle orbital ϕ_i localized at site i . In condensed matter applications one can assume the ϕ_i 's to be Wannier weave functions (Fourier transform of Bloch orbitals). Obviously, the operators obey $\{c_{\sigma}^{\dagger}(i), c_{\sigma'}(k)\} = \delta_{ik} \delta_{\sigma\sigma'}$. Other anti-commutators equals zero. The coefficients $t(i,k)$ characterize the single-particle matrix elements and is called the hopping of charges between sites given by

$$t(i,k) = \left\langle i \left| \left(-\frac{\hbar^2 \nabla^2}{2m} + \hat{V} \right) \right| k \right\rangle = \int d\mathbf{r} \phi_i(\mathbf{r}) \left(-\frac{\hbar^2 \nabla^2}{2m} + V(\mathbf{r}) \right) \phi_k(\mathbf{r}). \quad (3.64)$$

Now, let us consider the electron-electron interaction \mathcal{H}_U . The most general form of interaction in second quantization representation that can be added to \mathcal{H}_0 is of the form of equation (2.30). The most important contribution of all possibilities is

$$\mathcal{H}_U = U \sum_i n_{\uparrow}(i) n_{\downarrow}(i). \quad (3.65)$$

In the limit of large U , the charge fluctuations are frozen and only the spin of electrons can fluctuate, thereby reducing to spin physics described by the so called t-J model.

At last, we add a term containing the chemical potential $\mu(i)$ that regulates the filling. Therefore, we write the full Hubbard Hamiltonian as

$$\mathcal{H}_H = \sum_{i,k} \sum_{\sigma} t(i,k) c_{\sigma}^{\dagger}(i) c_{\sigma}(k) + U \sum_i n_{\uparrow}(i) n_{\downarrow}(i) - \sum_{i,\sigma} \mu(i) n_{\sigma}(i). \quad (3.66)$$

This is the Hubbard model, which has vast applications in systems with strongly correlated

electrons. Our task, now, is to extend this model to include the effective interaction $V(i)$ expected from the theory of phase separation, whose phenomenology will be introduced in the next chapter.

3.4.2 The extended Hubbard Hamiltonian

Here in particular, we extend the Hubbard model to describe d-wave superconductors. We prefer to work with a discrete space for computational convenience. One can always rewrite the Hamiltonian in continuous (integral) form if necessary. The discrete extended Hubbard Hamiltonian reads

$$\begin{aligned} \mathcal{H} = & \overbrace{\sum_{\langle i,k \rangle} \sum_{\sigma} t(i,k) c_{\sigma}^{\dagger}(i) c_{\sigma}(k) - \sum_{i,\sigma} \mu(i) n_{\sigma}(i) + U \sum_i n_{\uparrow}(i) n_{\downarrow}(i)}^{\mathcal{H}_H} \\ & + \frac{1}{2} \overbrace{\sum_{\langle i,k \rangle} \sum_{\substack{\sigma, \sigma' \\ \sigma \neq \sigma'}} V(i) n_{\sigma}(i) n_{\sigma'}(k)}^{\mathcal{H}_V}. \end{aligned} \quad (3.67)$$

The term \mathcal{H}_V is the extended part that provides the interaction $V(i)$ between the charges within the first few neighbours denoted by $\langle i, k \rangle$. The chemical potential $\mu(i)$ regulates the local density, and U is the one site Coulomb repulsion. If we make $V(i) = 0$ and $U < 0$, the gaps are of the s-wave type [21]. Here, where $V(i) < 0$ and $U > 0$ we also will obtain d-wave gaps [20]. In order to hope for a relatively simple solution of the model, we perform a number of simplifications on each term of (3.67). We start with \mathcal{H}_V .

Simplifying the extended Hamiltonian \mathcal{H}_V

Summing \mathcal{H}_V over the spins σ and σ' gives

$$\begin{aligned} \frac{1}{2} \sum_{\langle i,k \rangle} \sum_{\substack{\sigma, \sigma' \\ \sigma \neq \sigma'}} V(i) n_{\sigma}(i) n_{\sigma'}(k) = \\ \frac{1}{2} \sum_{\langle i,k \rangle} V(i) \left[c_{\uparrow}^{\dagger}(i) c_{\uparrow}(i) c_{\uparrow}^{\dagger}(k) c_{\uparrow}(k) + c_{\downarrow}^{\dagger}(i) c_{\downarrow}(i) c_{\downarrow}^{\dagger}(k) c_{\downarrow}(k) \right. \\ \left. + c_{\uparrow}^{\dagger}(i) c_{\uparrow}(i) c_{\downarrow}^{\dagger}(k) c_{\downarrow}(k) + c_{\downarrow}^{\dagger}(i) c_{\downarrow}(i) c_{\uparrow}^{\dagger}(k) c_{\uparrow}(k) \right]. \end{aligned} \quad (3.68)$$

This last equation should lead to an interesting superconducting amplitude. By inspecting the four terms we see that there is nothing special about the first two terms. However, the

last two terms should yield some interesting new physics. Both last terms share the same structure and since we will take thermal averages of pairs of operators, it will suffice to consider only the last term to retain the essential physics. Therefore,

$$\mathcal{H}_V = \sum_{\langle i,k \rangle} \frac{V(i)}{2} c_{\uparrow}^{\dagger}(k) c_{\downarrow}^{\dagger}(i) c_{\downarrow}(i) c_{\uparrow}(k). \quad (3.69)$$

A product of four field (site) operators is not pleasant to handle. For this reason we apply the mean field approximation (2.37) with thermal averages to (3.69), which yields

$$\mathcal{H}_V = \sum_{\langle i,k \rangle} \left[\overbrace{\frac{V(i)}{2} \langle c_{\uparrow}^{\dagger}(k) c_{\downarrow}^{\dagger}(i) \rangle}_{\Delta_{\delta}^*(i)} c_{\downarrow}(i) c_{\uparrow}(k) + \overbrace{\frac{V(i)}{2} \langle c_{\downarrow}(i) c_{\uparrow}(k) \rangle}_{\Delta_{\delta}(i)} c_{\uparrow}^{\dagger}(k) c_{\downarrow}^{\dagger}(i)} \right], \quad (3.70)$$

where we have defined the amplitude $\Delta_{\delta}(i)$ that in advance is the d-wave gap parameter.

Simplifying the on-site repulsive Hamiltonian \mathcal{H}_U

To simplify the term responsible for the onsite repulsion we recur to the sometimes so called Hartree-Fock Bogoliubov approximation (2.39) [53]. Doing so, we write

$$\mathcal{H}_U = \frac{U}{3} \sum_i \left[\langle n_{\uparrow} \rangle n_{\downarrow} + \langle n_{\downarrow} \rangle n_{\uparrow} + 2 \langle c_{\downarrow} c_{\uparrow} \rangle c_{\uparrow}^{\dagger} c_{\downarrow}^{\dagger} + 2 \langle c_{\uparrow}^{\dagger} c_{\downarrow}^{\dagger} \rangle c_{\downarrow} c_{\uparrow} \right]. \quad (3.71)$$

In this equation we have omitted the argument because it is the same for all operators. If there are no external electromagnetic fields, then $\langle n_{\uparrow} \rangle = \langle n_{\downarrow} \rangle$. This permits us to resume our notation further defining $n = n_{\uparrow} + n_{\downarrow} = \sum_{\sigma} n_{\sigma}$. With these considerations we rewrite equation (3.71) defining new amplitudes:

$$\mathcal{H}_U = \sum_i \left[\frac{U}{6} \langle n \rangle n + \underbrace{\frac{2U}{3} \langle c_{\downarrow} c_{\uparrow} \rangle}_{\Delta_U(i)} c_{\uparrow}^{\dagger} c_{\downarrow}^{\dagger} + \underbrace{\frac{2U}{3} \langle c_{\uparrow}^{\dagger} c_{\downarrow}^{\dagger} \rangle}_{\Delta_U^*(i)} c_{\downarrow} c_{\uparrow} \right]. \quad (3.72)$$

The gap appears naturally with energy dimensions. If $U < 0$ and $V(i) = 0$, then $\Delta_U(i)$ would simply be the isotropic s-wave gap.

Writing the effective Hamiltonian \mathcal{H}_e

The term $\sum_i \frac{U}{6} \langle n \rangle n$ from (3.72) can be combined with the similar term $-\sum_{i,\sigma} \mu(i) n_{\sigma}(i)$ from (3.67) to give $\sum_i \bar{\mu}(i) n$, where

$$\bar{\mu}(i) = \mu(i) - \frac{U}{6} \langle n \rangle n \quad (3.73)$$

is the chemical potential that contains the Hartree-shift [21] $\frac{U}{6}\langle n \rangle n$ and has to be used for an inhomogeneous charge distribution $\rho(i)$. With this in mind, we assemble equations (3.70) and (3.72) back into equation (3.67) obtaining now our effective extended Hubbard Hamiltonian

$$\begin{aligned} \mathcal{H}_e = & \sum_{\langle i,k \rangle} \sum_{\sigma} t(i,k) c_{\sigma}^{\dagger}(i) c_{\sigma}(k) - \sum_i \bar{\mu}(i) n(i) \\ & + \sum_{\langle i,k \rangle} \left[\Delta_{\delta}(i) c_{\uparrow}^{\dagger}(k) c_{\downarrow}^{\dagger}(i) + \Delta_{\delta}^*(i) c_{\downarrow}(i) c_{\uparrow}(k) \right] \\ & + \sum_i \left[\Delta_U(i) c_{\uparrow}^{\dagger}(i) c_{\downarrow}^{\dagger}(i) + \Delta_U^*(i) c_{\downarrow}(i) c_{\uparrow}(i) \right]. \end{aligned} \quad (3.74)$$

In the next section we diagonalize this Hamiltonian using the Bogoliubov transformation. We will obtain the Hamiltonian's eigenvalues E_n and eigenvectors. Our mission now is to calculate $\Delta_U(i)$, $\Delta_{\delta}(i)$, $\rho(i)$ and $\langle \rho \rangle$.

3.4.3 Bogoliubov equations

The effective Hamiltonian (3.74) is now quadratic in the operators. Let us introduce the generalized Bogoliubov transformation in neat notation in analogy to (3.57) as

$$c_{\sigma}(i) = \sum_n \left[u_n(i) \gamma_{n\sigma} - \sigma v_n^*(i) \gamma_{n,-\sigma}^{\dagger} \right], \quad (3.75)$$

where the $\gamma_{n\sigma}$'s are quasi-particle operators, and $u_n(i)$ and $v_n(i)$ are probability amplitudes to be determined. The spin σ as usual can assume two possibilities: up \uparrow with a plus sign, and down \downarrow with a minus sign. Remember that that the quantum number n summarizes all necessary quantum numbers necessary to describe the system. Equation (3.75) diagonalizes (3.74) into

$$\mathcal{H}_e^D = \sum_{n,\sigma} E_n \gamma_{n\sigma}^{\dagger} \gamma_{n\sigma}, \quad (3.76)$$

where the eigenvalue of \mathcal{H}_e^D is measured from the ground state. This structure is pleasing because it reminds the quantum mechanics of the harmonic oscillator. Our next task is to establish proper communication between (3.74) and (3.76), which must be the same. We strategically calculate the commutators $[c_{\downarrow}(i), \mathcal{H}_e]$ and $[c_{\downarrow}(i), \mathcal{H}_e^D]$. Then, we Bogoliubov transform and equate them. This will lead us to the Bogoliubov equations that we are seeking for. In the process of these calculations, commutators such as $[\gamma_{n\sigma}, \mathcal{H}_e^D]$ will appear. Therefore, we calculate the following two commutators using (3.76) and $\{\gamma_{n\sigma}^{\dagger}, \gamma_{m\sigma'}\} = \delta_{nm} \delta_{\sigma\sigma'}$ in advance to give

$$[\gamma_{n\sigma}, \mathcal{H}_e^D] = E_n \gamma_{n\sigma} \quad \text{and} \quad [\gamma_{n\sigma}^\dagger, \mathcal{H}_e^D] = -E_n \gamma_{n\sigma}^\dagger. \quad (3.77)$$

Now let us proceed and calculate $[c_\downarrow(i), \mathcal{H}_e^{(D)}]$, where we have chosen the case $\sigma = \downarrow$ for no special reason. We would arrive at the same result calculating $[c_\uparrow^\dagger(i), \mathcal{H}_e^{(D)}]$. First, using the diagonal form of the effective Hamiltonian (3.76) together with (3.75) and (3.77) gives

$$[c_\downarrow(i), \mathcal{H}_e^D] = \sum_n E_n \left(u_n(i) \gamma_{n\downarrow} - v_n^*(i) \gamma_{n\uparrow}^\dagger \right). \quad (3.78)$$

In the same way we calculate $[c_\downarrow(i), \mathcal{H}_e]$ using (3.74) and after some longer manipulation we get

$$[c_\downarrow(i), \mathcal{H}_e] = \sum_k t(i, k) c_\downarrow(k) - \bar{\mu}(i) c_\downarrow(i) - \sum_k \Delta_\delta(i) c_\uparrow^\dagger(k) - \Delta_U(i) c_\uparrow^\dagger(i). \quad (3.79)$$

The first two terms were obtained from the first line of equation (3.74), and the other terms from the other two lines. In order to compare (3.79) with (3.78) we must Bogoliubov transform it giving

$$\begin{aligned} [c_\downarrow(i), \mathcal{H}_e] = & \\ & \sum_n \left(\sum_k u_n(k) t(i, k) - \bar{\mu}(i) u_n(i) + \sum_k v_n(k) \Delta_\delta(i) + v_n(i) \Delta_U(i) \right) \gamma_{n\downarrow} + \\ & \sum_n \left(\sum_k v_n^*(k) t(i, k) - \bar{\mu}(i) v_n^*(i) - \sum_k u_n^*(k) \Delta_\delta(i) - u_n^*(i) \Delta_U(i) \right) \gamma_{n\uparrow}^\dagger. \end{aligned} \quad (3.80)$$

We establish our so desired communication by comparing the coefficients $\gamma_{n\downarrow}$ and $\gamma_{n\uparrow}^\dagger$ in (3.78) and (3.80), obtaining

$$E_n u_n(i) = \sum_k u_n(k) t(i, k) - \bar{\mu}(i) u_n(i) + \sum_k v_n(k) \Delta_\delta(i) + v_n(i) \Delta_U(i), \quad (3.81)$$

and

$$-E_n v_n^*(i) = \sum_k v_n^*(k) t(i, k) - \bar{\mu}(i) v_n^*(i) - \sum_k u_n^*(k) \Delta_\delta(i) - u_n^*(i) \Delta_U(i). \quad (3.82)$$

These two equations are the Bogoliubov Equations of our problem. As customary, we wish to write this in standard matrix notation as

$$\begin{pmatrix} K & \Delta \\ \Delta^* & -K^* \end{pmatrix} \begin{pmatrix} u_n(i) \\ v_n(i) \end{pmatrix} = E_n \begin{pmatrix} u_n(i) \\ v_n(i) \end{pmatrix}. \quad (3.83)$$

The effect of the operators K and Δ over the amplitudes u_n and v_n is established by comparing equations (3.81) and (3.82) with (3.83). For (3.81) this yields

$$E_n u_n(i) = \overbrace{\sum_k u_n(k) t(i, k) - \bar{\mu}(i) u_n(i)}^{K u_n(i)} + \overbrace{\sum_k v_n(k) \Delta_\delta(i) + v_n(i) \Delta_U(i)}^{\Delta v_n(i)}, \quad (3.84)$$

and an analogous equation for (3.82). By definition $E_n \geq 0$. The equations (3.83) are the Bogoliubov-deGennes equations for our problem. They provide the eigenvalue excitation energy spectrum $\{E_n\}$. Also, they determine the eigenvector composed of the quasi-particle amplitudes

$$\begin{pmatrix} u_n(i) \\ v_n(i) \end{pmatrix}. \quad (3.85)$$

This is done with computational implementation. Once we know $\{E_n\}$ and (3.85), we can write $\Delta_U(i)$, $\Delta_\delta(i)$, $\rho(i)$ and $\langle \rho \rangle$ in terms of these quantities. This quantifies all necessary parameters to describe the system.

3.4.4 The gaps and the electronic density

Calculation of the gap amplitude $\Delta_U(i)$

In perfect analogy to (3.58) we can calculate the gap $\Delta_U(i) = U \langle c_\downarrow(i) c_\uparrow(i) \rangle$, where the constant was absorbed into the potential U . We have

$$\Delta_U(i) = -U \sum_n u_n(i) v_n^*(i) \tanh\left(\frac{\beta E_n}{2}\right). \quad (3.86)$$

Calculation of the gap amplitude $\Delta_\delta(i)$

We proceed calculating $\Delta_\delta(i) = V(i) \langle c_\downarrow(i) c_\uparrow(k) \rangle$. Bogoliubov transforming this and remembering the properties of thermal averages ($\langle \gamma_{n\sigma}^\dagger \gamma_{m\sigma'} \rangle = \delta_{nm} \delta_{\sigma\sigma'} f_n$), we get

$$\Delta_\delta(i) = V(i) \sum_n [v_n^*(i) u_n(k) f_n - u_n(i) v_n^*(k) (1 - f_n)]. \quad (3.87)$$

We can simplify this by establishing a relationship between the coefficients. We know that $\{c_\downarrow(i), c_\uparrow(k)\} = 0$. If we Bogoliubov transform this we obtain the relationship

$u_n(i)v_n^*(k) = u_n(k)v_n^*(i)$. With this we have

$$\Delta_\delta(i) = -V(i) \sum_n u_n(i)v_n^*(k) \tanh\left(\frac{\beta E_n}{2}\right). \quad (3.88)$$

Symmetry

One can see from (3.74) that $\Delta_\delta(i)$ is summed over the nearest neighbours $\langle i, k \rangle$. Now is the convenient time to define those neighbours. We can explicitly identify them by writing $k \equiv i + \delta$, where δ is a vector pointing from the point i to the nearest neighbour $k \equiv i + \delta$. If we consider a two dimensional square lattice, then the point i has four nearest neighbours, namely $i \pm \hat{x}$ and $i \pm \hat{y}$. One can easily verify that $\Delta_{\hat{x}}(i) = \Delta_{-\hat{x}}(i + \hat{x})$. Therefore, the components of $\Delta_\delta(i)$ present the symmetry

$$\Delta_\delta(i) = \Delta_{-\delta}(k), \quad (3.89)$$

which is characteristic for d-wave gaps.

Calculation of $\rho(i) = \langle n(i) \rangle$

At last we calculate $\rho(i) = \langle n(i) \rangle$, which yields

$$\rho(i) = 2 \sum_n [|u_n(i)|^2 f_n + |v_n(i)|^2 (1 - f_n)]. \quad (3.90)$$

The d-wave gap $\Delta_\delta(i)$ and the hole concentration $\rho(i)$ are determined and compared by computer simulations.

3.4.5 Numerical evaluation

Equations (3.88) and (3.90) were numerically evaluated in self-consistent manner using the Fortran programming language over a square lattice of many sizes [34], which represents a section of the cooper-oxide plane, characteristic of all cuprates. In figure 3.5 we show typical results for calculations with $T = 50$ K and $T = 190$ K, respectively. These figures show the correlation between the hole concentration and the d-wave superconducting gap in the pseudogap region. One can clearly see that a higher hole concentration ρ generates a higher gap value. The reddish plateaus are the regions with low electronic charge densities (high hole concentration ρ), separated by the bluish valleys. This shows that the electronic inhomogeneity plays a crucial role in studying the local gaps throughout the sample – the pseudogap region.

One of the great advantages of the formalism of Bogoliubov-deGennes is that it permits us to analyse a problem where the charge density varies. Another interesting graph is shown in figure 3.6. Here we show the evolution of the d-wave gap parameter. According

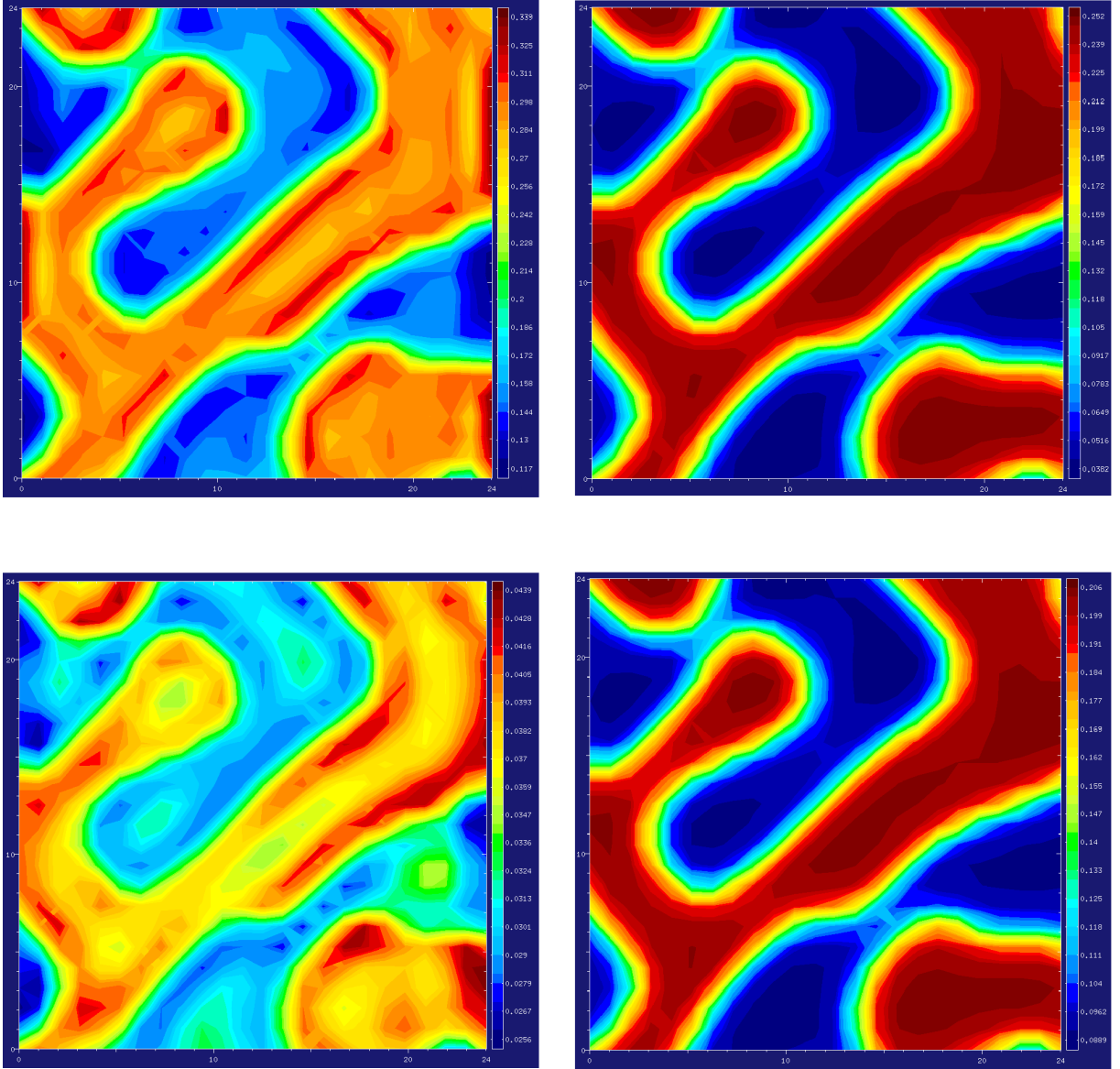


Figure 3.5: **Top left:** The values of the gap of $\Delta_\delta(i)$ varying in a 24 x 24 square lattice at temperature 50 K. **Top right:** Correspondent hole concentration $\rho(i)$ also at 50 K. **Bottom left:** The gaps at 190 K. **Bottom right:** Hole concentration at 190 K.

to figure 3.5 we see that the gap varies throughout the plane. This means that randomly chosen sites will have different initial values. However, whatever initial value the gap has, all will vanish at the same temperature around 165 K, as shown in figure 3.6.

In chapter five we will use the formalism discussed here to predict the onset of spontaneous ferromagnetism observed in YBCO samples.

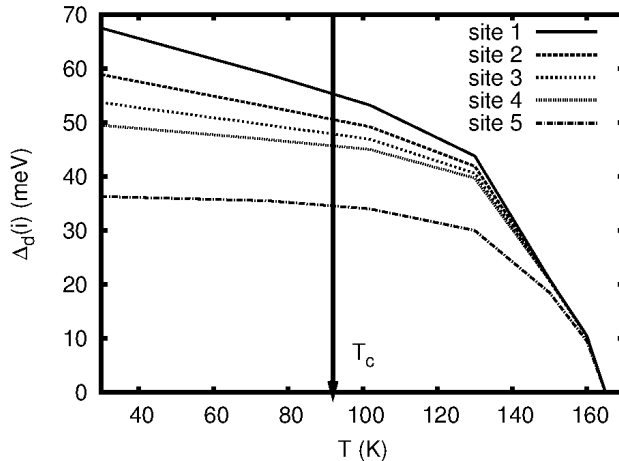


Figure 3.6: The temperature evolution of $\Delta_{\delta}(i)$ at five randomly chosen locations i of an average $\bar{\rho} = 0.15$ compound. The mean field Bogoliubov-deGennes calculations vanish at the same temperature $T^*(0.15) = 165$ K, above $T_c(0.15) = 92$ K.

3.5 Concluding remarks

In this chapter we surveyed relevant elements of the microscopic theory of superconductivity for this dissertation. The Cooper problem provided the foundation for the description of the superconducting condensate. Further, we introduced some elements of BCS theory in such a way that the formalism of Bogoliubov-deGennes could be naturally followed. The basic machinery of this chapter showed us how to determine the correct Bogoliubov equations for a given Hamiltonian. The Bogoliubov equations consist of two non-linear coupled equations that must be solved self-consistently with the definition of the gap parameters. The simulations obtained by the formalism of Bogoliubov-deGennes will integrate nicely with the experiments and theory of electronic phase separation presented in the next chapter.

Phenomenological theory of superconductivity

4.1 Introductory remarks

In this chapter we introduce the phenomenological theory of superconductivity, which will include the general Ginzburg-Landau theory of second order phase transitions, the Josephson effect, a short survey on recent experiments about the pseudogap region and intrinsic inhomogeneity of high- T_c superconductors, and a model of electronic phase separation to describe the features of copper-oxide planes of cuprates.

4.2 Ginzburg-Landau theory

The Ginzburg-Landau theory is a general approach to the theory of second-order phase transitions, that is, where the order parameter varies continuously under a phase transition. In the case of a ferromagnet, a suitable order parameter would be the magnetization. In the case of superconductivity, however, the order parameter was proposed to be the wavefunction $\psi(\mathbf{r})$, which was Ginzburg's genius choice. In the words of Tinkham, "this theory was a triumph of physical intuition" [48]. Although very successful, this theory was given limited attention because of its phenomenological foundation. This changed in 1959, when Gor'kov derived the Ginzburg-Landau theory from the microscopic BCS Theory near T_c . He showed that the order parameter ψ is essentially the same as the gap parameter Δ , except for some numerical constants [23]. This allowed to write the superconducting wavefunction as

$$\psi(\mathbf{r}) = |\Delta(\mathbf{r})|e^{i\varphi(\mathbf{r})}, \quad (4.1)$$

where φ is the phase of the superconductor. The order parameter describes the phase of matter of interest obtained by a second-order phase transition at a critical temperature T_c . In our case, the wavefunction $\psi(\mathbf{r})$ describes the macroscopic condensed superconducting state below a critical temperature T_c . Since there is no condensing of Cooper pairs in the normal state above T_c , the order parameter is assumed to obey

$$\psi = \begin{cases} 0 & T > T_c \\ \psi(T) \neq 0 & T < T_c. \end{cases}$$

This makes sense, since equation (4.1) implies that Cooper pairs with binding energy Δ only appear below T_c . The basic postulate of Ginzburg and Landau was that the superconducting free-energy density $f_s(T)$ could be expanded in terms of the wavefunction $\psi(\mathbf{r})$ as

$$f_s(T) = f_n(T) + a(T)|\psi(\mathbf{r})|^2 + \frac{b(T)}{2}|\psi(\mathbf{r})|^4 + \frac{1}{2m} \left| \left(\frac{\hbar}{i} \nabla - q\mathbf{A} \right) \psi(\mathbf{r}) \right|^2 + \frac{B^2}{2\mu_0}. \quad (4.2)$$

The first term $f_n(T)$ is the normal state free energy density, $a(T)$ and $b(T)$ are phenomenological parameters, the third term is associated with gradients in the magnitude of the order parameter and electronic transport; and the last term accounts for external magnetic influence. Note that if $\psi(\mathbf{r}) = 0$, equation (4.2) reduces to

$$f_s(T) = f_n(T) + \frac{B^2}{2\mu_0}, \quad (4.3)$$

which is simply the normal state free energy subjected to external magnetic influences. Let us examine the features of (4.2) first considering $\Delta f \equiv f_s(T) - f_n(T)$ with no gradients and no magnetic influences.

4.2.1 The phenomenological parameters

Without the last two terms of equation (4.2), we have

$$\Delta f = a(T)|\psi(\mathbf{r})|^2 + \frac{b(T)}{2}|\psi(\mathbf{r})|^4. \quad (4.4)$$

Proper inspection of this shows us that $b(T)$ must be positive if the theory is to be useful; otherwise the free energy density would have no minimum. We are left to examine the cases in which $a(T) > 0$ and $a(T) < 0$. In the first case one sees that there is one minimum for Δf at $\psi = 0$. More interestingly, in the second case, we have two minima where $|\psi|^2 = -a/b$. The parameter a plays a crucial role in the behaviour of the system. For this reason, Landau and Ginzburg assumed that $a(T) > 0$ characterizes the normal state, while $a(T) < 0$ characterizes the superconducting state.

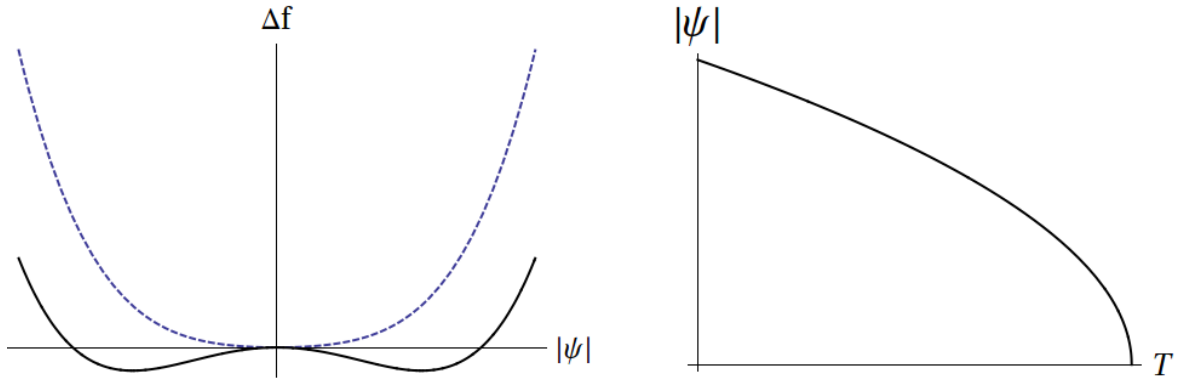


Figure 4.1: **Left** (Equation 4.4): The free energy density difference between the superconducting and the normal state. The dashed line describes the normal state in which $a(T) > 0$, admitting one minimum. The continuous line describes the superconducting state in which $a(T) < 0$ with two minima at $\pm\sqrt{\alpha(T_c - T)}/\beta$. **Right** (Equation 4.5): The order parameter magnitude $|\psi|$ as a function of the temperature in the Ginzburg-Landau model. This is worth comparing with figure 3.3.

Assuming that the parameters $a(T)$ and $b(T)$ change smoothly at the critical temperature T_c we can Taylor expand these to obtain $a(T) \approx \alpha(T - T_c) + \dots$ and $b(T) \approx \beta + \dots$. Note that both α and β are positive. Therefore, we obtain

$$|\psi|^2 = \frac{\alpha(T_c - T)}{\beta}, \quad \text{for } T < T_c. \quad (4.5)$$

This permits us to rewrite (4.4) as

$$\Delta f = -\frac{\alpha^2}{2\beta}(T_c - T)^2, \quad (4.6)$$

which means that $f_s < f_n$, as expected. Figure 4.1 shows the basic idea of phase separation used in the Cahn Hilliard theory discussed further. As one can see on the left there are two solutions with the same minimum value of the Ginzburg-Landau free energy corresponding to two equilibrium values of the order parameter.

4.2.2 The Ginzburg-Landau differential equations

Equations (4.5) and (4.6) describe our simplified model with no electronic transport and no magnetic influence. Evidently, such a model is useless for superconducting samples. For a useful theory of superconductivity we must find the minima of equation (4.2). This will yield differential equations to which one can provide appropriate boundary conditions to describe the system of interest.

Derivation

In order to minimize the free energy for the general case (4.2), we employ the method provided by functional derivatives. First we write the total free energy

$$\Delta F(T) = \int d\mathbf{r} \left(a(T)|\psi(\mathbf{r})|^2 + \frac{b(T)}{2}|\psi(\mathbf{r})|^4 + \frac{1}{2m} \left| \left(\frac{\hbar}{i}\nabla - q\mathbf{A} \right) \psi(\mathbf{r}) \right|^2 + \frac{B^2}{2\mu_0} \right). \quad (4.7)$$

Recalling the basic axiom of functional derivatives, which are

$$\frac{\delta}{\delta f(\mathbf{r})} f(\mathbf{r}') = \delta(\mathbf{r} - \mathbf{r}') \quad \text{or equivalently} \quad \frac{\delta}{\delta f(\mathbf{r})} \int d\mathbf{r}' f(\mathbf{r}') \eta(\mathbf{r}') = \eta(\mathbf{r}), \quad (4.8)$$

where both f and η are well behaved functions, we calculate the functional derivatives

$$\frac{\delta}{\delta \psi^*(\mathbf{r})} \Delta F = 0 \quad \text{and} \quad \frac{\delta}{\delta A_\nu(\mathbf{r})} \Delta F = 0, \quad (4.9)$$

that will give us the Ginzburg-Landau differential equations. The subscript ν just stands for a generic component of \mathbf{A} . After some lengthy calculations we obtain the Ginzburg-Landau differential equations:

$$a(T)\psi(\mathbf{r}) + b(T)|\psi(\mathbf{r})|^2\psi(\mathbf{r}) + \frac{1}{2m} \left(\frac{\hbar}{i}\nabla - q\mathbf{A}(\mathbf{r}) \right)^2 \psi(\mathbf{r}) = 0 \quad (4.10)$$

$$\frac{qi\hbar}{2m} (\psi^*\nabla\psi - \psi\nabla\psi^*) + \frac{q^2}{m} |\psi|^2 \mathbf{A} + \frac{1}{\mu_0} \nabla \times \mathbf{B} = 0. \quad (4.11)$$

In the second equation (4.11) we have used the fact that $\mathbf{B} = \nabla \times \mathbf{A}$. In the same equation, we can identify the current $\mu_0 \mathbf{J} = \nabla \times \mathbf{B}$ from Ampère's Law with negligible displacement current. If one wants to study the effects of a varying external magnetic field, then the displacement current must be included. We also know that the current is given by $\mathbf{J} = \rho \mathbf{v}$, where ρ is the (super)-current density. We can identify \mathbf{v} in (4.11) by rewriting it in terms of the phase φ . Therefore, we substitute $\psi = |\Delta|e^{i\varphi}$ in (4.11) to obtain

$$\mathbf{J} = \frac{q}{m} |\Delta|^2 (\hbar\nabla\varphi - q\mathbf{A}) = q|\Delta|^2 \mathbf{v}. \quad (4.12)$$

We also identify $\rho = q|\Delta|^2$. The charge unit q in superconductivity is a Cooper pair, and therefore $q \equiv 2e$.

Boundary conditions

When applying the Ginzburg-Landau theory to a superconducting sample one must provide the appropriate boundary conditions to the two differential equations established above. The two most common boundary interfaces are: the superconductor-insulator in-

terface, and the superconductor-metal interface. In the superconductor-insulator interface one must be sure that no current passes through the surface. Investigation of equation (4.12) suggests the following boundary condition

$$\left(\frac{\hbar}{i}\nabla - q\mathbf{A}\right)\Big|_n \psi = 0. \quad (4.13)$$

If one deals with a superconductor-metal interface one must generalize this to

$$\left(\frac{\hbar}{i}\nabla - q\mathbf{A}\right)\Big|_n \psi = \frac{i\hbar}{b}\psi, \quad (4.14)$$

where the value of b will depend on the nature of the material to which contact is made, approaching zero for a magnetic material, and infinity for an insulator.

4.2.3 Flux quantization

Let us study the features of a current flowing through a closed loop with no spacial extension. Since we are dealing with a loop, and the current density is given by (4.12), let us investigate the line integral $\oint_C \mathbf{dl} \cdot \mathbf{J}$. From equation (4.12) we have the condition

$$\oint_C \mathbf{dl} \cdot \left(\nabla\varphi - \frac{q}{\hbar}\mathbf{A}\right) = \oint_C \mathbf{dl} \cdot \frac{m\mathbf{v}}{\hbar}. \quad (4.15)$$

We can rewrite this as

$$\delta\varphi - \frac{q}{\hbar}\Phi = \oint_C \mathbf{dl} \cdot \frac{m\mathbf{v}}{\hbar}, \quad (4.16)$$

where $\delta\varphi$ is the change of phase of ψ after going around the loop and Φ is the magnetic flux which we identified by applying Stoke's theorem to the second term. Since the macroscopic wavefunction $\psi = |\Delta|e^{i\varphi}$ must be defined uniquely, we must have $\delta\varphi = 2\pi n$, where n is an integer. Therefore

$$\Phi = n \overbrace{\frac{\hbar}{q}}^{\Phi_0} - \oint_C \mathbf{dl} \cdot \frac{m\mathbf{v}}{q}, \quad (4.17)$$

where we have used the definition of the reduced Planck constant $\hbar = h/2\pi$. The fundamental result here is that the magnetic flux Φ is quantized in steps of Φ_0 .

4.3 The Josephson Effect

In the year of 1962, Brian David Josephson predicted that a supercurrent of the type

$$I_s = I_c \sin \Delta\varphi \quad (4.18)$$

flows between two superconductors separated by a thin barrier. Here, I_c is the maximum critical current that the junction can manage, and $\Delta\varphi$ is the phase difference of $\psi = |\Delta|e^{i\varphi}$ between the two superconductors. This phenomena was somehow expected because of the well known phenomena of quantum tunnelling. It was a remarkable prediction since I_s maintains itself with no potential difference across the junction. Josephson predicted that if a potential difference ΔV were maintained, then $\Delta\varphi$ evolves according to

$$\frac{d}{dt} \Delta\varphi = \frac{q}{\hbar} \Delta V, \quad (4.19)$$

with $q \equiv 2e$. In this case the supercurrent would have the form

$$I_s = I_c \sin (\Delta\varphi + \nu t), \quad (4.20)$$

which is an alternating current of amplitude I_c and frequency $\nu = q\Delta V/\hbar$. These two cases, (4.18) and (4.20) are respectively known as the dc and ac Josephson effects.

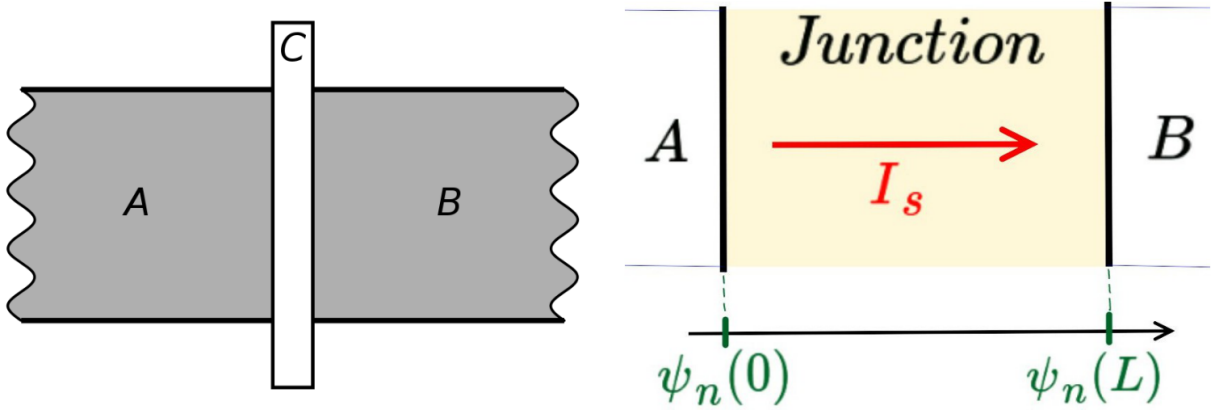


Figure 4.2: **Left:** Diagram of a single Josephson junction. A and B represent superconductors, and C the weak link between them. **Right:** Boundary conditions of the junction as described by equation (4.24).

The barrier (junction) could be insulating, metallic, or another "weak link" of a different nature. In the high- T_c superconductors, a simple grain boundary can serve as a weak link because these materials have such short coherence lengths. One can calculate the electrical free energy stored in the junction. Using equation (4.20) we calculate

$$F = \int_0^t dt' I_s \Delta V = E_J [\cos \Delta\varphi - \cos (\Delta\varphi + \nu t)], \quad (4.21)$$

where $E_J \equiv \hbar I_c / q$ measures how strongly the two phases are coupled through the weak link. Note that the free energy F is minimum when the two phases are equal.

4.3.1 Deriving the Josephson equations

Here we derive the equations presented above from the Ginzburg-Landau theory introduced in the previous section. To do so, we first define a conveniently normalized wave function $\psi_n = \psi / \psi_m$, where ψ_m is the wavefunction describing a stable superconducting state with minimized free energy, that is, $|\psi_m|^2 = -a/b$, where $|\psi_n|^2 = 1$. Now we rewrite the first Ginzburg-Landau differential equation (4.10) in terms of ψ_n considering ψ real to obtain

$$\left(\frac{\xi}{i} \nabla - q \mathbf{A} \right)^2 \psi_n + \psi_n - \psi_n^3 = 0, \quad \text{with} \quad \xi = \frac{\hbar}{\sqrt{2ma}}. \quad (4.22)$$

The quantity ξ is called the *coherence length*. In order to simplify the discussion further we assume uniformity over the cross section A of the junction. Therefore, we can treat our junction in one dimension with length L . With this, the last equation becomes

$$\left(\frac{\xi}{i} \frac{d^2}{dx^2} - qA(x) \right)^2 \psi_n + \psi_n - \psi_n^3 = 0. \quad (4.23)$$

We can assume that both left and right superconductors connected by the junction are in equilibrium with minimized energy, but may have different phases (see right figure 4.2). Therefore, the boundary conditions for equation (4.23) are

$$\psi_n(0) = 1 \quad \text{and} \quad \psi_n(L) = \exp i \left(\Delta\varphi - \frac{2\pi}{\Phi_0} \int_0^L dl A(x) \right). \quad (4.24)$$

In the second boundary condition at $x = L$ we have absorbed the influence of \mathbf{A} into the wavefunction. See reference [35] for a review on this. Further, if $L \ll \xi$, then the term with ξ^2 dominates over all the others. Thus, the differential equation (4.23) reduces to Laplace's equation $d^2\psi_n/dx^2 = 0$, for which the most general solution is $\psi_n = a + bx$. Applying the boundary conditions (4.24) we obtain the solution

$$\psi_n = \overbrace{\left(1 - \frac{x}{L}\right)}^{\text{left}} + \overbrace{\frac{x}{L} \exp i \left(\Delta\varphi - \frac{2\pi}{\Phi_0} \int_0^L dl A(x) \right)}^{\text{right}}. \quad (4.25)$$

We finally use the second Ginzburg-Landau differential equation (4.11) to obtain

$$I_s = I_c \sin \left(\Delta\varphi - \frac{2\pi}{\Phi_0} \int_0^L dl A(x) \right) \quad \text{where} \quad I_c = -\frac{q\hbar a A}{m b L} > 0. \quad (4.26)$$

Let us examine what happens if we apply a constant electric field E_0 in the x direction. From the electromagnetic relation $\mathbf{E} = -\partial\mathbf{A}/\partial t$ we have that $A(x) = -E_0 t$. Substituting this into equation (4.26) we have

$$I_s = I_c \sin \left(\Delta\varphi + \frac{2\pi}{\Phi_0} \Delta V t \right), \quad (4.27)$$

where $\Delta V \equiv LE_0$. This equation is precisely the same as (4.20). Observe that a static (dc) electric field has produced an alternating (ac) current.

4.4 Intermission – experimental survey

Before presenting the theory of electronic phase separation, we shortly survey some of the most prominent experiments on the pseudogap and electronic inhomogeneities of high- T_c superconductors.

4.4.1 Evidence for the pseudogap from ARPES

Simply put, Angle-resolved photoemission spectroscopy (ARPES) is a direct experimental technique to observe the charge distribution in \mathbf{k} -space of solids. It is one of the most effective methods, until now, to study the electronic structure of the surface of solids. This technique is regarded as a refinement of the ordinary photoemission spectroscopy. It has shown itself very useful to study cuprates, because it yields the energy and momentum of the filled electronic states below the Fermi surface. This makes it possible to analyse the copper-oxide planes of cuprates, which is the main locus of superconductivity in these materials.

Figure 4.3 illustrates several measurements performed along the red line in the Brillouin zone that trespasses the Fermi surface as depicted in (c). The graphs show the probability of extracting an electron as a function of the energy. The gap, with zero probability around the Fermi energy is clearly visible.

4.4.2 Evidence for inhomogeneity

In this section we wish to describe the inhomogeneity (disorder) observed in high- T_c superconductors by many experiments. There is substantial evidence from many experiments on different materials that support the existence of intrinsic inhomogeneities. We list the most important experiments below:

- Neutron diffraction [49, 6];
- Muon spin relaxation [43];

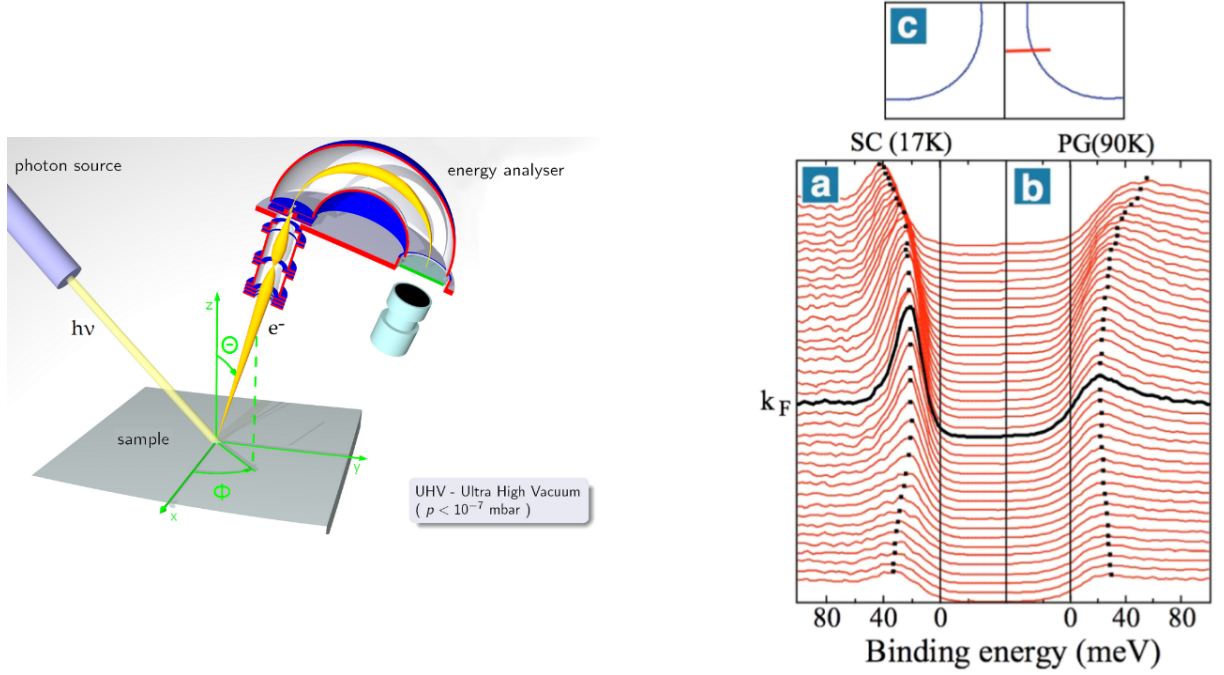


Figure 4.3: **Left:** An experimental setup of ARPES. **Right:** ARPES measurements through the Fermi surface (c) of a film of Bi2212 showing the superconducting gaps defined by the dots in (a) and (b) [27].

- Nuclear quadrupole resonance [42];
- Nuclear magnetic resonance [37];
- Scanning tunnelling microscopy (STM) measured spatial variations of the gap amplitude $\Delta(\vec{r})$, which is possibly related to the charge inhomogeneities [33, 22, 39];
- Angle resolved photon emission spectroscopy (ARPES) found a large anisotropy in \mathbf{k} -space [12, 28];
- Electronic Raman scattering showed that the nodal gap is connected with T_c and the antinodal gap with the pseudogap temperature T^* [24].

Below we summarize the most important features of some of these experiments.

Neutron diffraction

This experimental technique is an application of neutron scattering to determine the atomic and magnetic structure of a material. The sample to be analysed is placed in a beam of neutrons to obtain a diffraction pattern that provides information of the material's structure. The technique is similar, but more powerful than X-ray diffraction. Recent measurements have detected small variations in the diffraction signals that were interpreted as small variations in the charge distributions around the ions in the copper-oxide planes of the $\text{La}_{2-x}\text{Sr}_x\text{CuO}_4$ series. Bozin et. al. [7] reported local structural

evidence that supports the fact that the charges are inhomogeneous in the underdoped and optimally doped region of the $\text{La}_{2-x}\text{Sr}_x\text{CuO}_4$ phase diagram, consistent with the presence of charge domains or dynamic charge stripes.

In this context, stripe configurations were discovered [49]. Stripes are linear segments that lack holes. In the regions with high density of charges, anti-ferromagnetic order is destroyed and these distinct regions remain separated by barriers, which are periodically spaced. See figure 4.4.

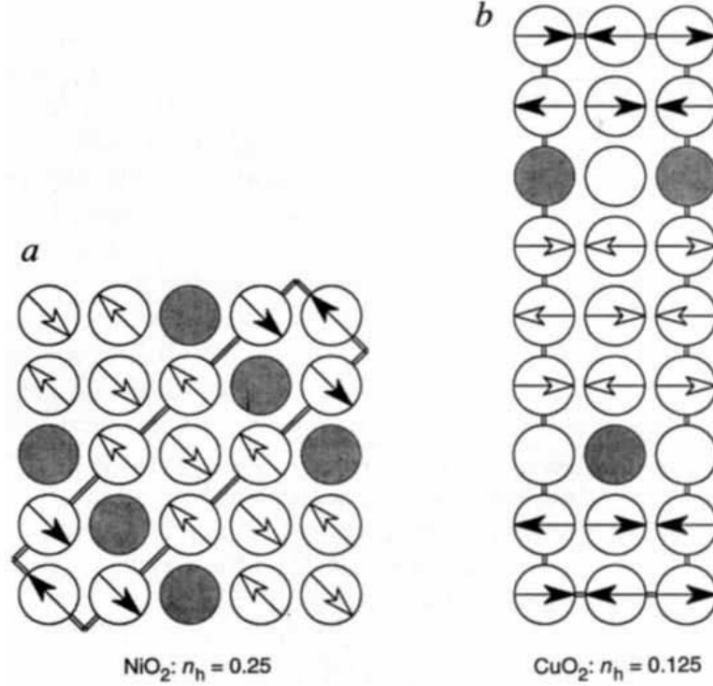


Figure 4.4: **Left:** Idealized diagram of the spin and charge stripe pattern within a Ni_2 plane observed in hole doped La_2Ni_4 with the hole density of 25%. **Right:** Hypothesized stripe pattern in a copper-oxide plane of hole doped oxygen atoms, which surround the metal sites in a square planar array. Arrows indicate the orientation of magnetic moments on metal atoms, which are locally anti-parallel.

The discovery of stripe configurations had a major impact and was confirmed by other research groups [6].

Nuclear quadrupole resonance

Singer et. al. [42] reported experimental evidence for the spatial variation of hole concentration of under-doped compounds (x_{hole} in their notation) in the high- T_c superconductor $\text{La}_{2-x}\text{Sr}_x\text{CuO}_4$ ($0.04 \leq x \leq 0.16$). They showed that the variation Δx_{hole} increases below 500 K. Moreover, this experiment is capable to estimate the length scale of the spatial variation of the hole concentration.

This experiment is important because it probes the spatial inhomogeneity at short length scales in the copper-oxide planes. Most of the theoretical debates rely on the

assumption that holes are homogeneously doped in the copper-oxide planes of cuprates. We already saw that the stripe configurations of the previous section [49] is a strong and widely accepted counterexample. The importance of quadrupole resonance is that it provided an independent, accurate and more general evidence for intrinsic electronic inhomogeneity. It determines the inhomogeneity of the charge density as a function of the temperature. They measure a nuclear resonance frequency of nucleons that is unique if the nucleon's neighbours are of the same kind (electrons). If the neighbourhood changes, the frequency varies – indicating surrounding charge inhomogeneities.

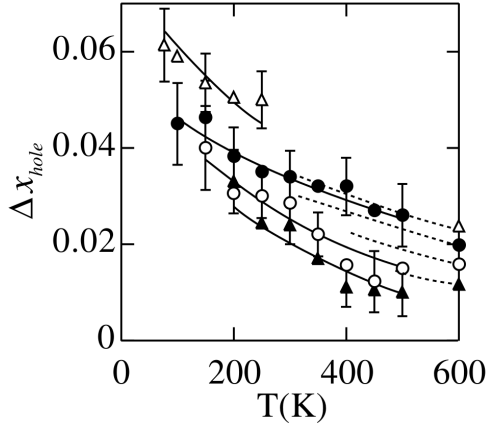


Figure 4.5: Temperature dependence of the distribution in local hole concentration Δx_{hole} as deduced by ^{63}Cu nuclear quadrupole resonance in $\text{La}_{2-x}\text{Sr}_x\text{CuO}_4$ [(\blacktriangle) $x = 0.04$, (\circ) $x = 0.07$, (\bullet) $x = 0.115$, (\triangle) $x = 0.16$].

Contrary to common assumptions that doped holes are uniformly distributed (i.e. $\Delta x_{\text{hole}} = 0$), figure 4.5 shows that $\Delta x_{\text{hole}} \neq 0$ exists at all temperatures in the graphs range. Also, the nuclear quadrupole resonance spectrum is consistent with our theory of phase separation, where the spatial variation in x_{hole} takes the form of patches in the copper-oxide plane. Some of these patches are metallic, and other are insulating in character. This experiment indicates a temperature dependent electronic phase transition occurring in high- T_c superconductors, which is an essential assumption for this dissertation.

Scanning tunnelling microscopy

A scanning tunneling microscope (STM) images surfaces at atomic precision. Good STM precision is held to be around 0.1 nm, which means that individual atoms can be mapped and manipulated. The basic principle used by the microscope is quantum tunneling that permits to map the local density of states of a superconducting sample. Observe the gap measurements over a sample of $\text{Bi}_2\text{Sr}_2\text{CaCu}_2\text{O}_{8+x}$ on the 50 nm copper-oxide square planes in figure 4.6. These images help us elucidate how the microscopic electronic inhomogeneity is distributed on the planes, which is a fundamental problem for high- T_c superconductivity. Beyond that, McElroy et. al. [33] showed how the electronic distribu-

tion evolves upon doping. Many STM experiments confirmed a check-board like charge order in strongly correlated superconducting $\text{Bi}_2\text{Sr}_2\text{CaCu}_2\text{O}_{8+x}$ [38, 33, 22]. These experiments reported the presence of electronic inhomogeneity that is manifested as spatial variations in both the local density of states spectrum and the superconducting gap amplitude. Moreover, they show that their data suggests that the measured inhomogeneity is not due to crystallographic errors or impurities; but rather indicates a universal behaviour of cuprates. This was confirmed after repeating the experiment over different samples. These STM studies show two important aspects:

1. The inhomogeneity in the local density of states is present from underdoped to overdoped compounds;
2. Local gaps vary substantially with doping.

Furthermore, they reported a strong spatial correlation between the local density of states (LDOS) and the superconducting gap by observing the similar patterns in each map. Recent STM experiments [33] provided important informations regarding the evolution of a Mott insulator into a d-wave superconductor under doping.

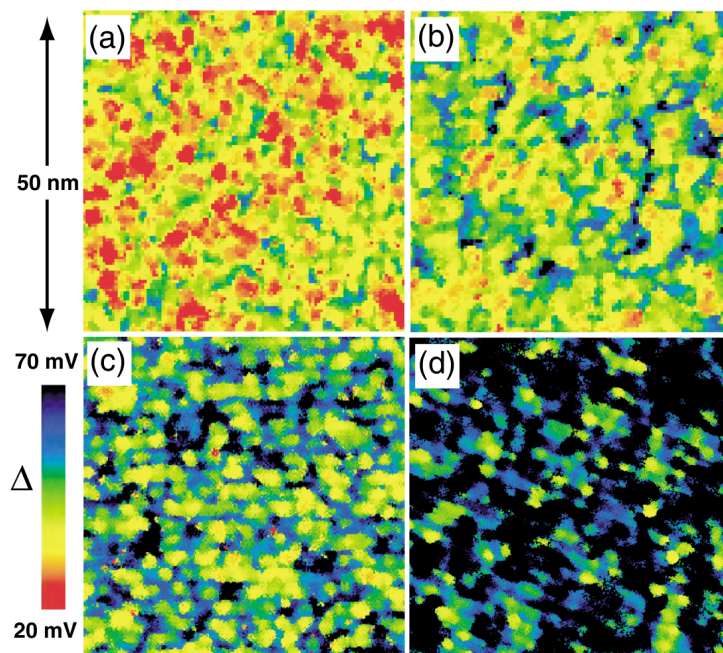


Figure 4.6: Measured $\Delta(\mathbf{r})$, gap maps, of four different hole dopings: (a) 89 K with $\rho = 0.19$; (b) 79 K with $\rho = 0.15$; (c) 75 K with $\rho = 0.13$; and (d) 65 K with $\rho = 0.11$ [33].

4.5 Theory of electronic phase separation

In this section we present a model of electronic phase separation to describe the features of the copper-oxide planes of cuprates. This model considers the two anomalous characteristics of cuprates: the anti-ferromagnetic normal phase with pseudogap regions, and the intrinsic electronic inhomogeneity.

4.5.1 Cahn-Hilliard theory of phase separation

To simulate the STM measurements shown in the last section, Mello et. al. [16] introduced a model of phase separation based on the theory of Cahn-Hilliard [9]. As we mentioned in Section 4.2.1, this theory is based on the Ginzburg Landau expansion (4.2) and the two minima in the free energy corresponding to two phases as shown in figure 4.1 and in the inset of figure 4.7. They showed that the potential responsible for the second order electronic phase separation, also generates an effective interaction between the charges responsible for superconductivity at high temperatures. Similarly to the Ginzburg-Landau theory, there should appear a local potential that separates the charge densities into two regions: one with low and another with high density of electrons per unit cell. Therefore, the charges are segregated into specific regions – the grains – and the potential barrier generates an effective attraction between the charges in a single grain – originating a stable superconducting amplitude throughout the grain.

As we saw in figure 1.2, cuprates with a low hole concentration have the antiferromagnetic phase destroyed with the insulator-metal transition, which completely changes the electronic transport properties. There are two possibilities for a doped cuprate: it presents a homogeneous charge distribution, or inhomogeneous with metallic domains in a anti-ferromagnetic background. According to several experiments, the second case is more likely [49, 6, 43, 42, 37, 33, 22, 39, 12, 28]. Mello et al [15] showed that the free energy of the inhomogeneous system is lower than the homogeneous one when the temperature is lower than the pseudogap curve $T^*(x)$. The lower free energy of the inhomogeneous distribution provides a physical interpretation for the origin of the thermodynamic electronic phase separation. In order to quantify the regions with different dopings as a function of the temperature, we employ a suitable framework for phase separations – the Cahn-Hilliard theory [9, 16].

Calculation procedure

In order to introduce a quantitative parameter – the order parameter – of our second order phase transition, we define the variation in the charge density in the site i of the square lattice as

$$u = \Delta\rho(i, T) \equiv \frac{\rho(i, T) - \bar{\rho}}{\bar{\rho}}, \quad (4.28)$$

where u is our order parameter, $\rho(i, T)$ is the local density of holes, and $\bar{\rho}$ is the average density of the compound. Clearly $|u| \leq 1$. The case with $u(i, T) = 0$ corresponds to a homogeneous system above the phase separation temperature $T_{\text{PS}}(\rho)$. Then, the typical Ginzburg-Landau free energy functional, in analogy to equation (4.2) with no external magnetic, can be written as

$$f[u] = \overbrace{\frac{A^2(T)}{2}u^2 - \frac{B^2}{4}u^4}^{V[u]} + \frac{1}{2}\epsilon^2|\nabla u|^2, \quad (4.29)$$

where $V[u]$ is the potential responsible for the origin of Cooper pair formation in cuprates. The form of the phenomenological constants were so defined for convenience. We Taylor expand the phenomenological parameter A^2 to give

$$A^2(T) \approx \alpha (T_{\text{PS}}(\rho) - T), \quad (4.30)$$

where now α and B are constants that lead to lines of fixed values of $A(T)/B$, parallel to $T_{\text{PS}}(\rho)$, as shown in figure 4.7. The parameter ϵ determines the size of the grain boundaries between the low and high density phases. The energy barrier between the grains of distinct phases is $E_g(T) = A^4(T)/B$, which is proportional to $(T_{\text{PS}} - T)^2$ near the transition, and becomes nearly constant for temperatures close to $T_{\text{PS}}(\rho)$.

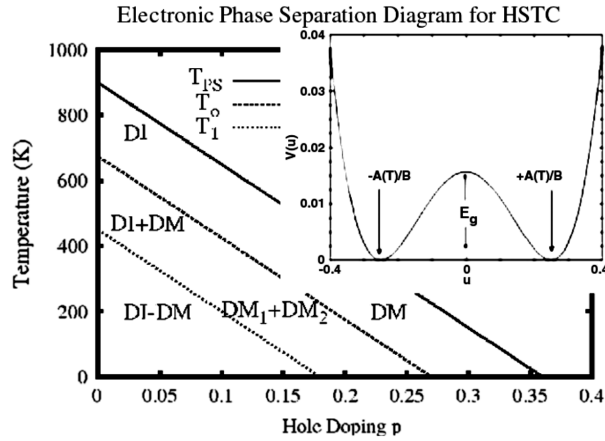


Figure 4.7: Electronic phase diagram for cuprates. The temperature $T_{\text{PS}}(\rho)$ marks the onset of phase separation into two main densities corresponding to the two minima of the Ginzburg-Landau potential. As the temperature decreases below $T_{\text{PS}}(\rho)$, the potential barrier E_g increases and the two minima $\pm A(T)/B$ separate from each other.

Following the Ginzburg-Landau equation (4.29) and the order parameter in (4.28), Cahn-Hilliard [9] derived a differential equation that governs the phase separation of the system from a homogeneous state $u = 0$ into two phases with $u = \pm A(T)/B$. This can be elegantly achieved in terms of a continuity equation $\partial_t u + \nabla \cdot \mathbf{J} = 0$, because the total number of charges is fixed, the volume integral over the charge density distribution is

fixed. Therefore, we identify the current density as

$$\mathbf{J} = M\nabla \left(\frac{\delta f}{\delta u} \right), \quad (4.31)$$

where M is the mobility or the charge transport coefficient. With this, we obtain

$$\frac{\partial u}{\partial t} = -M\nabla^2 (\epsilon^2 \nabla^2 u + A^2(T)u - B^2 u^3), \quad (4.32)$$

which is called the Cahn-Hilliard equation.

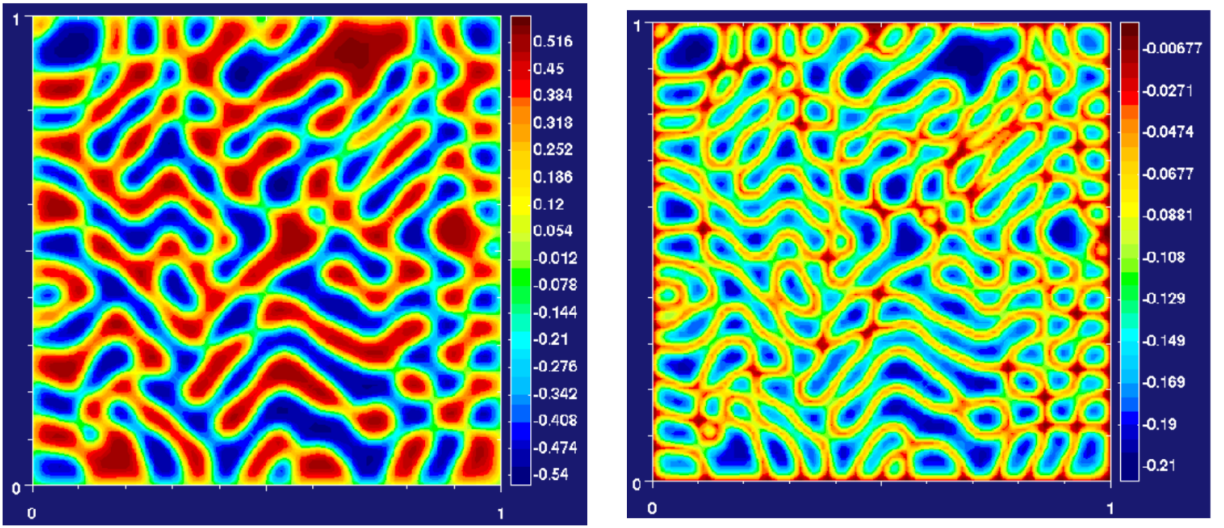


Figure 4.8: **Left:** The charge density on a 105×105 square lattice system after 6400 time steps. The fraction $A(T)/B = 0.6$, which corresponds to values of T close to the line T_1 plotted in figure 4.7 – with $0.05 < \rho < 0.18$. The dark blue grains are in the verge of becoming insulators (low density) and the red ones have metallic character (high density). **Right:** Density profile of the local free energy in the same location and temperature as in the left figure. The red lines show the potential barrier between the grain boundaries. The system becomes a mixture of two disordered metals with high and low densities (DM1+DM2).

Equation (4.32) is numerically solved, which is well described by Mello in [18]. The Cahn-Hilliard approach provides a quantitative approach to describe the motivated electronic phase separation, which in turn is capable to explain many features of the pseudogap phase of cuprates. A central point of this approach is that the free energy potential of segregation or confining $V[u]$ is the dominant factor of the creation of Cooper pairs in cuprates. This idea is based in experiments on Bi cluster [50].

4.6 Concluding remarks

We analysed different experimental techniques which support the case for intrinsic inhomogeneous high- T_c superconductors. Nuclear quadrupole resonance [42] in particular, suggests a temperature dependent electronic phase separation [18] as the mechanism behind the inhomogeneities. According to this, the charges are segregated into specific regions called grains. This generates low and high density regions separated by a thin potential barrier. A typical simulation of the potential responsible for the segregation of charges is depicted in figure 4.7.

As discussed by Ginzburg-Landau and Cahn-Hilliard, the phase separation process is caused by the two minima of the free energy corresponding to two phases [18]. In a real system this corresponds to the segregation of the electronic charges in low and high density domains, or islands bounded by free energy barriers. The formation of these isolated islands, where the charges are confined in nanometre domains, favours the development of a sustainable superconducting amplitude. This is analogous to a granular superconductor. The difference is that instead of impurities assuming the role of grains, the local charge densities act as grains. These little charge islands, the grains, may be weakly connected with the other grains. The barriers act as "weak links" and the system resembles a granular superconductor with very small grains. These little charge islands can be modelled by Josephson junctions. As a consequence, one models the whole sample as a network of Josephson junctions [34].

This chapter laid the relevant elements of the phenomenological theory describing superconductors. The basic model proposed in chapter five relies on the Josephson mechanism. The phenomenological character of the Ginzburg-Landau permits a relatively intuitive interpretation of the Josephson effect. The ideas developed in this chapter will be useful in understanding chapter five.

Ferromagnetism in high temperature superconductors

In this chapter we use the model for high- T_c superconductors developed in the last chapter to describe the weak ferromagnetic signal observed in some compounds of the YBCO family.

5.1 Introductory remarks

Understanding the "normal" state pseudogap phase of high- T_c superconductors endures as a major problem in condensed matter physics. The reason is the existence of localized energy gaps above T_c and below a certain temperature T^* that marks the crossover temperature of the pseudogap phase. The lack of a largely accepted theory persists because of the nanoscale complexity and intrinsic inhomogeneous electronic distributions that vary according to specific families of cuprates [11].

Many anomalies are present in the normal pseudogap phase that are not understood, which do not have a widely accepted explanation. Here we address the spontaneous weak ferromagnetic signal observed in $\text{YBa}_2\text{Cu}_3\text{O}_{6+x}$. Such measurements were made by sensitive experiments, namely zero-field muon spin relaxation (μSR) [44] and polar Kerr-effect (PKE) [52]. Both experiments identify a hole concentration ρ dependent signal T_s that agrees closely with the crossover values of $T^*(\rho)$ from many experiments [47, 30]. In figure 5.1, the authors of [52] identify that the signal T_s is much larger than T_c in the underdoped region, but decreases rapidly with increasing ρ , and becomes smaller than T_c near the optimally doped concentration which is $\rho = 0.16$. It is worth noting that ρ is a monotonic function of the oxygen concentration x .

In this dissertation, we attempt to reproduce the measured signals from references [44] and [52] from theoretical grounds.

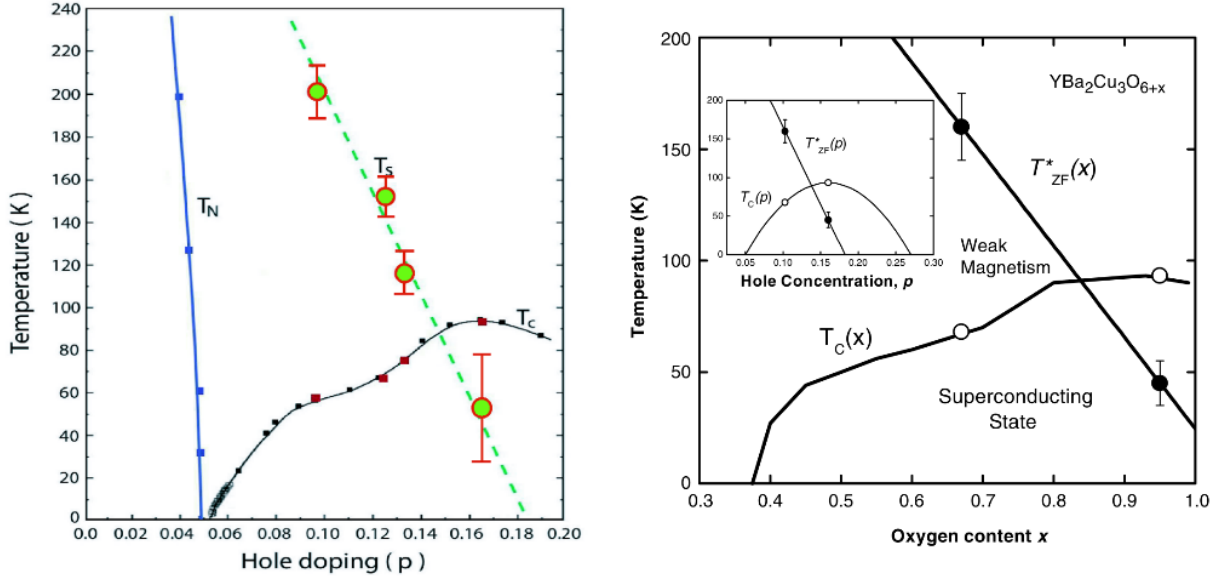


Figure 5.1: **Left:** The onset of the polar Kerr-effect signal T_s in circles and T_c as red squares for $\text{YBa}_2\text{Cu}_3\text{O}_{6+x}$ samples [52]. **Right:** The same behaviour is confirmed by zero field muon spin relaxation [44].

5.2 Paramagnetic effect in cuprates

After its discovery, high- T_c superconductors were in the form of powder and only more recently single crystals large enough to be measured were synthesized. The powders were formed by grains of typically micrometers in diameters. Therefore, early susceptibility measurements in cuprates discovered an unusual weak paramagnetic response, also called Wohllenben effect [41]. Sigrist and Rice [41] explained that this effect is due to the random crystal orientations of the many grains and the d-wave symmetry of the superconducting order parameter. Neighbour grains form weak links and are connected by Josephson coupling that depends on the relative phase of the superconducting wave function. The combination of crystal orientation and superconducting phase may lead to what is known as a π -junction.

The π -junction

Simply defined, a π -junction is a Josephson junction with a negative critical (coupling) current. In equation (4.18) the super-current threading the junction was described by a strictly positive critical current, that is, $I_s = |I_c| \sin \Delta\varphi$. Since, by definition, the Josephson coupling in a π -junction is negative, we write $I_s^\pi = -|I_s| \sin \Delta\varphi$, which is the super-current for a π -junction. This can be equivalently written as

$$I_s^\pi = |I_s| \sin(\Delta\varphi - \pi), \quad (5.1)$$

which is simply a Josephson junction with a π -shift in the phase. Therefore, the name π -junction is justified in contrast to the regular (Josephson) 0-junction.

Standard granular superconductors are often modelled as a network of 0-junctions. Good coupling between the sample's grains guarantees the percolation of superconductivity throughout the whole granular sample. If we consider that each grain i is described by a phase φ_i , a simplified model for the Hamiltonian of such a network would be

$$\mathcal{H} = - \sum_{i,j} |E_{ij}| \cos(\varphi_i - \varphi_j). \quad (5.2)$$

Such a system is unfrustrated, and the lowest energy state is for φ_i constant throughout all i , minimizing the energy of all junctions simultaneously. One way to frustrate this network would be to apply an external magnetic field. The the phase φ_i is subject to gauge effects:

$$\varphi_i - \varphi_j \longrightarrow \varphi_i - \varphi_j - \frac{2\pi}{\Phi_0} \int_i^j \mathbf{dl} \cdot \mathbf{A}. \quad (5.3)$$

In such a system, there is a phase shift (not necessarily π) induced by the vector potential \mathbf{A} , and the energy cannot be minimized for each junction independently and is frustrated.

However, in the case of powder-like high- T_c superconductors this is not the case. Since Sigrist and Rice already supposed the pairing wavefunction to be of the d-wave type, measurable consequences should arise. In ordinary s-wave grain boundaries, electrons tunnel perpendicularly through the junction. Nevertheless, the Josephson tunnelling is a direction sensitive effect. This means that for d-wave twin boundaries, the strength of Josephson tunnelling will depend on a weighted average over the d-wavefunction, weighted in favour of electronic momenta in this perpendicular direction. Sigrist and Rice showed that such a twin boundary, as shown in figure 5.2, generates a π -junction. The internal angular structure of the pair wavefunction leads to intriguing new effects. We will discuss the π -junction and its connection with frustration effects in more detail in section 5.4.

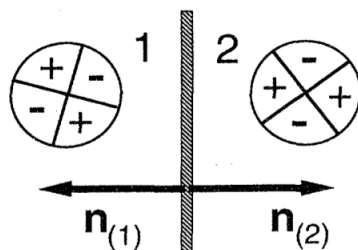


Figure 5.2: Josephson junction between two d-wave superconductors. The circles show the orientation of the crystal lattice and the pair wave function $\psi(\mathbf{k}) \propto \cos k_x - \cos k_y$ on both sides of the junction. This example corresponds to a π -junction.

Thus it is possible that this weak paramagnetic effect in the magnetic susceptibility is associated to frustration of the Josephson network [41]. In ordinary granular super-

conductors, frustration of the Josephson network arise due to the misorientation of the crystal axis with respect to the d-wave order parameter. Sigrist and Rice [41] demonstrated this frustration through a simplified model in an array of π -junctions, which are a direct consequence of d-wave symmetry. These π -junctions give a negative contribution to the junction's energy because of the phase shift π . In this case the current is negative. They also showed that there is no way to minimize the free energy of all junctions in an array of an odd numbers of junctions. Therefore, an array of odd π -junctions is frustrated, and a spontaneous current may arise if the coupling is sufficiently strong.

5.3 Phase fluctuations

We cannot apply the ideas above about paramagnetism to our Josephson network of grains of low or high local densities because they are formed in single crystals and consequently all these grains have the same crystal orientation. In this context, π -junctions cannot be generated by the mechanism described by Sigrist and Rice [41]. However, there is another mechanism particular to electronic inhomogeneities that leads to a negative Josephson coupling (a π shift).

We saw in section 3.2.6 that the number operator N is the conjugate variable to the phase φ , such that $[N, \varphi] = 1$. A specific region \mathcal{R} is characterized by a phase angle $\varphi_{\mathcal{R}}$, and its dynamically conjugate variable $N_{\mathcal{R}}$ [19, 1]. The "stiffness" of the system to phase fluctuations is determined by the local density of charges; the smaller the superfluid density, the more significant the phase fluctuations. In our case the isolated grain islands are characterized by low charge densities, and hence the local phase fluctuates substantially. Spivak and Kivelson showed that large fluctuations in the local densities lead to a negative Josephson coupling [45]. They considered the case of two Josephson-coupled grains. The Josephson current is guaranteed to be positive in the absence of spin-orbit coupling. However, if the electron tunneling is indirect, through a localized state between the grains (the junction), the transfer Hamiltonian can be modelled by

$$\mathcal{H}_T = \sum_{j=1,2} \sum_{k,s} T_k(j) \left(c_{k,\sigma}^\dagger(j) c_\sigma(I) + c_\sigma^\dagger(I) c_{k,\sigma}(j) \right) + \epsilon_0 n_0 + U, \quad (5.4)$$

where $c_{k,\sigma}^\dagger(j)$ creates an electron with spin σ and other quantum numbers represented by k on grain j which assumes the values 1 or 2. The other operator $c_\sigma^\dagger(I)$ creates an electron of spin σ in the junction which is the localized intermediate state. The number $n_0 = 0, 1$ or 2 is the number of electrons in the junction. $T_k(j)$ is the hopping matrix element, ϵ_0 is the energy of the junction, and U is a very large interaction energy. Spivak and Kivelson assumed that $T_k(j)$ is a small perturbation. By using perturbation theory up to fourth order, they showed that correlation effects produce a negative Josephson coupling J across the junction – a π -junction. We can demonstrate the appearance of the negative sign using

arguments from second quantization, that is, from the ant-commutation relations. In one of the figures of [45], Spivak and Kivelson show the tunneling process from one grain to another, mediated by the junction. We reproduce a similar table in 5.3.

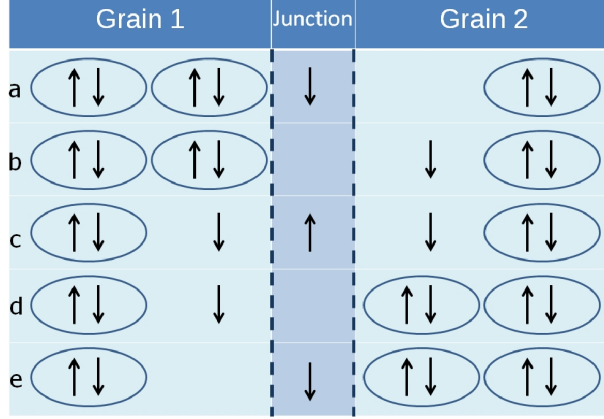


Figure 5.3: A schematic example of a sequence of intermediate states for a Cooper pair tunnelling across a barrier that contains a spin up and leads to a negative coupling along the junction. Between steps c and d it is necessary to permute the two electrons to be in canonical order of a pair, and this exchange is responsible for the negative sign [45].

In summary, the electronic phase separation generates regions with strong fluctuations in the charge densities due to $[N_{\mathcal{R}}, \varphi_{\mathcal{R}}] = 1$, which generate π -junctions. We explore the mechanism of π -junctions better in the next section.

5.4 Spontaneous frustration

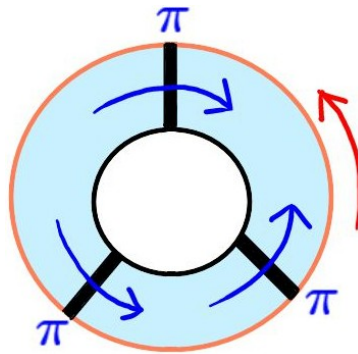


Figure 5.4: Superconducting loop with three π -junctions. If there were only two junctions, the system would manage to minimize the overall free energy and no current would arise. With an odd number of junctions (three in this case) the system is frustrated and the overall effect of one junction generates a spontaneous current around the loop.

We saw in equation (4.21) that the free energy of a junction of two coupled superconductors is proportional to $-\cos \Delta\varphi$, where $\Delta\varphi$ is the phase difference between the two superconductors. In our case, these two superconductors are grains. These two grains

are connected by a π -junction through the strong fluctuations in the charge densities. Thus, the electrical free energy stored in this junction is proportional to $-\cos(\Delta\varphi - \pi)$. Nevertheless, the fact that the weak link is a π -junction does not lead to any special observable effects. Let us explain that. The phases of both grains would simply manage to minimize the junction's free energy by setting $\Delta\varphi = \pi$. We cannot measure the existence of a π -junction directly. It merely is equivalent to a phase change in one of the grains by π , such that one would return to a normal 0-junction.

However, measurable consequences arise in multiply connected geometries, for instance, an array of π -junctions. The phase change transmitted along the array by the π -junctions will be noticed. In the case of a loop with three connected grains, that is, grain one is connected with grain two, grain two with grain three, and grain three with grain one, there is no way to remove all three π -junctions. At least one π -junction has to survive. Therefore, a loop of connected grains is frustrated and may produce spontaneous currents! See figure 5.4.

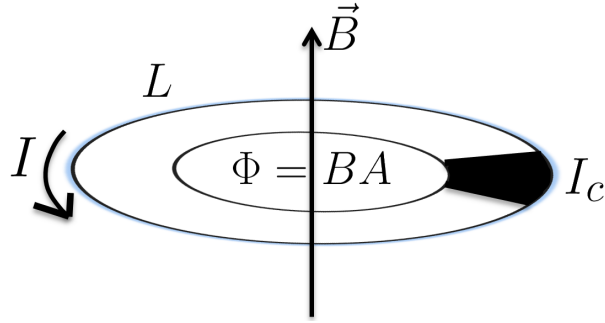


Figure 5.5: The simplest model for a frustrated loop with a single junction.

Sigrist and Rice [41] analysed the simplest case of frustration and spontaneous currents in multiply connected geometries. Consider a single loop with a single junction see figure 5.5. This could be the idealization of a loop with many strong and just one rather weak junction. As the weakest link, it will determine the properties of the whole loop. We assume that the current I that flows through the loop is $I \ll I_c$. Inspired on equation (4.21) we can write the loop's electrical free energy as

$$F(I, \Delta\varphi) = \underbrace{\frac{1}{2}LI^2}_{\text{Current}} - \underbrace{\frac{\Phi_0 I_c}{2\pi} \cos(\Delta\varphi - \pi)}_{\pi\text{-Junction}}, \quad (5.5)$$

where L is the self-inductance of the loop and I_c is the critical current tolerated by the junction. Note that the Josephson coupling energy $E_J = \Phi_0 I_c / 2\pi$ is exactly the same as in (4.21) but written in terms of the flux quantum Φ_0 . The relation between the phase difference $\Delta\varphi$ and the current I can be found from equation (4.15) which reads

$$\oint_C d\mathbf{l} \cdot \left(\nabla\varphi - \frac{2\pi}{\Phi_0} \mathbf{A} \right) = \oint_C d\mathbf{l} \cdot \frac{m\mathbf{v}}{\hbar}. \quad (5.6)$$

The path C is deep enough inside the superconductor so that the velocity \mathbf{v} vanishes due to the Meissner screening effect. Therefore equation (5.6) gives

$$\Delta\varphi = \frac{2\pi}{\Phi_0} \Phi = \frac{2\pi}{\Phi_0} (\Phi_{ex} + LI). \quad (5.7)$$

We have used Stoke's theorem for the second term on the left hand side of (5.6) and identified the magnetic flux. Substituting this back to equation (5.5) we obtain an explicit expression for the electrical free energy in terms of the current. This reads

$$F(I, \Delta\varphi) = \frac{1}{2}LI^2 - \frac{\Phi_0 I_c}{2\pi} \cos\left(\frac{2\pi}{\Phi_0} (\Phi_{ex} + LI) - \pi\right). \quad (5.8)$$

In order to obtain an equation that relates the current threading the loop with an external magnetic influence Φ_{ex} we minimize $F(I, \Delta\varphi)$ with respect to I for a given Φ_{ex} . This gives us

$$\gamma + \gamma_c \sin\left(2\pi\frac{\Phi_{ex}}{\Phi_0} + \gamma - \pi\right) = 0, \quad (5.9)$$

where the dimensionless parameters γ and γ_c are given by

$$\gamma_{(c)} = 2\pi\frac{LI_{(c)}}{\Phi_0}. \quad (5.10)$$

The parameter γ is proportional to the current I passing through the loop, and γ_c is a parameter that is proportional to the critical current I_c tolerated by the π -junction. We are interested in the case where $\Phi_{ex} \approx 0$ because the contribution from the other loops should be small. From figure 5.6 it is possible to see that for $\gamma_c > 1$, spontaneous currents arise. The onset of spontaneous currents, a consequence of frustration, may be the reason for the appearance of the ferromagnetic signal. Therefore we restate this dissertation's main point: ***the low electronic density of the grains in conjunction with correlation effects, produce a negative Josephson coupling that provokes spontaneous frustration.***

As the dimensionless parameter γ_c increases above one, a spontaneous current flows around frustrated loops producing weak local magnetic signals. The first few spontaneous currents that arise in the sample generate a magnetic field that will dictate the direction of the adjacent currents. Therefore, there will be several small local inhomogeneous ferromagnetic signals throughout the sample that arise near T^* . Such a magnetic signal was observed by sensitive muon spin relaxation [44] and polar Kerr effect [52] and is much weaker than the paramagnetic response to external fields [41]. To compare our proposal with these experimental results we need to study the temperature and doping dependence of γ_c .

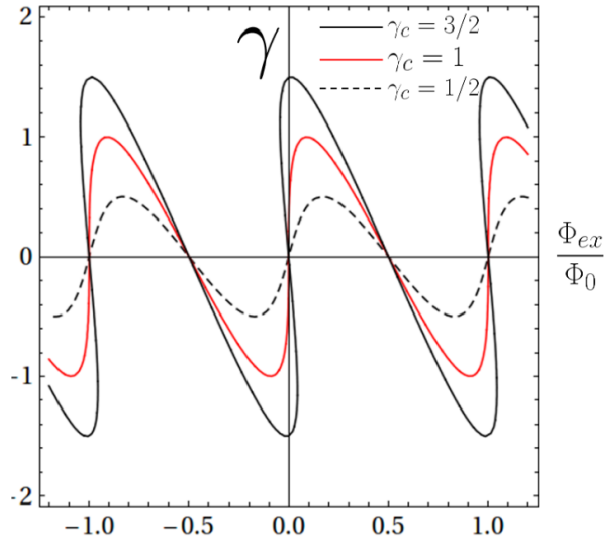


Figure 5.6: The induced current in a frustrated loop for three values of the parameter γ_c as a function of the external flux. For the zero flux case $\Phi_{ex} = 0$, the figure shows that for $\gamma_c > 1$ a spontaneous current may arise while there is none for $\gamma_c < 1$.

5.5 Doping and temperature dependence

We saw that the parameter γ_c controls the arising of spontaneous currents. Therefore, we must investigate how I_c depends on T and ρ . This was studied in detail for d-wave superconductors by many authors [4, 8]. Bruder et al [8] calculated the supercurrent tunnel matrix elements up to second order perturbation theory for two d-wave superconductors with amplitudes

$$\Delta_{\delta,R(L)}(i, T, \phi) = \Delta_0(i, T) \cos [2(\phi - \phi_{R(L)})], \quad (5.11)$$

where $R(L)$ refers to the right(left) superconductor, and the angles ϕ_R and ϕ_L determine the relative orientation of the two superconductors. In our case we make $\phi_{R(L)} = 0$, because the electronic domains are in a single crystal. They show that the dominant contribution to I_c is from "node to node" tunnelling. For this reason, the overall behaviour is like an s-wave superconductor. This result is in agreement with the calculations of an s-wave Josephson junction [29], where

$$I_c \propto \frac{\Delta_R \Delta_L}{\Delta_R + \Delta_L}. \quad (5.12)$$

5.6 Bogoliubov-deGennes calculations

According to the formalism of Bogoliubov deGennes studied in the previous chapter, the values of $\Delta_\delta(i)$ in (3.89) vary in a system with electronic inhomogeneity [15, 14]. Review figure 3.6. The inhomogeneity of the local gaps is responsible for different values of the tunnelling matrix elements between different grains. Consequently, the parameter γ_c also

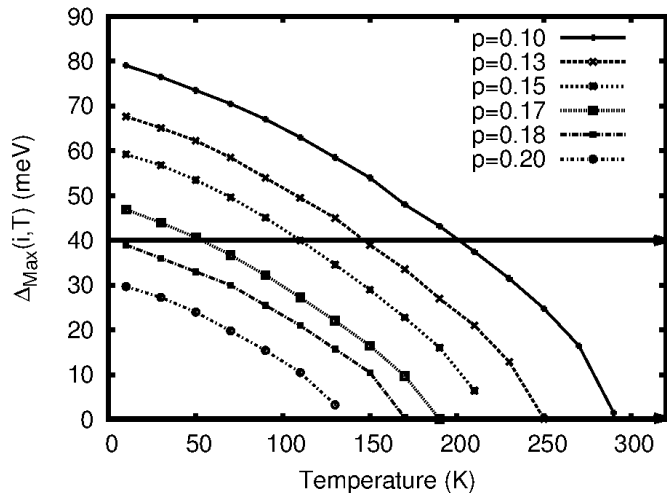


Figure 5.7: The temperature evolution of $\Delta_{\delta,max}(\rho, T)$ of six different values of the average doping $\bar{\rho}$. The line at ≈ 40 meV shows the experimental onset of spontaneous magnetization and the intersections yield the temperature onset for different compounds.

varies through the sample. The values of the γ_c increases with $\Delta_{\delta}(i, T)$, while the temperature is lowered. Spontaneous currents reach their maximum value for maximum $\Delta_{\delta}(i, T)$, causing some loops to have $\gamma_{c,max} \geq 1$ at zero external field. In such an inhomogeneous system, an analytical expression for $\gamma_c(i)$ is difficult to achieve. However, it is reasonable to assume that $\Delta_{\delta}(i, T)$ is the only parameter that controls $\gamma_c(i)$ as the hole doping ρ varies. Since underdoped systems are generally more inhomogeneous, there may be more loops that influence the ferromagnetic signal. Indeed, the Polar Kerr-effect signal T_s is much stronger than in the optimally doped region.

Since the ferromagnetic signal vanishes about $\rho = 0.18$, we use the gap values $\Delta_{\delta}(i, T)$ that trigger the spontaneous current at $\Delta_{\delta,max}(\rho = 0.18, T = 0) \approx 40$ meV. With this minimum energy established, we guarantee $\gamma_c \geq 1$. We then can follow the temperature evolution of the maximum gap of each compound with the horizontal line drawn in figure 5.7. The results for five doping values are shown in the right figure 5.8, together with the experimental results from muon spin relaxation (open circles) and polar Kerr-effect (black squares). This is the main result of this dissertation and shows that our results are in good agreement with the experimental data [17].

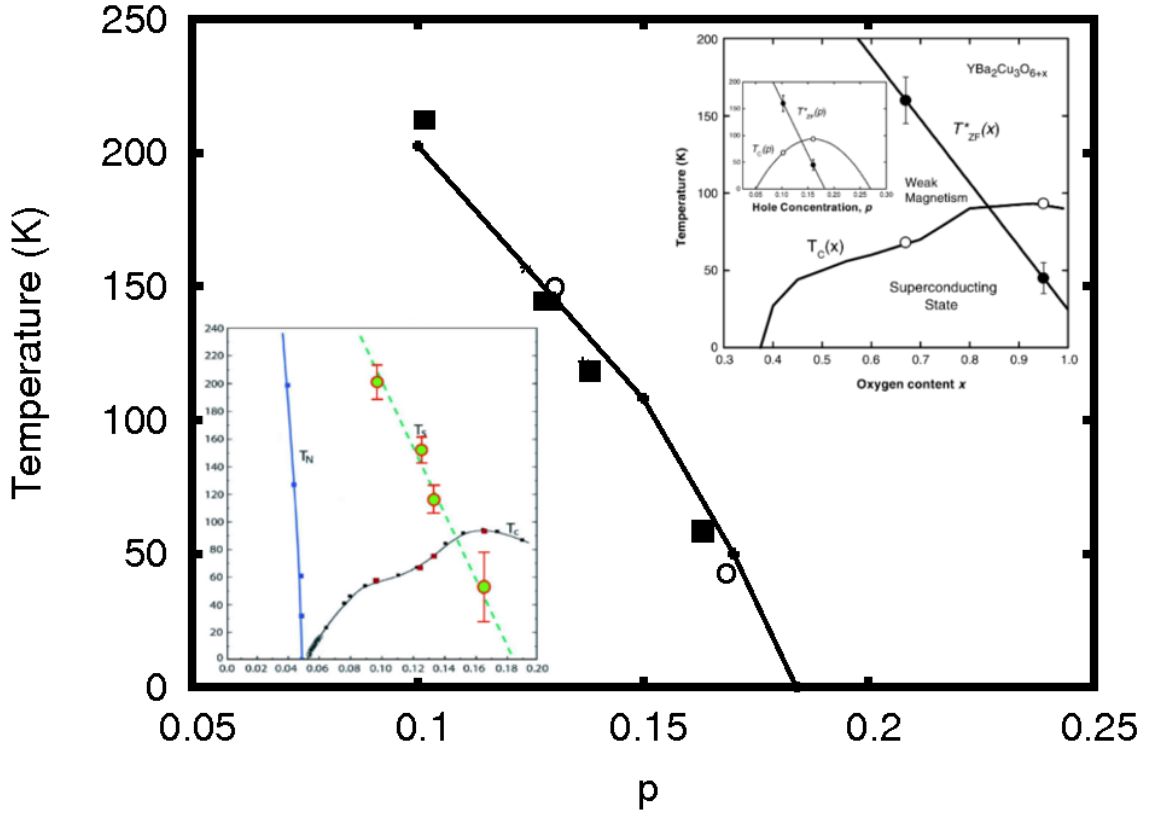


Figure 5.8: This dissertations' main result [17]: The calculated onset of spontaneous magnetization derived from from the intersections in figure 5.7. The results from polar Kerr-effect are drawn as black squares, while muon spin relaxation is indicated by open circles. The line connecting the theoretical points is just a guide to the eye. The insets from left to right are respectively from polar Kerr-effect and muon spin relaxation.

5.7 Concluding remarks

We used the fact that cuprate superconductors have an intrinsic inhomogeneous state where the charges are segregated into a few nanometers of high and low density grains, separated by thin potential barriers. As in Bi-clusters [50] this charge confinement may be the origin of the local superconducting interaction. We then calculate the superconducting properties by the Bogoliubov deGennes method using a phenomenological two-body potential proportional to the energy barriers between the grains. The distinct regions are coupled forming a Josephson network that promotes the resistivity transition at low temperatures. The phase-number quantum fluctuations together with correlation effects are large enough to frustrate arrays of π -junctions. This leads to spontaneous currents with an overall magnetization. These theoretical calculations provide an interpretation to this intriguing weak ferromagnetic phenomenon in good quantitative agreement with the experiments.

Conclusion and perspectives

We have proposed a theory on the onset of ferromagnetic order detected in two very sensitive experiments and, as far as we know, without an explanation. The main ingredient of our model is a phase separation transition that segregates the system into islands of low and high densities where the charges can be confined and Cooper pairs develop locally. These regions are connected by Josephson coupling as in a granular superconductor. Since the charge density is very low in these regions, a well known feature of high- T_c superconductors, the superconducting phase of each grain has a large uncertainty, what causes the spontaneous formation of π -junctions and frustration effects.

This approach is also in agreement with many experimental facts of the high- T_c superconductors, like the pseudogap phase that is composed of local superconducting amplitudes without phase coherence. This model has shown itself to be effective in explaining the features of cuprate superconductors. The general model described here to deal with the spontaneous ferromagnetism may also provide some clues to the important problem that is the pseudogap phase of high- T_c superconductors. In this context we gave a new interpretation for the pseudogap region of $\text{YBa}_2\text{Cu}_3\text{O}_{6+x}$, capable to set a framework to explain experimental data [44, 52] that were lacking a theoretical model.

The studies and simulations developed in this dissertation have a general scope of applications and can be used to deal with other unconventional properties of high- T_c superconductors measured by experiments. Therefore we expect to apply it in the near future to interpret other measurements that so far have not a consensus explanation. High- T_c superconductivity is one of the major problems of Condensed Matter Physics and we believe that using this model of phase separation and inhomogeneous superconductivity can help to understand the physics of these materials.

Bibliography

- [1] P. Anderson. Considerations on the Flow of Superfluid Helium. *Reviews of Modern Physics*, 38(2):298–310, April 1966.
- [2] James F. Annett. *Superconductivity, Superfluids and Condensates*. Oxford University Press, New York, 2004.
- [3] Leslie E Ballentine. *Quantum Mechanics - A Modern Development*, 1998.
- [4] Yu. Barash, A. Galaktionov, and A. Zaikin. Charge transport in junctions between d-wave superconductors. *Physical Review B*, 52(1):665–682, July 1995.
- [5] JG Bednorz and KA Müller. Possible highT c superconductivity in the Ba²⁺La²⁺Cu²⁺O system. *Zeitschrift für Physik B Condensed Matter*, 1986.
- [6] A Bianconi, N. Saini, A Lanzara, M Missori, T Rossetti, H Oyanagi, H Yamaguchi, K Oka, and T Ito. Determination of the Local Lattice Distortions in the CuO₂ Plane of La_{1.85}Sr_{0.15}CuO₄. *Physical Review Letters*, 76(18):3412–3415, April 1996.
- [7] E S Bozin, G H Kwei, H Takagi, and S J Billinge. Neutron diffraction evidence of microscopic charge inhomogeneities in the CuO₂ plane of superconducting La_{2-x}Sr_xCuO₄ (0 ≤ x ≤ 0.30). *Physical review letters*, 84(25):5856–9, June 2000.
- [8] C. Bruder, A. van Otterlo, and G. Zimanyi. Tunnel junctions of unconventional superconductors. *Physical Review B*, 51(18):12904–12907, May 1995.
- [9] John W. Cahn and John E. Hilliard. Free Energy of a Nonuniform System. I. Interfacial Free Energy. *The Journal of Chemical Physics*, 28(2):258, 1958.
- [10] Leon Cooper. Bound Electron Pairs in a Degenerate Fermi Gas. *Physical Review*, 104(4):1189–1190, November 1956.
- [11] Elbio Dagotto. Complexity in strongly correlated electronic systems. *Science (New York, N. Y.)*, 309(5732):257–62, July 2005.
- [12] Andrea Damascelli and Zhi-xun Shen. Angle-resolved photoemission studies of the cuprate superconductors. *Reviews of Modern Physics*, 75(2):473–541, April 2003.

- [13] P G De Gennes. *Superconductivity of metals and alloys*. Frontiers in physics. {W.A.} Benjamin, 1966.
- [14] E. V. L de Mello. Disordered-based theory of pseudogap, superconducting gap, and Fermi arc of cuprates. *EPL (Europhysics Letters)*, 99(3):37003, August 2012.
- [15] E V L De Mello, R B Kasal, Otton S T Filho, and C A C Passos. Electronic phase separation transition as the origin of the superconductivity and pseudogap phase of cuprates. *Journal of physics Condensed matter an Institute of Physics journal*, 21(23):4, 2008.
- [16] E V L de Mello, R B Kasal, and C a C Passos. Electronic phase separation transition as the origin of the superconductivity and pseudogap phase of cuprates. *Journal of physics. Condensed matter : an Institute of Physics journal*, 21(23):235701, June 2009.
- [17] E. V. L de Mello and David Möckli. Weak Magnetic Order in High-Tc Superconductors Produced by Spontaneous Josephon Currents. *Sent to Europhysics Letters*, 2013.
- [18] Evandro Vidor Lins de Mello. Teoria para os supercondutores de altas temperaturas críticas com transição de desordem eletrônica, 2009.
- [19] V. J. Emery and S. A. Kivelson. Importance of phase fluctuations in superconductors with small superfluid density. *Nature*, 374(6521):434–437, March 1995.
- [20] M Franz, C Kallin, and A J Berlinsky. Impurity scattering and localization in d-wave superconductors. *Physical review B Condensed matter*, 54(10):4, 1996.
- [21] Amit Ghosal, Mohit Randeria, and Nandini Trivedi. Inhomogeneous pairing in highly disordered s-wave superconductors. *Physical Review B*, 65(1):1–13, November 2001.
- [22] Kenjiro K Gomes, Abhay N Pasupathy, Aakash Pushp, Shimpei Ono, Yoichi Ando, and Ali Yazdani. Visualizing pair formation on the atomic scale in the high-Tc superconductor Bi2Sr2CaCu2O8+delta. *Nature*, 447(7144):569–72, May 2007.
- [23] Lev P. Gor'kov. Microscopic Derivation of the Ginzburg-Landau Equations in the Theory of Superconductivity. *Soviet Physics JETP*, 36(9)(6), 1959.
- [24] W. Guyard, A. Sacuto, M. Cazayous, Y. Gallais, M. Le Tacon, D. Colson, and A. Forget. Temperature Dependence of the Gap Size near the Brillouin-Zone Nodes of HgBa2CuO4+delta Superconductors. *Physical Review Letters*, 101(9):1–4, August 2008.
- [25] C. Howald, P. Fournier, and a. Kapitulnik. Inherent inhomogeneities in tunneling spectra of Bi2Sr2CaCu2O8-x crystals in the superconducting state. *Physical Review B*, 64(10):100504, August 2001.
- [26] J. R. Schrieffer J. Bardeen, L. N. Cooper. Theory of superconductivity. *Physical Review*, 108(5), 1957.

- [27] Kanigel, U. Chatterjee, M. Randeria, M. Norman, G. Koren, K. Kadowaki, and J. Campuzano. Evidence for Pairing above the Transition Temperature of Cuprate Superconductors from the Electronic Dispersion in the Pseudogap Phase. *Physical Review Letters*, 101(13):137002, September 2008.
- [28] Kanigel, U. Chatterjee, M. Randeria, M. Norman, S. Souma, M. Shi, Z. Li, H. Raffy, and J. Campuzano. Protected Nodes and the Collapse of Fermi Arcs in High-Tc Cuprate Superconductors. *Physical Review Letters*, 99(15):1–4, October 2007.
- [29] J B Ketterson and S N Song. *Superconductivity*. Cambridge University Press, New York, 1999.
- [30] S A Kivelson, I P Bindloss, V Oganessian, J M Tranquada, A Kapitulnik, and C Howald. How to detect fluctuating stripes in the high-temperature superconductors. *Reviews of Modern Physics*, 75(4):1201–1241, October 2003.
- [31] A. J. Leggett. *Quantum Liquids*. Oxford University Press, New York, 2011.
- [32] Deltlef Lehman. *Mathematical Methods of Many-Body Quantum Field Theory*. Chapman & Hall/CRC, London, 2005.
- [33] K. McElroy, D.-H. Lee, J. Hoffman, K. Lang, J. Lee, E. Hudson, H. Eisaki, S. Uchida, and J. Davis. Coincidence of Checkerboard Charge Order and Antinodal State Decoherence in Strongly Underdoped Superconducting $\text{Bi}_2\text{Sr}_2\text{CaCu}_2\text{O}_{8+\delta}$. *Physical Review Letters*, 94(19):1–4, May 2005.
- [34] E V L De Mello. Description and connection between the oxygen order evolution and the superconducting transition in La_2CuO_4 . 98, 2012.
- [35] HJW Müller-Kirsten. *Electrodynamics: an introduction including quantum effects*. World Scientific, 2004.
- [36] Antonio H. Castro Neto. *Elementary Condensed Matter Physics*, 2003.
- [37] Rinat Ofer and Amit Keren. Nutation versus angular-dependent NQR spectroscopy and impact of underdoping on charge inhomogeneities in $\text{YBa}_2\text{Cu}_3\text{O}_{7-y}$. *Physical Review B*, 80(22):1–8, December 2009.
- [38] S H Pan, J P O’Neal, R L Badzey, C Chamon, H Ding, J R Engelbrecht, Z Wang, H Eisaki, S Uchida, A K Gupta, K W Ng, E W Hudson, K M Lang, and J C Davis. Microscopic electronic inhomogeneity in the high-Tc superconductor $\text{Bi}_2\text{Sr}_2\text{CaCu}_2\text{O}_{8+x}$. *Nature*, 413(6853):282–5, September 2001.
- [39] Aakash Pushp, Colin V Parker, Abhay N Pasupathy, Kenjiro K Gomes, Shimpei Ono, Jinsheng Wen, Zhijun Xu, Genda Gu, and Ali Yazdani. Extending universal nodal excitations optimizes superconductivity in $\text{Bi}_2\text{Sr}_2\text{CaCu}_2\text{O}_{8+\delta}$. *Science (New York, N.Y.)*, 324(5935):1689–93, June 2009.
- [40] J Quintanilla and C Hooley. The strong-correlations puzzle. *Physics World*, (June), 2009.
- [41] Manfred Sigrist and TM Rice. Unusual paramagnetic phenomena in granular high-temperature superconductors—A consequence of d- wave pairing? *Reviews of Modern Physics*, 67(2):503–513, 1995.

- [42] P. Singer, A. Hunt, and T. Imai. ^{63}Cu NQR Evidence for Spatial Variation of Hole Concentration in $\text{La}_{2-x}\text{Sr}_x\text{CuO}_4$. *Physical Review Letters*, 88(4):4–7, January 2002.
- [43] J. Sonier, M. Ilton, V. Pacradouni, C. Kaiser, S. Sabok-Sayr, Y. Ando, S. Komiya, W. Hardy, D. Bonn, R. Liang, and W. Atkinson. Inhomogeneous Magnetic-Field Response of $\text{YBa}_2\text{Cu}_3\text{O}_y$ and $\text{La}_{2-x}\text{Sr}_x\text{CuO}_4$ Persisting above the Bulk Superconducting Transition Temperature. *Physical Review Letters*, 101(11):2–5, September 2008.
- [44] J E Sonier, J H Brewer, R F Kiefl, R I Miller, G D Morris, C E Stronach, J S Gardner, S R Dunsiger, D a Bonn, W N Hardy, R Liang, and R H Heffner. Anomalous weak magnetism in superconducting $\text{YBa}_2\text{Cu}_3\text{O}_{6+x}$. *Science (New York, N.Y.)*, 292(5522):1692–5, June 2001.
- [45] B I Spivak and S A Kivelson. Negative local superfluid densities: The difference between dirty superconductors and dirty Bose liquids. *Physical Review B*, 43(4):3740–3743, 1991.
- [46] Philip L. Taylor and Olle Heinonen. *A Quantum Approach to Condensed Matter Physics*. Cambridge University Press, New York, 2002.
- [47] T Timusk and B W Statt. The pseudogap in high-temperature superconductors: an experimental survey. *Reports on Progress in Physics*, 62(1):54, 1999.
- [48] Michael Tinkham. *Introduction to Superconductivity*. Dover Publications, Inc, New York, second edition, 1996.
- [49] J. M. Tranquada, B. J. Sternlieb, J. D. Axe, Y. Nakamura, and S. Uchida. Evidence for stripe correlations of spins and holes in copper oxide superconductors. *Nature*, 375(6532):561–563, June 1995.
- [50] B. Weitzel and H Micklitz. Superconductivity in granular systems built from well-defined rhombohedral Bi-clusters: Evidence for Bi-surface superconductivity. *Physical Review Letters*, 66(3):385–388, January 1991.
- [51] M. Wu, J. Ashburn, C. Torng, P. Hor, R. Meng, L. Gao, Z. Huang, Y. Wang, and C. Chu. Superconductivity at 93 K in a new mixed-phase Y-Ba-Cu-O compound system at ambient pressure. *Physical Review Letters*, 58(9):908–910, March 1987.
- [52] Jing Xia, Elizabeth Schemm, G Deutscher, S A Kivelson, D A Bonn, W N Hardy, R Liang, W Siemons, G Koster, M M Fejer, and A Kapitulnik. Polar Kerr-Effect Measurements of the High-Temperature $\text{YBa}_2\text{Cu}_3\text{O}_{6+x}$ Superconductor : Evidence for Broken Symmetry near the Pseudogap Temperature. *Physical Review Letters*, 100(12):3–6, 2008.
- [53] V. Yukalov and E. Yukalova. Mesoscopic phase separation in anisotropic superconductors. *Physical Review B*, 70(22):1–12, December 2004.